

Utah State University

DigitalCommons@USU

---

Theses and Dissertations

Materials Physics

---

Summer 8-2020

## Electron Emission and Transport Properties Database for Spacecraft Charging Models

Phil Lundgreen

Follow this and additional works at: [https://digitalcommons.usu.edu/mp\\_etd](https://digitalcommons.usu.edu/mp_etd)



Part of the [Condensed Matter Physics Commons](#), and the [Engineering Physics Commons](#)

---

### Recommended Citation

Lundgreen, Phil, "Electron Emission and Transport Properties Database for Spacecraft Charging Models" (2020). *Theses and Dissertations*. 18.

[https://digitalcommons.usu.edu/mp\\_etd/18](https://digitalcommons.usu.edu/mp_etd/18)

This Thesis is brought to you for free and open access by the Materials Physics at DigitalCommons@USU. It has been accepted for inclusion in Theses and Dissertations by an authorized administrator of DigitalCommons@USU. For more information, please contact [digitalcommons@usu.edu](mailto:digitalcommons@usu.edu).



THE DEVELOPMENT AND USE OF A SECONDARY ELECTRON YIELD  
DATABASE FOR SPACECRAFT CHARGE MODELING

by

Phillip Lundgreen

A thesis submitted in partial fulfillment  
of the requirements for the degree

of

MASTER OF SCIENCE

in

Physics

Approved:

---

JR Dennison  
Major Professor

---

Tonya Triplett  
Committee Member

---

Ludger Scherliess  
Committee Member

---

D. Richard Cutler, Ph.D.  
Interim Vice Provost  
of Graduate Studies

UTAH STATE UNIVERSITY  
Logan, Utah

2020



Copyright © Phillip Lundgreen 2020

All Rights Reserved

## ABSTRACT

The Development and Use of a Secondary Electron Yield Database for  
Spacecraft Charge Modeling

by

Phillip Lundgreen, Master of Science

Utah State University, 2020

Major Professor: Dr. JR Dennison  
Department: Physics

Modeling the rate and likelihood of spacecraft charging during spacecraft mission is critical to determine mission length, proposed spacecraft attitude, and spacecraft design. The focus of this work is the creation and utilization of a database of secondary electron yield (SEY) measurements for a host of materials to increase accuracy in spacecraft modeling. Traditional methods of SEY data selection for input into spacecraft charging codes typically include the use of compiled materials databases incorporated in charging codes or selecting values from a specific scientific study. The SEY database allows users to select data inputs based upon the details associated with the studies used to generate the data. Qualifications of data based upon surface morphology, surface contamination, and data origin are all included as well as a brief guide to assist researchers in understanding the way to best determine which dataset would best model their craft in its proposed environment. Such qualifications of data allow for more accurate modeling and for the amount of fault tree analysis utilized in spacecraft monitoring to be decreased as a more accurate root cause analysis can be performed preflight.

(109 pages)

## PUBLIC ABSTRACT

The Development and Use of a Secondary Electron Yield Database for  
Spacecraft Charge Modeling

Phillip Lundgreen

Charge modeling of electron-solid interactions requires a detailed and accurate compilation of experimental data on which to base its physics and against which to test its predictions. Historically researchers used methods involving individual research or information taken from existing, vague, databases that were often found wanting. To streamline the charge modeling process, a collection of data has been assembled and categorized based upon surface morphology and contamination from various published sources and existing databases. The quality and quantity of the compilation vary widely with very little information offered with regards to surface conditions of various materials (contamination, morphology, etc. ...). Included in the database are 34 elements and over 100 different sources. Using this database, physics principles have been found which allow for the quantification of material surface conditions, and more accurate SEY modeling to be accomplished.

## ACKNOWLEDGMENTS

I want to acknowledge the kindness, love, and patience of my wife who encouraged me to return to school and pursue this degree. Her constant support of me as I worked through homework, grading, and finally thesis writing sustained me as nothing else could. Her love was unflagging even as I justified the development of minor Mountain Dew and fishing addictions to cope with the rigors of grad-school.

I was brought up in a household of education. My parents would not let me miss a day of school, much less a homework assignment. They gave me the motivation to pursue education and do my best. Without the guiding influence they had on me I don't know that I would have had the motivation to even contemplate a goal as lofty as a Master's Degree in Physics.

Without Tonya Triplett, I never would have been offered this opportunity. She found me in a cluttered high school chemistry classroom and championed my return to USU. Her belief in me, her guidance, and her never-ending supply of snacks helped motivate me through all the difficult studying I had to do to remember all the physics that I had forgotten.

Lastly, JR Dennison, never gave up on me even when my ideas about what this database could and should be differed from what he had in mind. He had the patience and trust to leave me alone long enough with the data so I could develop the proof of concept that eventually became this database. His trust went further when he let me work with a number of undergraduate students so that this database could be pushed further along (Thanks Trace, Jenny, and Ben).

I feel like the young Wart in T.H. White's "Once and Future King" As I came to work on this thesis all those I know who loved me were there encouraging me and offering wisdom to help me live up to my true potential.

Phillip Lundgreen

## CONTENTS

	Page
ABSTRACT.....	iii
PUBLIC ABSTRACT .....	iv
ACKNOWLEDGMENTS .....	v
LIST OF TABLES.....	viii
LIST OF FIGURES .....	ix
LIST OF SYMBOLS .....	xi
LIST OF ABBREVIATIONS.....	xiii
INTRODUCTION.....	1
Purpose and Scope.....	1
Outline .....	3
BASICS AND THEORY .....	5
State of Research .....	5
Space is Not Nice.....	5
Basics of Electron Emission and Charging.....	6
Theoretical Foundations.....	10
Spacecraft Charge Modeling Software .....	10
SEY Models .....	12
Material Parameter Inputs Required for Charging Codes.....	13
Limitations Associated with Historical Databases.....	17
Origination of NASCAP Aluminum Values.....	22
The Need for a Better Database .....	23
DEVELOPMENT OF DATABASE .....	29
Data Acquisition .....	29
Analysis and Qualification of Surface Conditions.....	31

Contamination/Oxidation.....	32
Surface Morphology (Roughness) .....	36
Data Compilation .....	39
Database Options .....	42
Report Types.....	42
Data Filters.....	43
RESULTS.....	48
Verification of Prior Established Physics Principles .....	49
Contamination Affects Yield .....	50
Roughness Affects Yield .....	53
Selecting Data for More Accurate Charge Modeling .....	55
Method 1: Select Parameterized Yield Properties .....	57
Method 2: Review of Available Literature .....	59
Establishment of New Physics Principles.....	62
Determining Spacecraft Environment.....	62
Method to Quantify Contamination and Morphology .....	65
CONCLUSION AND OUTLOOK .....	71
Conclusion .....	71
Further Developments.....	73
REFERENCES .....	76
APPENDIX A: LIBRARIES USED IN CODING .....	86
APPENDIX B: EXAMPLES OF VARIOUS REPORTS AND HOW TO USE THEM .....	89
Removing Gaps Between Datapoints .....	89
A Table Report.....	90
APPENDIX C: BRUINING ARTICLE PERMISSIONS.....	92
CURRICULUM VITAE.....	93

## LIST OF TABLES

Table	Page
2.1. Various space environments. ....	5
2.2. Comparison between several range and SEY models with their associated coefficients (Lundgreen and Dennison, 2020) .....	13
2.3. NASCAP materials parameters for copper .....	15
2.4. Materials with charging properties found in the NASCAP database. (Mandell, 1977) .....	17
2.5. Materials with charging properties found in the SEE database .....	19
2.6. Materials with charging properties found in the SPENVIS database .....	19
2.7. Elements reported in the USU SEY Database. ....	20
2.8. Composite materials featured in the Joy database of material Electron- Solid Interactions .....	21
2.9. SEY parameters in the default materials database included with NASCAP (Mandell, 1993). ....	22
2.10. Spacecraft charging and transport code input requirements. ....	26
3.1. Chart types available in USU SEY database. ....	43
4.1. SEY data for various Cu studies .....	52
4.2. The different symbols used in the comparison of different SEY fitting parameters. ....	53
4.3. SEY data for various Al studies .....	58
5.1. Fitting parameters for aluminum .....	74

## LIST OF FIGURES

Figure	Page
1.1. Linear plot of SEY versus energy.....	2
2.1. Pie graph showing the cause of environmentally induced spacecraft anomalies. After, Koons, 1999.....	6
2.2. Emission spectra for an arbitrary material.....	7
2.3. Steps associated with SEY.....	9
2.4. Various Cu SEY measurements as functions of incident electron energy.....	10
2.5. Generic model of a satellite modeled in NASCAP.....	11
2.6. Typical SEY yield curve with key features identified.....	14
2.7. NASCAP-2K Secondary Yield Fitting Tool example.....	16
2.8. Historical plots of reduced SEY. Plots as taken from Baroody (1950).....	24
3.1. A pair of SEY plots.....	29
3.2. The three main surface characteristics which affect SEY.....	31
3.3. Range versus energy plot for (a) different species of aluminum samples and (b) common spacecraft materials.....	33
3.4. Aggregate mole fraction of contaminants detected by the Columbia Orbiter.....	36
3.5. Values for different allotropes of carbon.....	41
3.6. SEY Values for Copper.....	41
3.7. Snapshot of the different reporting options available in the USU SEY database.....	42
3.8. The default USU SEY Pivot Tool settings.....	43
3.9. Screen shot of the USU SEY Database.....	45
3.10. Different copper SEY data sets sorted based upon surface morphology conditions.....	46
3.11. Different aluminum SEY data sets sorted based upon surface contamination conditions.....	47
4.1. $\delta_{max}$ values for two conducting materials.....	49

4.2.	Comparison of $E_{max}$ values for various conducting samples.....	50
4.3.	Roughness facilitates the recapture of emitted electrons. ....	54
4.4.	Round robin comparison of various SEY curves.....	57
4.5.	SEY curves versus energy for Al studies.....	60
4.6.	Entirety of the Cu SEY data.....	61
4.7.	Mean free paths versus altitude.....	64
4.8.	Log-log plot of reduced SEY, $\delta/\delta_{max}$ , versus reduced energy, $E_0/E_{max}$ .....	67
4.9.	Values of the high-energy SEY fitting parameter (n) used in Eq. 2.2 .....	68
4.10.	Values of the low-energy SEY fitting parameter (m) used in Eq. 2.2 .....	70
B.1.	First step to remove gaps between data points.....	89
B.2.	Second and third steps to remove gaps between data points .....	90
B.3.	Data reports for various materials.....	91

## LIST OF SYMBOLS

## Symbol

$b$	= constant related to material density
$b_1$	= first coefficient for bi-exponential range law
$b_2$	= second coefficient for bi-exponential range law
$E_0$	= incident energy
$E_a$	= first low energy value for determining $n$
$E_b$	= second low energy value for determining $n$
$E_c$	= first low energy value for determining $m$
$E_d$	= second low energy yield value for determining $m$
$E_{max}$	= energy associated with maximum SE yield for electron impact
$K_B$	= Boltzmann constant
$n$	= fitting parameter associated with high energy (surface morphology)
$n_1$	= first power for bi-exponential range law
$n_2$	= second power for bi-exponential range law
$N_D$	= number of molecules being desorbed from surface
$m$	= fitting parameter associated with low energy (surface contamination)
$Q_1$	= outgassing coefficient
$r_0$	= constant determined by $n$ , $m$ , and $E_{max}$
$R$	= maximum range an electron can penetrate for a specific energy
$R_0$	= radius of Earth
$R_{sc}$	= spacecraft radius
$T$	= temperature
$Z_{eff}$	= effective mean atomic number
$\alpha$	= coefficient of condensation
$\delta_a$	= first low energy yield value for determining $n$
$\delta_b$	= second low energy yield value for determining $n$

$\delta_c$	= first high energy yield value for determining $m$
$\delta_d$	= second low energy yield value for determining $m$
$\delta_{max}$	= maximum SE yield for electron
$\epsilon_r$	= relative dielectric constant
$\Phi$	= material work function
$\lambda_0$	= electron mean free path
$v_0$	= craft velocity
$v_D$	= velocity of desorbed molecules
$\sigma_0$	= bulk Conductivity

## LIST OF ABBREVIATIONS

AFRL	Airforce Research Lab
BSEY	Backscattered electron yield ( $\eta$ )
ESA	European Space Agency
JAXA	Japan Aerospace Exploration Agency
JSON	JavaScript Object Notation
keV	Kilo-electron volt
MUSCAT	Multi-Utility Spacecraft Charging Analysis Tool
MPG	Material physics group
NASA	National Aeronautics and Space Administration
NASCAP	NASA/Air Force Spacecraft Charging Analysis Program
PE	Primary electrons
SE	Secondary electrons
SEE	Space Environments and Effects
SEM	Scanning electron microscope
SEY	Secondary electron yield ( $\delta$ )
SPINE	Spacecraft Plasma Interactions Network in Europe
SPIS	Spacecraft Plasma Interaction System
TEY	Total electron yield ( $\sigma$ )
USU	Utah State University

## CHAPTER 1

### INTRODUCTION

The goal in undertaking the task of creating a secondary electron yield (SEY) database was to discern the reasons for the disparity of reported values from various respected researchers, as well as determining if there were any meaningful way to quantify this disparity and leverage it to achieve a more accurate method for SEY modeling. SEY is a count of electrons produced by a material when it is bombarded by highly energetic particles. SEY reported values have been compiled into a large (though not comprehensive) database. In doing this, the disparity of values has become at once evident through simple graphing of all reported values for a specific material.

Through careful study, it has been determined that the largest source of variation in reported SEY values for nominally similar materials is either contamination, oxidation, roughness, or some combination of the three surface properties. While investigating this, a novel method for determining coefficients to use in a SEY charge model for a specific set of surface conditions was developed. This model allows for charge modeling based upon surface characteristics as well as the maximum SEY value and the energy associated with it. This is an improvement over historical models that did not have a simple way to incorporate surface characteristics.

This thesis intends to communicate to interested parties the methods used to obtain, classify and present the myriad of SEY data that has been collected and categorized in this study. Also, this study demonstrates a method that can be used to identify the appropriate approximate coefficients requisite for SEY modeling based upon surface conditions determined through the analysis of a reduced SEY graph.

#### 1.1 Purpose and Scope

The study of SEY is not new. The earliest studies of SEY were made independently by Starke in Germany in 1898 (Starke, 1898), and by Swinton in England in 1899 (Swinton, 1899). Because the study of the number of electrons produced when a material is bombarded with highly energetic electrons is not a new study, huge quantities of data have been produced. This is where a primary problem with the field lays, and also the inspiration for the work here. In generating such vast quantities of data, huge discrepancies for

similar materials have been measured. SEY is an intrinsic material property, meaning, that regardless of where studies are performed the same SEY values should be returned for a specific material. This has proved not to be the case (see Fig. 1.1.). These discrepancies have been identified before, and databases have been developed in an attempt to determine a way to solve them (Joy, 1995). Unfortunately, a method to quantify the source of the differences, and use that to better model materials has not been determined historically.

SEY is of significance because of its use as an input value for spacecraft charge modeling, electron microscopy, and particle acceleration. Of particular interest is the relationship between spacecraft charge modeling and spacecraft preservation from differential charging. By improving charge modeling better decisions can be made by engineers and operators in the design and operation of spacecraft, which can result in diminished potential charge potential by adjustments in physical design, material selection, or flight attitude adjustment. Charging is a significant issue to spacecraft as it accounts for more than one-half of environmentally induced spacecraft anomalies (Koons *et al.*, 1999). Understanding and mitigating the risk caused by it is of significant importance to researchers as well as spacecraft designers.

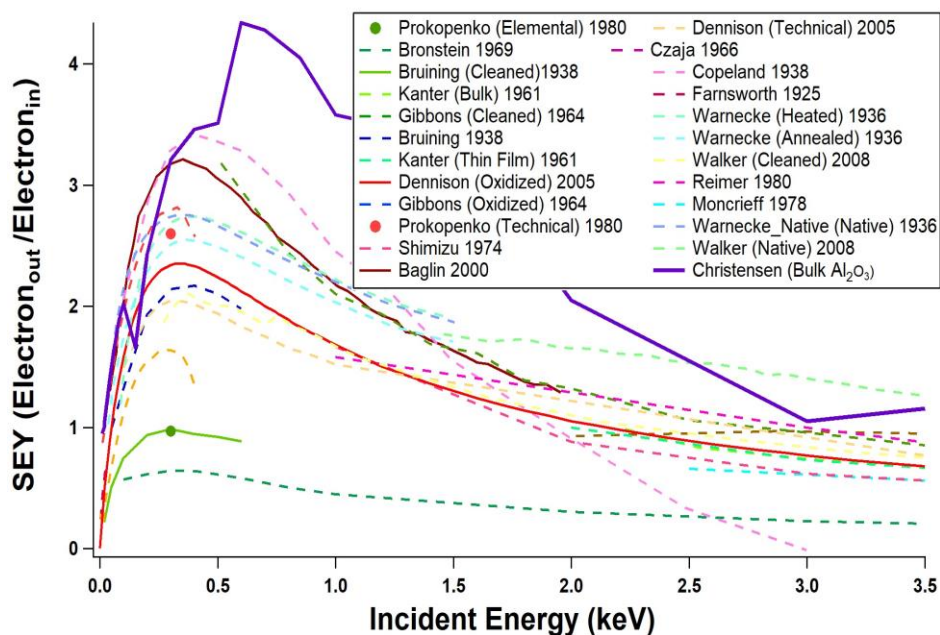


FIG. 1.1. Linear plot of SEY versus energy. The inset legend identifies the lines associated with each study. The “best” representative studies for various conditions selected are highlighted as solid lines.

To better model crafts and facilitate the use of the charging codes that were developed specifically for charge modeling purposes several data sets have been collected and made available to the public (Joy, 1995; Davis and Mandell, 2014; Wood *et al.*, 2007; Dennison *et al.*, 2005; Dennison *et al.*, 2007; Parker and Minow, 2018; SPENVIS, 2018). These historical databases have a few issues; namely paucity of data, incorrect data, lack of materials study background information, and poor user interface. Another problem that exists with these datasets does not have to do with the quality of data but is related to the use of the data. With such a variety of data available, selecting appropriate data for proper modeling of a specific application could prove to be quite difficult.

The key goals for this work were three-fold. Firstly the development of a quick, simple way to visualize a large quantity of data for a specific material was needed. Large amounts of data require a quick way to sort the data based upon surface characteristics of the material studied. The second goal was to make that data accessible to a wide user community in a manner consistent with the needs of a wide array of users. The final goal was to understand the cause of discrepancy of data and, if possible, find a way to use that understanding to add value to the various studies.

An online database of over 34 different elements and 100 different sources has been developed in the furtherance of these goals. These studies were classified based on surface conditions and data origination. An online database format allows for the presentation of data from multiple sources and even multiple types of materials at once. Analysis of the database has verified trends associated with low and high energy electron yields and their relation to materials surface characteristics (Baglin *et al.*, 2000), i.e., low energy yield is related to surface contamination and high energy yield is affected by surface morphology (roughness). When plotted in a reduced format it was found that a few points taken from the graph can be used to determine approximate  $n$  and  $m$  fitting parameters that are used in SEY modeling (Christensen, 2017; Lundgreen and Dennison, 2019), which allows researchers to adjust their model based upon predicted surface characteristics for materials.

## 1.2 Outline

This thesis begins with a brief review of the relevant background physics (Chapter 2). This review begins with a definition of electron yield and a short history of these measurements. It continues with an

examination of the space environment and the central role SEY plays in spacecraft charging. A brief analysis of the importance of databases and a review of existing SEY databases follows. Chapter 2 also outlines existing charging codes and the inputs of materials properties that they require. The output values will be briefly touched upon, but the main emphasis of this section will be the near-identical properties (with regards to spacecraft charging) that each of these codes possesses. Models used to parameterize the SEY data are also reviewed.

Chapter 3 then transitions into the methods used in this study to develop a SEY database. The content limitations and use of values in historical databases are discussed. There is a discussion of the source of data referenced, as well as the care taken to make the data readily accessible.

The results garnered by this new database are presented in Chapter 4. Methods of analysis, as well as important conclusions that can be drawn from a very large database, are demonstrated. In this chapter, we discuss the results in the context of both empirical and physics-based models.

Finally, the conclusions and potential future work are discussed in Chapter 6. Included, are appendices which highlight an updated materials report project, and advanced methods to create various reports using the Utah State University (USU) SEY Database.

## CHAPTER 2

## BASICS AND THEORY

## 2.1 State of Research

This chapter has been written to better acquaint the casual reader with some of the ideas that are pertinent to this thesis. In this chapter, brief explanations are given of the space environment, secondary electron emission modeling, electron emission, spacecraft charge modeling, and historical electron emission databases. This is, of course, a huge number of subjects to cover. Should the reader desire to learn more about any of the sections, they are encouraged to read the historically cited review articles. The author can honestly say that it is from those giants' shoulders that he has been able to view the new physics principles that will be discussed later in this thesis.

## 2.1.1 Space is Not Nice

The space environment is harsh, especially for sensitive instruments, power systems, and communication devices. Different environments require different methods of protection for each craft. There are a host of different environments to which spacecraft may be subject (see Table 2.1.) (Koons *et al.*, 1999; Hastings and Garrett, 2004). The methods that scientists and engineers use to protect their crafts from these harsh environments combine principles of spacecraft geometry design, altitude control (orbit),

Table 2.1. Various space environments.

- 
- Neutral Thermosphere
  - Thermal Environment
  - Plasma
  - Meteoroids and Orbital Debris
  - Solar Environment
  - Ionizing Radiation
  - Magnetic Field
  - Gravitational Field
  - Mesosphere

and selection of spacecraft material based on potential interactions between space environment and spacecraft elements.

When the space environment interacts with a craft, it can cause anomalies in mission parameters. A voluntary study done on these environmentally-induced anomalies shows the largest source of spacecraft anomalies to be some form of electrostatic discharge (see Fig. 2.1.) (Koons *et al.*, 1999; Bedingfield *et al.*, 1996). Koons took into account data spanning 1979 to 2000. Due to the proprietary nature of spacecraft data it is assumed that these data, while informative, do not represent a totality of environmentally induced spacecraft anomalies. However, the cited data, which shows charging related events account for between 50 and 65% of all such anomalies, indicate that spacecraft charging should receive specific attention from designers. Charging is directly related to the specified orbit of a craft and will affect contamination of the craft (see Section 4.3.1). Contamination of the surface of a craft is of concern, as it may increase or decrease the charging of spacecraft surfaces depending upon the variety of contaminants.

### 2.1.2 Basics of Electron Emission and Charging

The charging rate of a material or the rate at which the total number of electrons of the material changes are determined by electron flux, electron yield, and electron transport. Of particular interest to spacecraft charge modelers is electron yield. Electron yield is defined, for our purposes, as the total of secondary electron yield (SEY,  $\delta$ ) and backscattered electron yield (BSEY,  $\eta$ ).

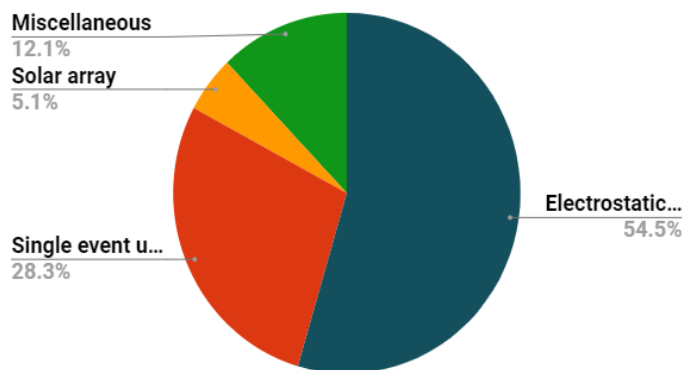


FIG. 2.1. Pie graph showing the cause of environmentally induced spacecraft anomalies. After, Koons, 1999.

$$\sigma_{Tot} = \delta + \eta \quad (2.1)$$

A word of clarification on the definition of SEY in the context of spacecraft charging codes is necessary. The electron yield of a material is universally defined as the ratio of emitted electrons per incident electron. This is traditionally separated into two subcategories, SEY and BSEY. From an operational perspective, the separation is made in terms of the energy of the emitted electrons: SEs are emitted with energies <50 eV, while BSEs are emitted with energies >50 eV (Sternglass, 1954) (See Fig. 2.2.). This operational distinction is used in the spacecraft charging community, in scanning electron microscopy literature (Reimer and Tollkamp, 1980; Joy, 1995), and numerous other fields. Therefore, this operational definition of SEY is also the one used for data presented in this thesis. From an alternate physics-based perspective, the separation is made in terms of the origin of the emitted electrons: backscattered electrons (BSEs) originate in the incident beam and can undergo one or more quasi-elastic collisions before escaping back out of the surface of the material. Alternately, secondary electrons (SEs) originate in the material, are excited into mobile states by energy deposited by incident electrons, and escape the material. These are sometimes referred to as “true secondary electrons” (Czaja, 1966). Physical

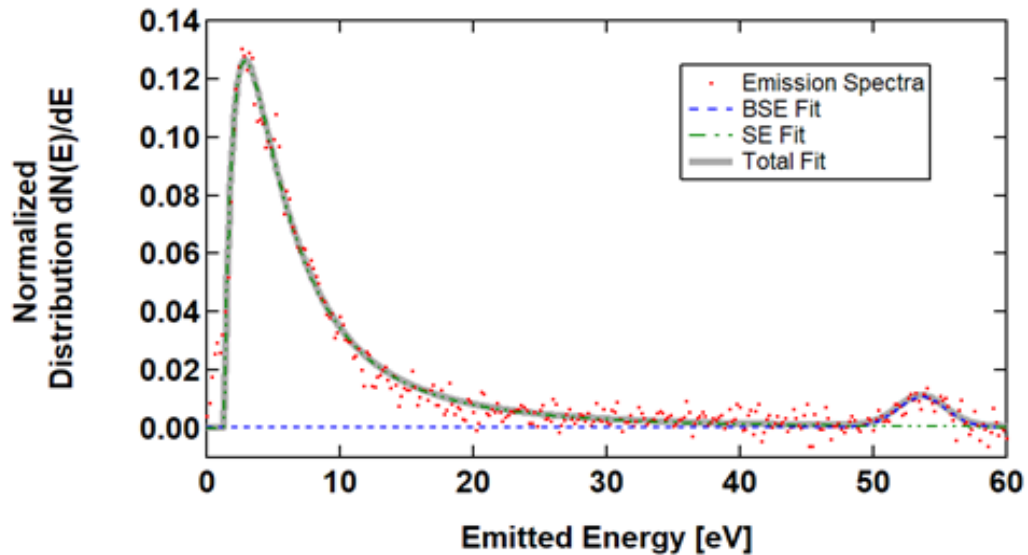


FIG. 2.2. Emission spectra for an arbitrary material. Showing the values reported for SEY ( $E < 50$  eV) and BSEY ( $E > 50$  eV).

models of electron emission—including Eq. 2.2 Presented in Section 2.3—are usually based on this physics perspective.

As mentioned before the sum of BSEY and SEY gives the total number of emitted electrons per incident electron, which is called the total electron yield (TEY). Some researchers use the term “secondary electron yield” to mean the same thing as total electron yield, without differentiating between the two mechanisms which produce emitted electrons. Most notably this potentially ambiguous use of “secondary electron yield” has been adopted by the European space community as a standard definition (Standards, 2008) even though the models used in SPENVIS make the clear distinction between SEY and BSEY as the two components for the total electron emission (SPENVIS, 2018). This fails to adequately model electron yield and often creates confusion, so it is important to distinguish between the two uses of SEY. Also, some studies of electron yield (Baglin *et al.*, 2000; Czaja, 1966)—or more commonly, some compilations of electron yield studies—fail to identify whether measured “secondary electron yield” refers to TEY or SEY. For many applications, the difference between TEY and SEY is not critical, as the BSEY yield is usually a modest fraction of the total yield and reasonably constant over intermediate incident energies. However—for more precise studies, especially for studies emphasizing low incident energies or high incident energies where BSEY have a smaller or larger contribution respectively, or for materials where the BSEY contribution is a larger fraction of TEY (e.g., higher atomic number metals)—misidentification of SEY or TEY values can introduce significant error.

The first discussions of electron yield occurred over a hundred years ago when energetic electrons were still referred to as cathode rays. Barely a year after Thomson identified the electron (Thomson, 1897) examinations of TEY were made independently by a German scientist (Starke, 1898) and an English scientist (Swinton, 1899). Thus, the study of electron emission was born.

As previously stated, the emission of electrons can be caused by energy deposition from highly energetic electrons. To help the reader better understand the emission process, the steps will be discussed herein (see Fig. 2.3.). The steps are as follows:

1. Entrance of and subsequent slowing of energetic primary electrons (PE) within the solid primarily due to low energy inelastic collisions.

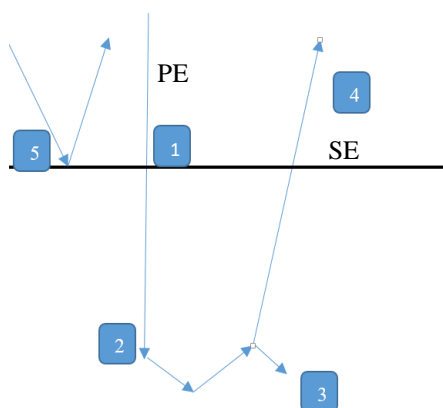


FIG. 2.3. Steps associated with SEY.

2. As the PE interacts with electrons within the material, it causes the production of excited internal secondary electrons (SE).
3. At this point in the process, there are two options for these electrons: absorption into the solid resulting in energy and charge being deposited directly into the material.
4. Or, if an electron has enough energy to overcome the attractive force of the solid a SE is emitted and can be measured typically by a tool such as a hemispherical grid. There are cases where a positively charged surface will re-attract emitted electrons preventing them from being measured by the hemispherical grid (this is of key importance when discussing spacecraft charged up to a positive surface potential.)
5. If the PE penetrates up to a finite range ( $r$ ) and undergoes elastic or quasi-elastic collision with atoms within the solid the PE can be emitted and backscattering of primary electrons occurs.

SEY is dependent upon the physical characteristics of a material (Sakai *et al.*, 1999), valence number (Ding *et al.*, 2001), and material density (Barut, 1954). As such, SEY is an intrinsic property, and identical materials should have constant SEY values dependent upon incident energy, as expressed by SE yield curves. However, SEY measurements exhibit great variability, as shown in Fig. 2.4. for Copper. Looking specifically at the maximum values for SEY ( $\delta_{max}$ ) a quantifiable variation is apparent with values available in the USU SEY Database ranging from 0.68 to 2.4, a 300% difference. As an example, Dennison *et al* (2007) found the modest changes of 10% and 18% for  $\delta_{max}$  and  $E_{max}$  can result in dramatic changes in

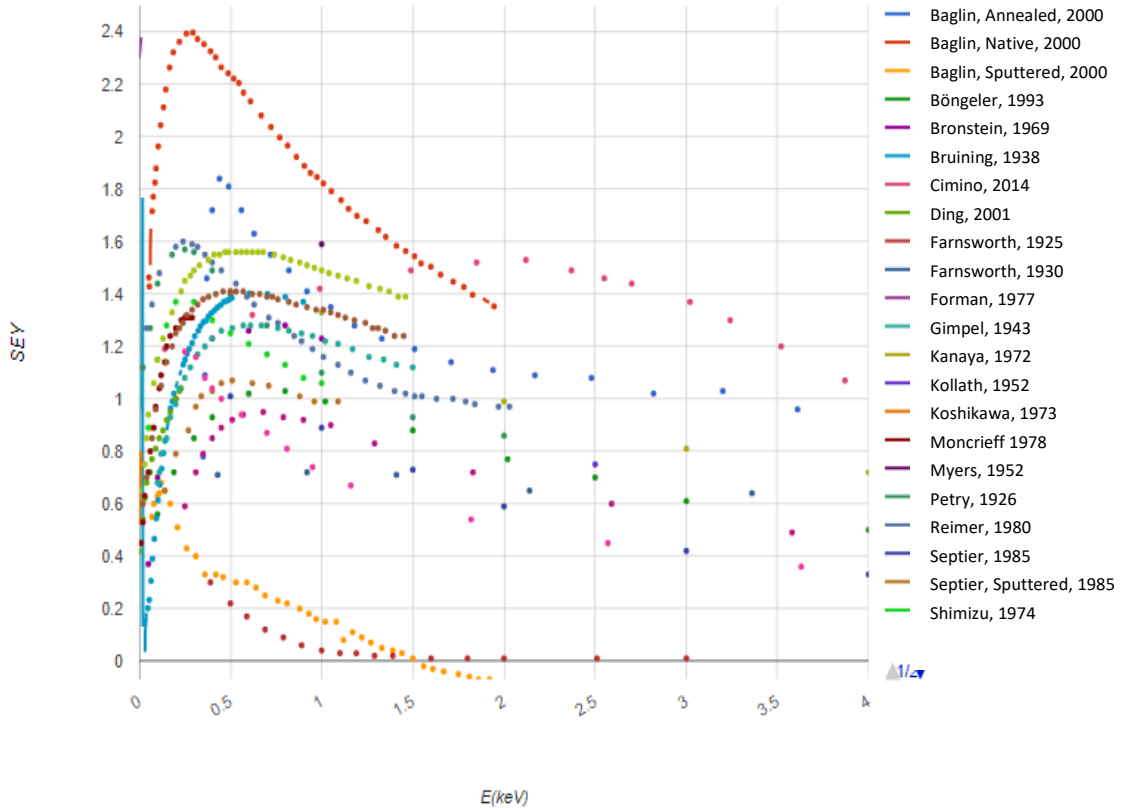


FIG. 2.4. Various Cu SEY measurements as functions of incident electron energy. As reported in the USU SEY Database.

spacecraft potential. For Gold variances in  $\delta_{max}$  of 11% and  $E_{max}$  of 26% result in swings of charge potential from +1.1 eV to -25.8 kilo-electron volts (keV) were witnessed. These swings are characteristic of threshold changing for very specific popular SEY models some of which we will discuss in Section 2.2.2.

## 2.2 Theoretical Foundations

### 2.2.1 Spacecraft Charge Modeling Software

To facilitate spacecraft charge modeling various agencies [e.g., Air Force Research Lab (AFRL), European Space Agency (ESA), Japan Aerospace Exploration Agency (JAXA), and National Aeronautics and Space Administration (NASA)] have devoted significant resources to develop modeling tools for spacecraft charging due to spacecraft interactions with the plasma. These codes require as inputs parameterized information regarding SEY to predict spacecraft charging rates (see Fig. 2.5.).

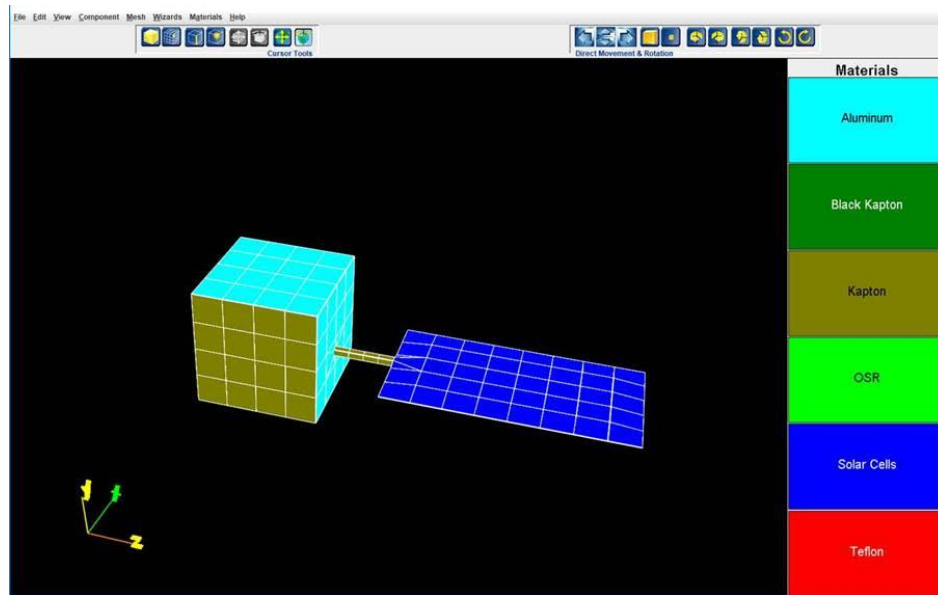


FIG. 2.5. Generic model of a satellite modeled in NASCAP. Visible are various geometries and multiple materials applied to the different geometries.

Initially, the only available spacecraft charging code available was the NASA/Air Force Spacecraft Charging Analysis Program (NASCAP) (Davis and Mandell, 2014; Katz *et al.*, 1977) and an accompanying example materials database. This program received an update in 2011 to become NASCAP-2K (Davis and Mandell, 2014). This update worked some of the bugs out of the system, increased functionality, and made the program more user friendly.

In 1996 the Space Environments and Effects (SEE) Charging Handbook was developed to be a browser-based, preliminary design spacecraft charging analysis tool with updated spacecraft charging models, updated design guidelines and analysis tools, including algorithms on deep dielectric charging, auroral charging, and a 3-D modeling tool (Pearson *et al.*, 1998).

To go along with the SEE Charging Handbook the SEE the Charge Collector database was made to provide a compilation of spacecraft charging-related products offered by NASA's SEE program. Within this collection is a series of data pertaining to materials charging parameters (Davis *et al.*, 2002). An update was made to this compilation in 2005 (Dennison *et al.*, 2005) and a final update was planned for the Charge Collector Database but was never made public due to budgetary constraints.

NASCAP-2k has not been made available outside the U.S. due to export control. For this reason, many international space agencies have seen fit to create their own spacecraft charging databases, many of them based upon the original NASCAP code. The Spacecraft Plasma Interaction System (SPIS) project began in 2000 as an open-source software developed by the European Space Agency (ESA) and maintained by Artenum, Paris (Matéo-Vélez *et al.*, 2012). The Spacecraft Plasma Interactions Network in Europe (SPINE) now maintains it. SPIS is a free program for members of SPINE. Just like NASCAP-2k, it allows users to create or import a 3D model of a spacecraft with specific materials attributed to various pieces of the craft (see Fig. 2.5.). The spacecraft model can be imported into a simulated space environment and charging simulations can be performed.

In 2004 Japan Aerospace Exploration Agency (JAXA), the Japanese equivalent of NASA developed a charging code (Cho *et al.*, 2012) and launched the final version of their software Multi-Utility Spacecraft Charging Analysis Tool (MUSCAT) in March 2007 (Muranaka *et al.*, 2008). The functionality and inputs of MUSCAT are very similar to those of NASCAP (see Section 2.3.2). The functionality and utility of the software were proved by (Cho *et al.*, 2012).

## 2.2.2 SEY Models

When discussing spacecraft charge modeling, there are two different types of charging to consider, surface charging and internal charging. For this thesis, a focus will be placed almost exclusively on surface charging, and leave the discussion of deep dielectric charging and charge propagation through a material to other researchers.

Critical to surface charge modeling is modeling SEY. In the pursuit of SEY modeling, various researchers have developed different parameterized SEY models. We will discuss the advantages and disadvantages of the various models in Section 2.3.2. For now, it is sufficient to note researchers in the USU Material Physics Group (MPG) have developed a 4-parameter semi-empirical reduced power-law SEY model (Wood *et al.*, 2019; Lundgreen and Dennison, 2020). This model is:

$$\frac{\delta(E_0)}{\delta_{max}} = \frac{1}{(1-e^{-r_0})} \cdot \left(\frac{E_0}{E_{max}}\right)^{1-n} \left[1 - e^{-r_0 \left(\frac{E_0}{E_{max}}\right)^{n-m}}\right] \quad (2.2)$$

where  $\delta_{max}$  is the maximum SEY,  $E_{max}$  is the energy at which  $\delta_{max}$  occurs, and  $m$  and  $n$  are power-law

exponents that characterize the SEY at energies well below and well above  $E_{max}$  respectively. Other common SEY models can be expressed as special cases of this 4-parameter reduced power-law model (see Table 2.2.) or a more general 5-parameter variation of the reduced Power Law model as discussed in Section 4.2.

The advantage of this 4-parameter power-law model is the ability to determine the fitting coefficients from experimentally determined values.  $\delta_{max}$ ,  $E_{max}$  are determined through examination of a simple SEY vs. energy graph. While  $n$ ,  $m$  are determined through examination of a reduced SEY vs reduced energy graph. This advantage, as well as methods utilized to determine these parameters, will be discussed further in slightly in the following section, and again more thoroughly in Section 4.3.

### 2.2.3 Material Parameter Inputs Required for Charging Codes

For spacecraft charging software, there are six SEY input parameters required by NASCAP, NASCAP-2K, and SEE Charging Handbook (also for SPIS and MUSCAT). However, only 5 are independent (Lundgreen and Dennison, 2020; Christensen *et al.*, 2018; Diaz-Aguado *et al.*, 2020;

Table 2.2. Comparison between several range and SEY models with their associated coefficients. (Lundgreen and Dennison, 2020)

Model / References	n	m	C <sub>1</sub>	C <sub>2</sub>
Young, 1957	1.35	0	1.114	2.283
Viatskin, 1958	1.4	0	1.1349	2.138
Lane and Zaffarano, 1954	1.66	0	1.24	1.629
Lin and Joy, 2005	1.67	0	1.28	1.614
Burke, 1980	1.725	0	1.284	1.526
Seiler, 1983	1.8	0	1.31	1.45
Whiddington, 1912a	2	0	1.396	1.256
Feldman, 1960	$\frac{n = (1 - e^{r_{max}})}{1 - (1 + r_{max}) \cdot e^{r_{max}}}$		$[1 - e^{-r_{max}}]^{-1}$	$r_{max}$
Sims, 1992	variable	0	$1 - n^{-1} [e^{(r-1)}]$	$x_m = \left(\frac{n-1}{n}\right) [e^{x_m} - 1]$
Variable n	$1 < n < 2$	0	$\left[1 - \exp(1 - n^{-1} [e^{(r-1)}])\right]^{-1}$	
Extended variable n	$1 < n < 2$	$0 < m < 1$		

Dennison *et al.*, 2007). Two of the exponents ( $b_1$ ,  $b_2$ ) are not independent, and thus can be replaced with a single variable. Most of these parameters are not physical constants and cannot be found experimentally, but need to be determined through specific fitting formulas. The inputs of particular interest are maximum SE yield for electron impact ( $\delta_{max}$ ), primary electron energy for  $\delta_{max}$  ( $E_{max}$ ), first coefficient for bi-exponential range law ( $b_1$ ), first power for bi-exponential range law ( $n_1$ ), second coefficient for bi-exponential range law ( $b_2$ ), and second power for bi-exponential range law ( $n_2$ ) (see Table 2.3.).

Maximum SE yield for electron impact ( $\delta_{max}$ ) and primary electron energy for  $\delta_{max}$  ( $E_{max}$ ) are related directly to a yield curve. Figure 2.6. effectively demonstrates the method to determine these two values.  $\delta_{max}$  is the maximum SEY of a material, and  $E_{max}$  is the energy at which that maximum yield can be achieved.  $\delta_{max}$  is unit-less and  $E_{max}$  is measured in keV.

- The first coefficient for bi-exponential range law  $b_1$  is related to the range of an electron, or the depth to which PE will travel with a given initial energy (Mandell *et al.*, 1993). For several SEY models,  $r_{max}$  is assumed constant regardless of material (see Table 2.2.).
- First power for bi-exponential range law,  $n_1$  this input is the power associated with the low energy electron yield (Mandell *et al.*, 1993). It has been found that for low energies the predominant surface condition that will affect yield is contamination (see Section 5.1.1).
- The second coefficient for bi-exponential range law  $b_2$  is related to the material density (Mandell *et al.*, 1993), and as such is directly related to the inelastic mean free path or the mean

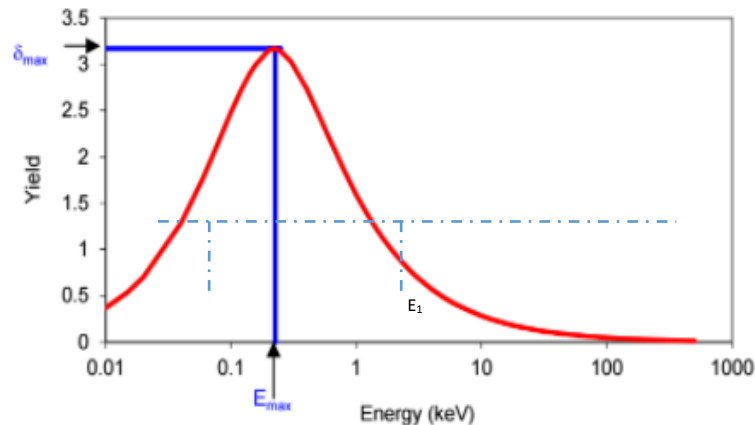


FIG. 2.6. Typical SEY yield curve with key features identified.

Table 2.3. NASCAP materials parameters for copper. As reported by the Space Environments and Effects Charge Collector Database. The red box highlights all the parameters that concern SEY. (Dennison *et al.*, 2003)

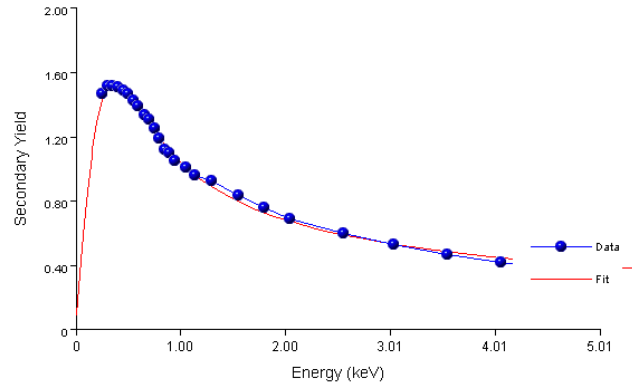
Parameter	Value
[1] Relative dielectric constant; $\epsilon_r$ (Input as 1 for conductors)	1, NA
[2] Dielectric film thickness; d	0 m, NA
[3] Bulk conductivity; $\sigma_b$ (Input as -1 for conductors)	-1; (2.655 $\pm$ 0.004) $\cdot 10^7$ ohm <sup>-1</sup> ·m <sup>-1</sup>
[4] Effective mean atomic number $\langle Z_{eff} \rangle$	16.1 $\pm$ 0.5
[5] Maximum SE yield for electron impact; $\delta_{max}$	2.47 $\pm$ 0.03
[6] Primary electron energy for $\delta_{max}$ ; $E_{max}$	(0.379 $\pm$ 0.012) keV
[7] First coefficient for bi-exponential range law, $b_1$	1 Å, NA
[8] First power for bi-exponential range law, $n_1$	1.73 $\pm$ 0.02
[9] Second coefficient for bi-exponential range law, $b_2$	0 Å
[10] Second power for bi-exponential range law, $n_2$	0
[11] SE yield due to proton impact $\delta^H(1keV)$	1.0882 $\pm$ 0.0007
[12] Incident proton energy for $\delta^H_{max}$ ; $E^H_{max}$	(1000 $\pm$ 250) keV
[13] Photoelectron yield, normally incident sunlight, $j_{pho}$	(4.88 $\pm$ 0.4) $\cdot 10^{-5}$ A <sup>-2</sup> ·m <sup>-2</sup>
[14] Surface resistivity; $\rho_s$ (Input as -1 for conductors)	-1 ohms-square <sup>-1</sup> , NA
[15] Maximum potential before discharge to space; $V_{max}$	10000 V, NA
[16] Maximum surface potential difference before dielectric breakdown discharge; $V_{punch}$	2000 V, NA
[17] Coefficient of radiation-induced conductivity, $\sigma_r$ ; k	0 ohms <sup>-1</sup> ·m <sup>-1</sup> , NA
[18] Power of radiation-induced conductivity, $\sigma_r$ ; $\Delta$	0, NA
[19] Density; $\rho$	(2.702 $\pm$ 0.002) $\cdot 10^3$ kg·m <sup>-3</sup>

travel time an electron experiences as it bounces from atom to atom within a solid.

- Second power for Bi-exponential range law  $n_2$  is believed to be the power associated with higher energy electron yield and so it will be associated with the surface morphology of the sample (i.e. roughness.) (See Section 5.1.2) The other NASCAP inputs are discussed at length in the NASCAP Programmers reference manual (Mandell *et al.*, 1993).

A special note should be made here concerning the NASCAP/ Katz 5 parameter fitting formula.

This formula is notoriously difficult to use when fitting a SEY curve. A tool has been created by Victoria Davis at NASA Marshall Space Flight Center to assist researchers in obtaining the NASCAP fitting parameters associated with a specific dataset (see Fig. 2.7.). The NASCAP-2K Secondary Yield Fitting Tool is mostly automated requiring inputs of specific SEY, energy, and standard deviation of SEY data



DeltaMax	0.5 <	1.5477993625911308	< 10.0
EMax	0.1 <	0.37727191001822524	< 1.0
RC1	0.0 <	0.1628894626774426	< 1.0
RExp1	0.4 <	0.6615000000000001	< 0.8
RC2	1.0 <	1.0	< 1.0
RExp2	1.5 <	1.6016614804352334	< 2.0
Chi-Squared	0.010651653862119245	Plot Fit	

FIG. 2.7. NASCAP-2K Secondary Yield Fitting Tool example. Showing the NASCAP-2K input options available.

values. An automatic fitting algorithm can be tuned to specific user input values of the fitting parameters, and accuracy of fit can be determined by a calculated chi-squared value.

The majority of the different models utilized to model SEY have been reconciled as special cases of the 4-parameter model by (Christensen *et al.*, 2018) (See Table 2.3.). The number of parameters required can characterize each of the various models.

- 1-parameter ( $r$ ) Feldman model which is a special case utilized by NASCAP, SPENVIS, and MUSCAT when nothing is known about the material besides its density and atomic weight, and are used to calculate range (SPENVIS, 2018; Mandell *et al.*, 1993; Standard, 2009; Feldman, 1960).
- 2 parameter ( $\delta_{max}$ ,  $E_{max}$ ) (Young, 1957; Whipple, 1982; Dionne, 1973; Lane and Zaffarano, 1954; Lin and Joy, 2005; Burke, 1980; Reimer and Tollkamp, 1980; Whiddington, 1912b; Terrill, 1923; Bruining and De Boer, 1938; Baroody, 1950; Viatskin, 1958)
- 3 Parameter ( $\delta_{max}$ ,  $E_{max}$ ,  $n$ ), ( $\delta_{max}$ ,  $E_{max}$ , variable  $n$ ) (Sims, 1992; Dennison *et al.*, 2009)
- 4 parameter ( $\delta_{max}$ ,  $E_{max}$ ,  $n$ ,  $m$ ) (Lundgreen and Dennison, 2020)
- 5 parameter ( $\delta_{max}$ ,  $E_{max}$ ,  $b_2/b_1$ ,  $n_1$ ,  $n_2$ ) NASCAP (Katz *et al.*, 1977)

The translation table (Table 2.3.) allows for interchange between any of the different models. More importantly, it allows for translation to be made from any of the models such as the Katz model (which uses parameters not related to physical, measurable, quantities) to the 4 parameter model which has real measurable quantities associated with each of the required parameters (see Section 4.3.2).

### 2.3 Limitations Associated with Historical Databases

Charge collector historical SEY databases already exist. The three most popular databases are Joy (Joy, 1995), NASCAP (Katz *et al.*, 1977), and the SEE Charge Collector Databases (Dennison *et al.*, 2005). These previous database instances each have positive aspects as well as limitations. It was determined that the limitations associated with the various databases were significant enough that the creation of a new database would be more advantageous than trying to repair the issues found in the historical databases.

The limitations associated with the original NASCAP charge-modeling program include a lack of variety in materials selection (see Table 2.4.). This database was intended to allow users to experiment with a few included materials data values, but for serious modeling, users were expected to identify data values from outside sources and input them into the code. In practice, this does not appear to be what has happened. Users of the NASCAP database seem to have largely accepted those values included in

Table 2.4. Materials with charging properties found in the NASCAP database. (Mandell *et al.*, 1977)

Conducting Materials				Spacecraft Materials	
Elemental Metals and Semiconductors	Alloys	Conductive Coatings		Conductors	Conductive coatings
(Amorphous) C	Al Alloy 6061-T6	Aquadag		Carbon Filled Polyester	Al on 2 $\mu\text{m}$ Kapton
Be				Black Kapton	Al on 8 $\mu\text{m}$ Kapton
Cu					Al on 25 $\mu\text{m}$ Kapton with ITO backing
Au					Al on 6.4 $\mu\text{m}$ PET
Ag					Ag/Inconel on 13 $\mu\text{m}$ FEP

NASCAP as gospel and never questioned their veracity, applicability, or provenance (see Section 4.2.1).

This has led to many misrepresentations of spacecraft models. One of the most prevalent misrepresentations has been the use of NASCAP's aluminum SEY value. In a study conducted by Dennison, it was shown that using significantly different yield values for materials in modeling can lead to substantially inaccurate results from charge modeling (Dennison *et al.*, 2007). Dennison showed that surface modifications can and often do lead to dramatic threshold charging effects (Dennison *et al.*, 2007; Chang *et al.*, 2000).

In researching the provenance of the NASCAP aluminum SEY parameter values they were found to originate with a clean, smooth, high purity, elemental sample (Bruining and De Boer, 1938) (see Sections 4.2.1). The significance of this is not immediately apparent unless it is understood that aluminum has a very high rate of oxidation when exposed to atmospheric conditions. Aluminum will develop an oxide layer 40 Å thick in a mere 260 ps. (Campbell *et al.*, 1999). The reported  $\delta_{max}$  value (0.98) appears to be significantly lower than the values found for technical aluminum (2.04-3.80) (Dennison *et al.*, 2007; Copeland, 1935; Baglin *et al.*, 2000; Warnecke, 1936; Walker *et al.*, 2008).

The SEE Charge Collector Database (Wood *et al.*, 2007) and follow-up unpublished updates to the SEE charge collector database (Dennison *et al.*, 2005) were very thorough in reporting information for a handful of materials. The material reports for each material in the database contain all the inputs required for modeling a spacecraft using the NASCAP charging code (see Table 2.3.), as well as information regarding the samples' provenance, surface condition, sample modifications, any instrumentation effects, contamination, and calibration techniques. Most materials reports included a bibliography of tests on similar materials. The SEY and BSEY data included fits to numerous fitting models including the NASCAP models. This plethora of information for each material is extremely useful; however, only sixteen materials had such detailed materials reports created (see Table 2.5.).

The SPENVIS database is based upon the values reported by NASCAP with a few additions that have been made and included by ESA SPINE. Along with those additions, several materials were excluded from the SPENVIS database. One improvement that SPENVIS has made which is of significance is the inclusion of oxidized and pure, elemental aluminum (See Table 2.6.).

Table 2.5. Materials with charging properties found in the SEE database.

Conducting Materials			Spacecraft Materials	
Conductors	Alloys	Conductive Coatings	Conductors	Conductive coatings
Aluminum	Al Alloy 6061-T6	Aquadag (C)	Carbon-filled polyester (Sheldahl Thick Film Black)	Al on 2 $\mu\text{m}$ Kapton (JPL "Solar Sail")
(Amorphous) C			Black Kapton (Sheldahl thermal control blanket)	Al on 8 $\mu\text{m}$ Kapton (Sheldahl thermal control blanket)
Be			Al on 25 $\mu\text{m}$ Kapton with ITO backing (Sheldahl thermal control blanket)	Al on 6.4 $\mu\text{m}$ PET (Sheldahl thermal control blanket)
Cu				Ag/Inconel on 13 $\mu\text{m}$ FEP (Sheldahl thermal control blanket)
Au				
C (HOPG graphite)				
Silver (Ag)				

Table 2.6. Materials with charging properties found in the SPENVIS database. After, EUROPEAN SPACE AGENCIES, 2018

Conducting Materials		Spacecraft Materials	
Elemental Metals and Semiconductors	Alloys	Coatings	Insulators
Ag	Steel	Material coated in (ITO)	Optical solar reflector (Cerium doped glass)
Oxidized Al SEE yields from DERTS		Epoxy resin on carbon Fiber (EPOX)	Optical solar reflector (Cerium doped glass with MgF2 coating)
Al		Non conductive black Paint (Electrodag 501 BLKP)	Kapton average values
Carbon Fiber (CFRP 1)		Non Conductive Black Paint (Herberts 1002)	Teflon DERTS
		Conductive black paint (Electrodag 501 BLKC1)	General Dielectric after 5 years in GEO
		White paint conductive (PCB-Z)	SiO <sub>2</sub>
		White paint PSG conductive (120 FD)	



Table 2.8. Composite materials featured in the Joy database of material Electron-Solid Interactions. These materials will be incorporated into the USU SEY Database in its next iteration.

Bulk Conductors	Bulk Insulators	Conductive coatings	Non-Conductive coatings	Compound Materials
Liquid water	Aclar	Liquid water (200 monolayers on copper)	COAT725 (wafer coat)	
KTCNQ (organic conductor)	Magnesium Oxide (MgO)	Indium Zinc Oxide	Resist (electron beam – PMMA)	Sodium Bromide (NaBr)
Stainless Steel	Copper dioxide (Cu <sub>2</sub> O)	Indium tin oxide (ITO)		KBr (Potassium Bromide)
TCNQ (organic conductor)	Chromium dioxide (Cr <sub>2</sub> O <sub>3</sub> )	PETEOS (organic)		KCl (Potassium Chloride)
Nickel chromide Alloy (NiCr)	Vanadium Pentoxide V <sub>2</sub> O <sub>5</sub>	Interconnect line aluminum		KI (Potassium Iodide)
Aluminum Beryllium Alloy (AlBe)	Alumina (Al <sub>2</sub> O <sub>3</sub> )			Tantalum Carbide (TaC)
	OW133 Spinel aluminum fosterite			Titanium Carbide (TiC)
	OW102 Fosterite			Titanium Nitride (TiN)
	OW137 Fosterite			Zirconium Carbide (ZrC)
	Silicon dioxide SiO <sub>2</sub> (steam formed)			Ammonia Ice (NH <sub>3</sub> )
	Boron Nitride (BN)			Methanol ice (CH <sub>3</sub> OH)
	Diamond (CVD diamond activated with CsI)			Carbon dioxide (“dry”) ice
	Kapton (polymer sheet)			Ice (H <sub>2</sub> O)
	Lucite (polymer sheet)			
	Nylon (polymer solid)			
	Polyethylene (polymer solid)			
	Polyurethane (polymer solid)			
	Teflon (polymer solid)			
	Di-Phenyl (C <sub>12</sub> H <sub>10</sub> )			
	Mylar (polymer sheet)			
	Anthracene (C <sub>14</sub> H <sub>10</sub> )			
	Xylene (organic solid)			
	Phenanthrene			
	Napthalene (C <sub>10</sub> H <sub>8</sub> )			

the data found in original journal articles have been identified. As an example compare Joy SEY reportings for Cu with original data reported by Bronstein, Warnecke, and Wittry (Wittry, 1966; Warnecke, 1936; Bronstein *et al.*, 1969). Lack of information regarding experiment procedures or material provenance is another issue concerning accurate modeling when using this database.

Historical databases lack specific spacecraft materials and new (since 2000) materials. Sometimes tabulated values are extracted from sources that are not fully documented. Even when specific references are cited, in many instances the sources are difficult to locate, do not provide necessary information to identify details about the materials studied, or do not reflect the nature of specific composition or surface modifications appropriate to spacecraft applications. As an example, consider the values of  $\delta_{max}$  and  $E_{max}$

for Al in the default NASCAP database (Mandell et al., 1977). These values are not well documented and appear to be significantly lower than many other SEY values for Al.

#### 2.4 Origination of NASCAP Aluminum Values

Table 2.9. lists the SEY parameters in the default materials database for five elemental conductors, three bulk insulating materials, and five spacecraft materials; these values are also included with current versions of SPENVIS and MUSCAT charging codes. The entries in the default material database in Table 2.9. are certainly severely limited in terms of the number of tabulated common spacecraft materials and do not contain novel designer materials or materials used for more demanding mission requirements.

In examining the values purported by the NASCAP database (Table 2.9.) it was found that no one in the spacecraft charging industry knew the origin for the Aluminum SEY value. For this reason, it is of value to include a brief section highlighting the provenance of the data, as we were able to determine it.

Mandell (1977) in his NASCAP overview and Katz (1977) in the NASCAP database both cited

Table 2.9. SEY parameters in the default materials database included with NASCAP (Mandell, 1993).

Material	$\delta_{max}$	$E_{max}$ (keV)	$b_1$ (Å)	$n_1$	$b_2$ (Å)	$n_2$
<b>Bulk Elemental Conductors</b>						
Aluminum (Al)	0.970	0.300	154	0.800	2200	1.76
*Aquadag (colloidal graphite, C)	1.00	0.300	374*	1.55*	2	12.0
Gold (Au)	0.880	0.800	88.8	0.920	53.50	1.73
*Magnesium (Mg)	0.920	0.250	399*	1.75*	1.74	24.3
Silver (Ag)	1.00	0.800	84.5	0.82	79.4	1.74
<b>Bulk Insulators</b>						
Kapton <sup>TM</sup>	2.10	0.150	71.5	0.600	312	1.77
Teflon <sup>TM</sup>	3.00	0.300	45.4	0.400	218	1.77
SiO <sub>2</sub>	2.40	0.400	116	0.81	183	1.86
<b>Spacecraft Materials</b>						
Conductive Paint	2.10	0.150	71.5	0.600	312	1.77
*Nonconductive Paint	2.10	0.150	55.6*	1.56*	1.05	0.98
Solar Cell with Coverglass	2.05	0.410	77.5	0.450	156	1.73
*Indium Tin Oxide (ITO) Coating	1.400	0.800	23.6*	2.29*	7.18	55.5
Screen (absorber)	0	1	10	1.5	0	1.0

Dekker and Van der Ziel (1958) as the source for the fitting parameters  $\delta_{max}$  and  $E_{max}$ . Within Dekker was found a plot of  $\delta_{max}$  versus work function ( $\Phi$ ) (See Fig. 3.2.). We traced this plot back to two different plots from Baroody (1950). One of the plots showed a reduced yield curve  $\delta/\delta_{max}$  versus  $E/E_{max}$  and another of  $\delta$  versus work function  $\Phi$ . Using these two plots in conjunction we were able to tease  $\delta_{max}$  out however  $E_{max}$  was left unknown. Baroody was not the originator of the data and it was found that he cited Bruining and De Boer (1938) (See Fig. 2.8.)<sup>1</sup>. Bruining does list his original data once again for  $\delta/\delta_{max}$  versus  $E/E_{max}$  and  $\delta_{max}$  vs  $W$  but does not include information on  $E_{max}$ . This dataset is for “Secondary electron emission of (an) aluminum layer deposited by sublimation in a vacuum” (Bruining and De Boer, 1938). While specifics of surface roughness, oxidation, and contamination are unknown and quite suspect given the use of vintage diffusion and getter pumps and glass vacuum systems the data appears to agree with modern elementally smooth samples (Walker *et al.*, 2008).

A cursory, though by no means exhaustive, investigation of recent studies returned a substantial list of references, which assumed the NASCAP default values for Al were appropriate for their spacecraft modeling (Hughes and Schaub, 2018; Schmidl *et al.*, 2018; Wolfley, 2018; Bengtson *et al.*, 2019; Pandya *et al.*, 2019; Wang *et al.*, 2017; Davis and Dennison, 1997; Marchand and Lira, 2017). It is significant to note that this ambiguity for Al has also been propagated by other international charging codes, including MUSCAT (Nakamura *et al.*, 2018) and SPENVIS (2018). A newer SPENVIS materials database does include a technical Al material, with a rougher more oxidized surface (Drolshagen, 1994).

## 2.5 The Need for a Better Database

During an analysis of one of the first iterations of an internal charging simulation tool NUMIT (Numerical Iteration) Insoo Jun, the current NASA administrator of NUMIT, expressed the desire for a more diverse material charging database (Jun *et al.*, 2008). There has been a variety of calls besides that one, however. From 2000 through 2006, the USU, MPG was contracted to develop the original SEE

---

<sup>1</sup> "Reprinted (figure) with permission from Baroody, E. Physical Review, 78, 6, 1950 Copyright (2020) by the American Physical Society (See Appendix C).  
<https://journals.aps.org/pr/abstract/10.1103/PhysRev.78.780>

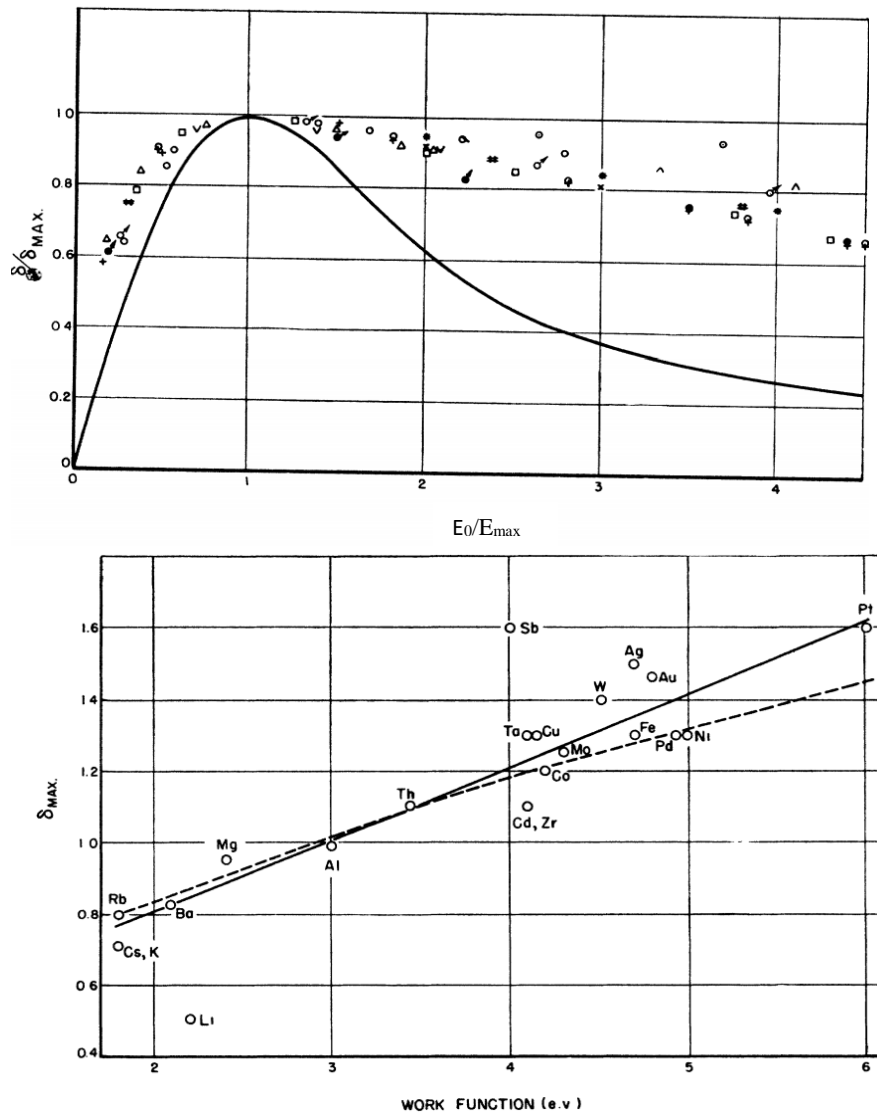


FIG. 2.8. Historical plots of reduced SEY. Plots as taken from Baroody (1950). Showing (a) reduced yield ( $\delta/\delta_{max}$ ) versus reduced Energy ( $E_0/E_{max}$ ) and (b) maximum yield ( $\delta_{max}$ ) versus work function ( $\Phi$ ).

charging database for the SEE Charge Collector Database (Dennison *et al.*, 2005; Dennison *et al.*, 2003). Katz, the originator of NASCAP stated that two things, in particular, are critical to giving good spacecraft potential predictions, “knowledge of both material properties and the ambient environment for both high and low energies” (Katz *et al.*, 1986). Linda Parker echoed these sentiments stating that spacecraft charge modeling requires, “knowledge of the fundamental physical and electrical properties of the materials exposed to the space environment” (Parker and Minow, 2018).

In his 2012 IEEE paper, Dale Fergusson echoed the need for good spacecraft charging theories to be grounded in good data: “Better theories are needed, which must be grounded in measurements. If you are modeling spacecraft charging, GIGO (garbage in – garbage out) still applies, no matter how good your model is,” (Ferguson, 2012). The goal of this work is to create the “more diverse” material-charging database that makes accessible to researchers the inputs required (Table 2.10.) for more accurate spacecraft charge modeling and to take data that has historically been categorized as “garbage” and find new value in it.

Table 2.10. Spacecraft charging and transport code input requirements.

Materials Properties	Terms	Spacecraft Charging Codes				Charge Transport Codes		
		NASCAP / NASCAP-2E / NASCAP-GEO [Karr 1977]	SEE Spacecraft Charging Handbook [Electr-A 2011]	SPENVIS [Rodgers 1999]	MSCAT [Standard 2012]	DICTAT [Rodgers 1999]	NUMITT [Jun 2008]	USU Range Tool [Whose 2019]
Basic Materials Properties	Stoichiometry	-	-	-	-	-	-	Chemical Formula (Param. # 2)
	Mean atomic number	-	-	-	-	-	-	Avg. atomic number (Z <sub>A</sub> ) [unitless] (Param. # 5)
	Mean atomic weight	-	-	Atomic weight Parameter 18	-	-	-	Avg. Atomic Weight (MA) Atmu (Param. # 5)
	Density	Density (ρ) [g cm <sup>-3</sup> ] (Param. # 19)	Density (ρ) [g cm <sup>-3</sup> ]	Density (ρ) [g cm <sup>-3</sup> ] (Param. # 8)	-	Density (ρ) [g cm <sup>-3</sup> ] (Param. # 3)	Dielectric's ρ density (ρ) [g cm <sup>-3</sup> ] (Param. # 7)	Material Density (ρ <sub>M</sub> ) [g cm <sup>-3</sup> ] (Param. # 4)
	Surface Roughness	-	-	-	-	-	-	-
	Dielectric film thickness	Dielectric Film Thickness (d) [m] (Param. # 2)	-	Thickness (d) [m] (Param. # 2)	Implied through Grant	Thickness (d) [m] (Param. # 1)	Dielectric thickness (d) [m] (Param. # 3)	-
	Number of layers	-	-	-	Implied through Grant	-	-	-
	Band Gap	-	-	-	-	-	-	Band Gap (E <sub>g</sub> ) eV (Param. # 7)
	Effective number of Valence Electrons	-	-	-	-	-	-	Effective number of valence electrons (N <sub>v</sub> ) [unitless] (Param. # 6)

Table 2.10. (Continued)

Materials Properties	Terms	Spacecraft Charging Codes					Charge Transport Codes			
		NASCAP / NASCAP-2E / NASCAP-GEO [Karr 1977]	SEE Spacecraft Charging Handbook [Electr-A 2011]	SPENVIS [Rodgers 1999]	MUSCAT [Standard 2012]	DICTAT [Rodgers 1999]	NUMINT [Fun 2008]	USU Range Tool [Wholen 2019]		
<b>Electron Emission</b>										
Photo-emission	Ion Induced Emission	BSEY	<b>Secondary Electron Yield</b>							
			Energy loss power (Sum SEY formula)	-	-	-	-	-	-	-
	SE yield due to proton impact at 1 keV	Effective atom atomic number (Z <sub>eff</sub> ) [unitless] (Param. # 4)	-	-	Atomic Number [unitless] (Param. # 4)	-	-	-	-	
	Incident proton energy at max. ion yield	SE yield due to proton impact (1keV) (S <sub>0</sub> ) [unitless] (Param. # 11)	-	-	SEE yield for 1keV protons [unitless] (Param. # 9)	-	-	-	-	
	Photoelectron yield, Normally incident sunlight (j <sub>max</sub> ) [A m <sup>-2</sup> ] (Param. # 13)	Incident Proton Energy at θ <sup>R</sup> <sub>max</sub> (E <sup>R</sup> <sub>max</sub> ) [keV] (Param. # 12)	-	-	Proton energy for max. SEE yield [keV] (Param. # 10)	-	-	-	-	
	Photoelectron yield, Normally incident sunlight (j <sub>max</sub> ) [A m <sup>-2</sup> ] (Param. # 13)	Photoelectric Current (j <sub>max</sub> ) [A m <sup>-2</sup> ] (Param. # 7)	-	-	Photoelectric current [A m <sup>-2</sup> ] (Param. # 11)	-	-	-	-	
	Photoelectron yield, Normally incident sunlight (j <sub>max</sub> ) [A m <sup>-2</sup> ] (Param. # 13)	Photoelectric Current (j <sub>max</sub> ) [A m <sup>-2</sup> ] (Param. # 7)	-	-	Photoelectric current [A m <sup>-2</sup> ] (Param. # 11)	-	-	-	-	

Table 2.10: (Continued)

Materials Properties	Terms	Spacecraft Charging Codes					Charge Transport Codes		
		NASCAP / NASCAP-2k / NASCAP-GEO [Katz 1977]	SEE Spacecraft Charging Handbook [Hecce-A 2011]	SPENVIS [Rodgers 1999]	MUSCAT [Sisander 2012]	DICTAT [Rodgers 1999]	NUMITT [Jua 2005]	USU Range Tool [Wilson 2019]	
Electron Transport	Relative permittivity (Dielectric Const)	Relative Dielectric Constant (a) [unitless] (Param. # 1)	-	Relative Permittivity - (Param. # 1)	Specific dielectric constant - (Param. # 4)	Dielectric constant - (Param. # 5)	Dielectric permittivity at 300°K (E) [F/m] (Param. # 6)	-	
	Bulk (Dark Current) Conductivity	Bulk Conductivity (a,b) [ $10^{-14} \text{ m}^{-1}$ ] (Param. # 3)	-	Conductivity - [ $10^{-14} \text{ m}^{-1}$ ] (Param. # 3)	-	Conductivity - [ $10^{-14} \text{ m}^{-1}$ ] (Param. # 4)	Dark Conductivity (G <sub>dark</sub> ) [ $10^{-14} \text{ m}^{-1}$ ] (Param. # 8)	-	
	Surface resistivity	Surface Resistivity (a,b) [ $\Omega \text{ cm}^{-1}$ ] (Param. # 14)	-	Surface resistivity (not used) - [ $\Omega \text{ cm}^{-1}$ ] (Param. # 12)	volume Resistivity - (Param. # 2)	-	-	-	
	Coefficient of RIC	Coefficient of Radiation induced Conductivity (a) [ $10^{-16} \text{ m}^{-1} \text{ rad}^{-1} \text{ s}^{-1}$ ] (Param. # 17)	-	-	RIC - (Param. # 3)	RIC dose rate factor (k <sub>d</sub> ) - (Param. # 7)	RIC k <sub>d</sub> [ $10^{-16} \text{ m}^{-1} \text{ rad}^{-1} \text{ s}^{-1}$ ] (Param. # 9)	-	
	Power of RIC	Power of Radiation-Induced Conductivity (a) [unitless] (Param. # 18)	-	-	-	Delta - (Param. # 8)	-	-	
Electrostatic Discharge	Dielectric Breakdown Potential	Max. surface potential difference before dielectric breakdown discharge V <sub>max</sub> [V] (Param. # 16)	-	-	Discharge generating threshold - (Param. # 5)	Breakdown electric field - [ $\text{V} \text{ m}^{-1}$ ] (Param. # 6)	-	-	
	Breakdown potential to space	Max. potential before discharge to space V <sub>max</sub> [V] (Param. # 15)	-	-	-	-	-	-	
Optical Properties	Absorptivity, $\alpha$	-	-	-	-	-	-	-	
	Emissivity, $\epsilon$	-	-	-	-	-	-	-	
	Reflectivity, R( $\lambda$ )	-	-	-	-	-	-	-	
	Photomission spectrum, $I_{\text{photo}}(\lambda)$	NASCAP-2k can input a four parameter fit to $I_{\text{photo}}(\lambda)$ or a tabulated spectrum							

## CHAPTER 3

## DEVELOPMENT OF DATABASE

It was determined that bringing together a large number of data sources, categorizing them, and analyzing them based on similar study characteristics would be useful in facilitating comparison through plots and tables. This has certainly yielded new and interesting physics, engineering guidelines, and trends in parameters and surface characteristics. The number of variables pertaining to materials preparation and experimental methods associated with specific SEY measurements is frequently large. This can prevent reaching a satisfactory agreement between datasets. However, it is possible to identify trends with a high degree of certainty by comparing multiple datasets (see Fig. 3.1.). In examining SEY for common elemental metals and qualifying data based upon surface characteristics, trends became obvious for  $\delta_{max}$  and  $E_{max}$  values.

## 3.1 Data Acquisition

We began developing the USU SEY Database by acquiring and logging the previously mentioned historical databases and merging them. Once again, the three most useful SEY databases available were the

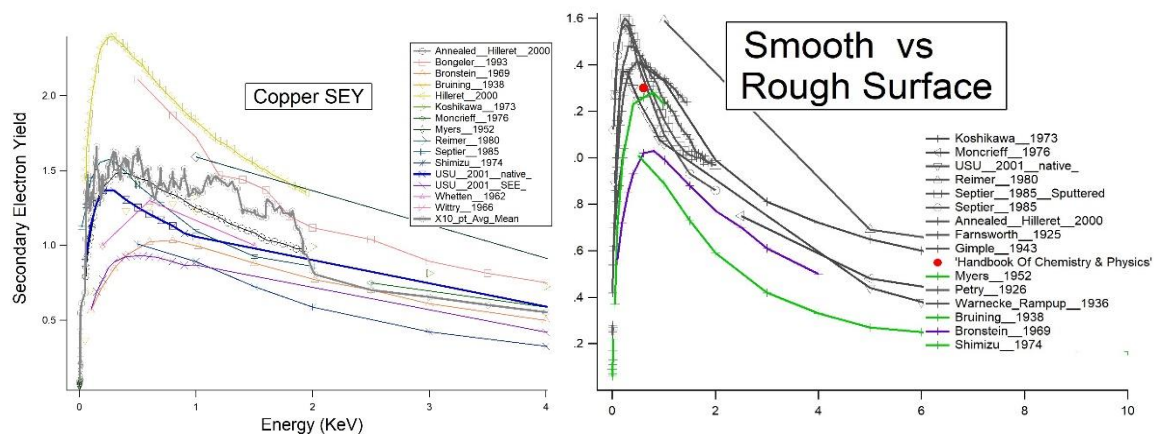


FIG. 3.1. A pair of SEY plots. Show (left) general Al SEY data and (right) the same data qualified. Clean (green), Oxidized (grey), default NASCAP (purple) values are shown. This process allows for trends associated with surface conditions to be pulled from the data.

Joy database (Joy, 1995), the SEE Charge Collector databases (Davis *et al.*, 2002), and the NASCAP database (Mandell *et al.*, 1977). Several different techniques were used to acquire these data. To flesh out these datasets, the origin of the reported data were located, verified, and any information regarding surface characteristics were uploaded to the USU SEY Database.

For each given material, data from the Joy database was acquired and matched with the digitized data reference. These digitized datasets for each reference are stored on an *Excel* worksheet for each material. This was done to facilitate future data references, as well as SEY curve fitting. Along with the expected SEY and E values specific information was collected with regards to surface characteristics, and data collection practices (see Section 3.2.1). The totality of SEY data from the SEE Charge Collector database was transferred directly into the Excel datasheet. The NASCAP fitting parameter values and original data from associated references were extracted directly from the NASCAP code. The NASCAP Programmers manual did not include full datasets.

Additional data has subsequently been collected from other published sources after combining the existing databases. When available, data regarding SEY values, information regarding the surface conditions, and the methods used to prepare the sample before SEY testing were also extracted from these new sources. The primary program used to acquire data from these various journals and texts was a *Java* Applet called *Datathief* (Tummers, 2006). *Datathief* allows screen-based capture of scanned plot images of both data points and data curves. Flower (2016) verified the effectiveness and accuracy of this program and found a correlation coefficient ( $r=0.999$ ).

While the total data imported into the database is by no means exhaustive, as of April 2020, it does contain data from over 90 different sources and over 4,000 thousand data points. Often those sources have data for more than one material or surface condition. As of April 2020, the USU database has data for 54 different elements (see Table 2.7.). A focus of ongoing work is to extend both the number of individual SEY data sets and the list of materials for which the database has entries.

### 3.2 Analysis and Qualification of Surface Conditions

As noted in Fig. 3.2, surface conditions are found to affect SEY curves and cause a nontrivial variance in the wide range of SEY values found for a known material. The surface conditions for each of the data sets were determined by analyzing the background information presented in each of the data's original papers. This was done to facilitate more accurate modeling of materials in the various charging codes. For example, using clean smooth elemental Al in place of rough, oxidized, contaminated technical Al can lead to lower predictions for charge modeling (Baglin *et al.*, 2000) (see Section 2.4).

Dennison *et al.*, (2007) performed trade studies of the effects of changing yields on the charging of hypothetical idealized spacecraft in representative space environments. They studied the evolution of SEY

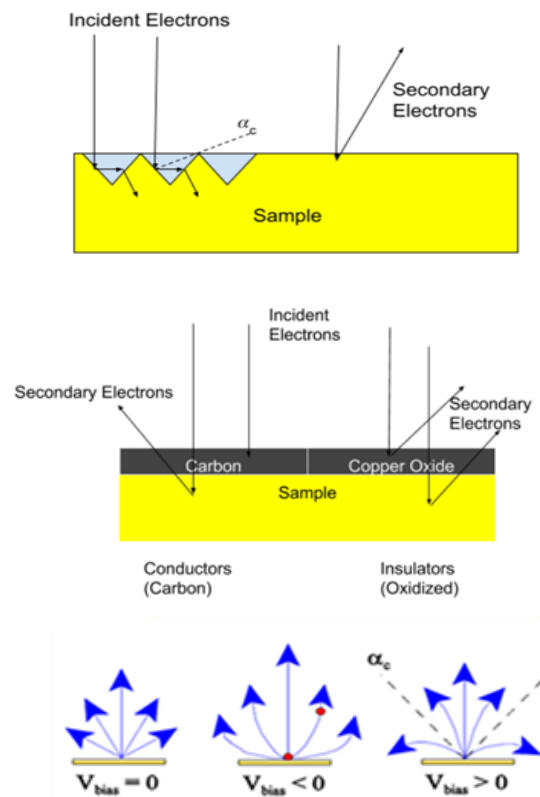


FIG. 3.2. The three main surface characteristics which affect SEY. Surface morphology (a), Surface contamination (b), and Surface Bias (c).

measurements of oxidized Al, clean Al, and carbon-contaminated Al (Davies and Dennison, 1997) as well as clean Au and carbon-contaminated Au (Chang *et al.*, 2000); they found that surface modification led to changes in SEY and potentially lead to dramatic threshold charging effects (Bergeret *et al.*, 1985; Dennison *et al.*, 2007; Chang *et al.*, 2000). For this reason, data collected for this database has been analyzed and qualified based upon surface conditions.

### 3.2.1 Contamination/Oxidation

For lower energies, surface contaminants have the highest effect on SEY (see Fig. 3.2.(b)). This is a rather simple concept as the kinetic energy of an incident electron is related directly to the maximum range that an electron can penetrate a material (R), at higher incident energies the range follows a simple power-law with energy (Reimer and Tollkamp, 1980; Wilson *et al.*, 2018b),

$$R(E_0; b, n) = bE_0^n \quad (3.1)$$

where  $n$  is a static exponential fitting parameter common to SEY charge modeling (see Section 4.3.2), and  $b$  is a constant that is related to material density. Lower energy electrons do not have sufficient energy to penetrate a contaminant layer and will, in essence, only see the contaminant, and not the bulk material. This is significant as various contamination levels can have vastly different effects upon range values Fig. 3.3. showcases the readily apparent differences in range values. Aluminum has a much lower range for energies <100 eV but has a larger range for energies >100 eV.

Wilson *et al.*, (2018a) provides examples for studies of thin graphitic carbon films on Au and tin Au films on HOPG graphite. Here the low energy SEY is dominated by the coating material and high energy SEY is dominated by the bulk substrate. Wilson found the transition energy from domination by coating to domination of substrate increases with increasing coating thickness.

To differentiate contamination values each data set was tagged as either “Clean,” “Contaminated,” “Oxidized,” or “Unknown.” The contamination level and species determination were reliant completely on the author-reported material background and knowledge of technologies that were in use by researchers at the time of data acquisition.

Some examples of phrases used to classify a “clean” sample are:

- “progressive heating to 650° C, maintained for 1 hour” (Warnecke, 1936)
- “Ion cleaned sample” (Walker *et al.*, 2008)

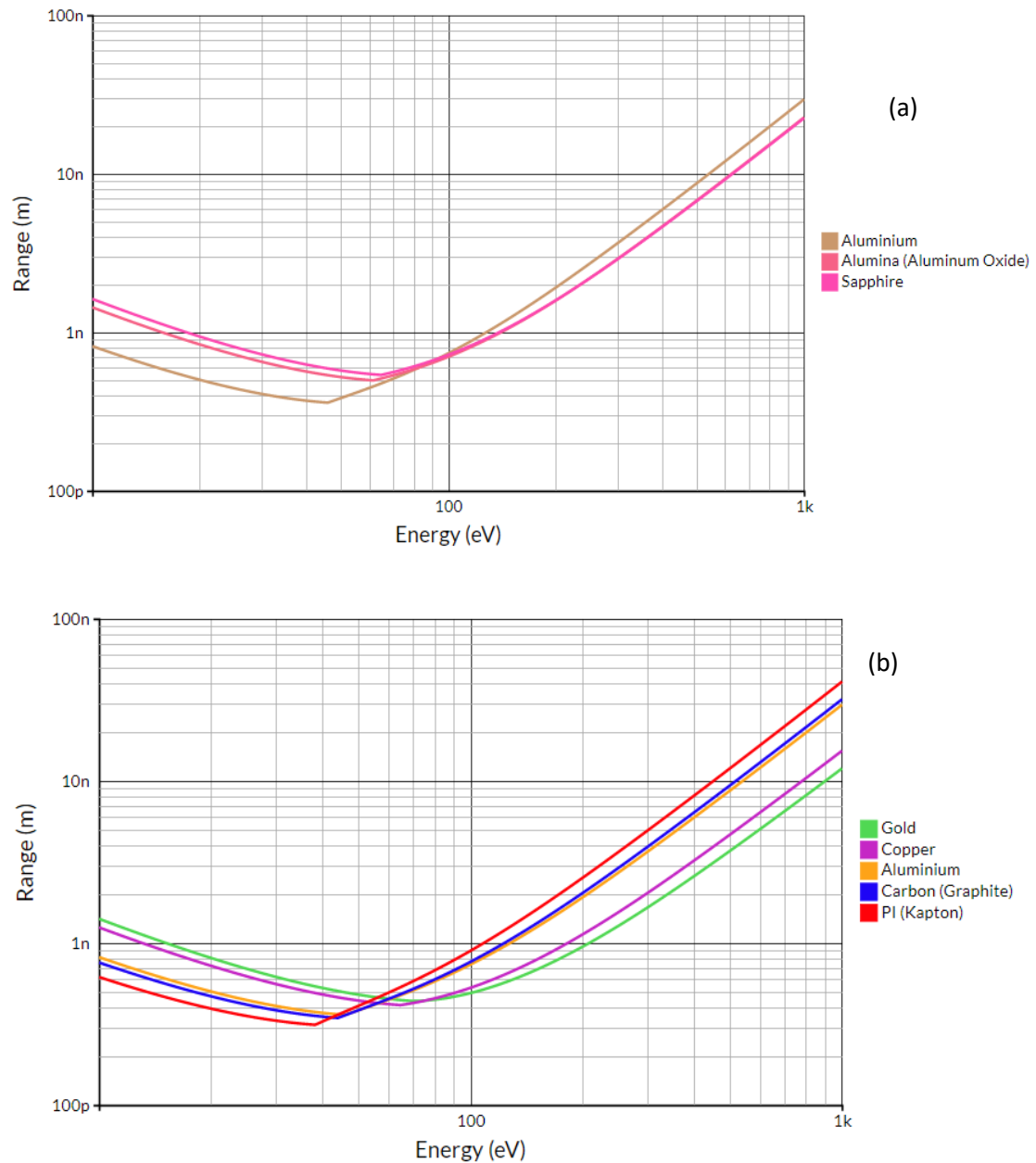


FIG. 3.3. Range versus energy plot for (a) different species of aluminum samples and (b) common spacecraft materials. Variance in minimum range and the energy associated with it is readily apparent when comparing aluminum samples with its various oxides. Plot generated with Electron Range Approximation Tool (Wilson, 2019).

- “...cleaning of the samples was done with argon ion bombardment” (Koshikawa and Shimizu, 1973)
- “Samples are mechanically polished, degreased, rinsed in deionized water and methanol, and then introduced wet in UHV” (Bergeret *et al.*, 1985)

Annealed materials may or may not be elementally clean. The cleanliness of an annealed sample depends upon the sample reaching a critical temperature for a sufficient duration of time. For example, annealed Cu samples are “clean” if the sample maintains a temperature of approximately 673 °C for at least an hour. Studies have shown that this combination of time and temperature have driven off enough of the oxide layer that XAES cannot detect it (Lee *et al.*, 2003). Phrases such as those used by Wood and Bergeret may not necessarily mean that a sample was clean on an atomic level and may have introduced uncertainty into material characterization values.

Some examples of phrases used to classify a “contaminated” sample are:

- “It was found that this gun was affected by the presence of contaminating layers on the electrodes” (Myers and Gwinn, 1952; Baroody, 1950)
- “as inserted” (Warnecke, 1936; Walker *et al.*, 2008)
- “...which shows the variation of the S.E.Y. measured for a copper sample in the as-received state” (Baglin *et al.*, 2000)
- “(The sample) is made of pure copper deposited electrolytically on a lead core. The core is melted away later.” (Gimpel and Richardson, 1943)
- “Thin films of aluminum were prepared by rapid evaporation... onto nitrocellulose films which were subsequently baked away in air” (Kanter, 1961)
- “pumped by diffusion pumps containing oil” (Darlington and Cosslett, 1972; Farnsworth, 1925)

Samples reported, “as received” or “as inserted” were classified as contaminated. As received samples come with several unknowns concerning surface conditions. To err on the side of caution, we labeled each of these samples as contaminated unless explicit information about cleaning procedures was

given within the text. Samples deposited on a substrate that is later heated until it “burns off” were also assumed contaminated. Perfect combustion of the substrate while ideal is often not likely. The residual substrate should have minimal effects; however, for low energies, the presence of contaminants could still have an effect. Another situation that prompts an assumption of contamination is the use of an oil diffusion pump (Sternglass, 1954). Indeed, most studies before the mid-1960s used diffusion pumps, leading to contamination (Goto and Ishikawa, 1968). Many vacuum systems from before the 1950’s used glass vacuum systems which outgassed heavily leading to contaminated samples (Starke, 1898; Swinton, 1899; Goto and Ishikawa, 1968). The use of getter pumps sealed in glass vacuum systems operated with great care were an exception to oil vapor contamination and lead to exceptional studies of elementally clean vapor-deposited films (Bronstein *et al.* 1969).

Some researchers have qualified their data with the source of the contaminant. Oxygen and carbon are the most commonly reported contaminant; however, more often than not the source of contaminants was not made known to the reader. A few studies have used Auger spectroscopy or photoemission spectroscopy to determine contamination species and occasionally even contamination thickness (Dennison *et al.*, 2016; Chang *et al.*, 2000)

A study on the contamination encountered by the Columbia Orbiter was carried out by Spacelab-1 (Miller, 1984). This study was able to collect contaminants associated with LEO as well as the contaminants associated with spacecraft outgassing. Utilizing an onboard scanning electron microscope (SEM), equipped with energy dispersive x-ray (EDX) analysis capabilities, an elemental analysis was performed. Elemental analysis returned a list of present elements (see Fig. 3.4.). However, because SEM cannot easily detect low *z* elements, SEM verification of contamination by C, O, and H was not possible. (Note: newer SEMs can detect elements down to beryllium on the periodic table.) While they are not included in the list, they are still very important to understand as films of hydrocarbon and oxygen have been found coated on craft in orbit (Silverman, 1995; Taylor *et al.*, 2020).

Aluminum and other materials with fast oxidation rates will negate any attempt made to clean them if exposed to the atmosphere. Aluminum can achieve an oxide layer of 33 Å after 260 ps of

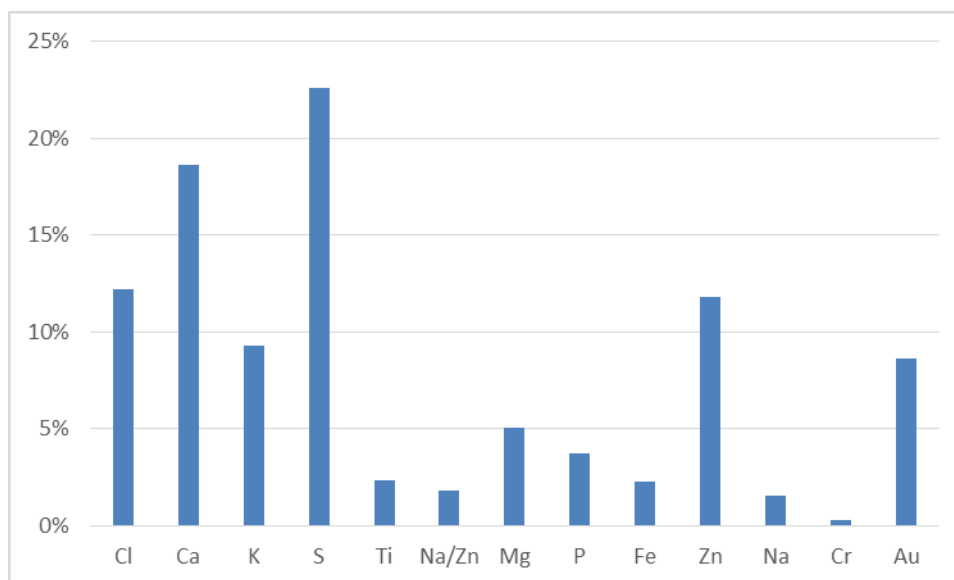


FIG. 3.4. Aggregate mole fraction of contaminants detected by the Columbia Orbiter. Due to the nature of SEM the Low Z atoms (C, Al, and Si) are not available in the Total Aggregate Mole Fraction. After (Miller, 1984)

atmospheric exposure (Campbell *et al.*, 1999), which can skew SEY values at low energies (Walker *et al.*, 2008).

Wilson provided examples for studies of thin graphitic carbon films on Au and thin Au films on HOPG graphite (Wilson *et al.*, 2018b). Here the low energy SEY is dominated by the coating material and high energy SEY is dominated by the substrate. The transition energy from domination by coating vs substrate increases with increasing coating thickness (Wood *et al.*, 2019). An example of this can be seen when comparing highly oxidized aluminum samples to a sapphire ( $\text{Al}_2\text{O}_3$ ) sample in Fig. 3.1.. For low energy, the highly oxidized aluminum appears to behave exactly as sapphire, but as energy and penetration depth increase the oxidized aluminum behaves more like bulk aluminum and less like sapphire.

### 3.2.2 Surface Morphology (Roughness)

Morphology or surface roughness can have serious effects on SEY values (see Fig. 3.2.a.). Roughened surface conditions typically lead to lower SEY values and thus facilitate charging (Reimer and Tollkamp, 1980; Baglin *et al.*, 2000; Olano *et al.*, 2017). Surfaces with less extreme morphology, here

categorized as smooth, typically increase SEY and decrease charge. Studies that contained rough surfaces or sputtered without annealing are classified as rough. Some examples of phrases used to classify a “smooth” surface:

- “Fine polishing was done using successive treatments of 3 $\mu$ m, 1 $\mu$ m and .25 $\mu$ m water-based diamond polishing compound” (Wood *et al.*, 2007)
- “...sample was electrolytically polished (Koshikawa and Shimizu, 1973)
- “annealed” (for low-enthalpy of formation oxides) (Warnecke, 1936; Farnsworth and Goerke, 1930)
- “formed by evaporation of the metal on to a suitable substrate” (Myers and Gwinn, 1952; Gimpel and Richardson, 1943)

Some examples of phrases used to classify a “rough” surface:

- “argon ion beam sputter texturing has been shown to effectively reduce secondary electron emission” (Wintucky *et al.*, 1981)
- “as received” (Baglin *et al.*, 2000; Bruining and De Boer, 1938)
- “mechanically polished” (Bergeret *et al.*, 1985)
- “1 mm diameter hole, 5 mm deep was drilled in the center of each to form a Faraday cage” (Moncrieff 1978)
- “pumped by diffusion pumps containing oil” (Farnsworth, 1925; Darlington and Cosslett, 1972; Shapiro and Hanyok, 1968)

Myers (1952) states: “A difficulty arising out of the use of evaporated metal is the uncertainty in the structure of the film” for this reason certain specific samples which were vapor-deposited and not annealed at sufficient temperature with sufficient time to allow for surface morphology extrema to decrease were categorized as rough. Au, Al, and Cu tend to be smooth when evaporated onto a surface, Si W, Mo, and Ni can form dendritic structures (or “whiskers”) which are very high aspect ratio growths (Voigt *et al.*, 2003; Shen *et al.*, 2000; Bilgin *et al.*, 2015; Grimmer *et al.*, 1978). In most cases, subsequent high-temperature annealing gives a smoother surface. Carbon nanotube forests are an example of extreme

dendritic surfaces. However, C bonds are very strong so even high-temperature annealing will not change this.

A drilled Faraday cup, as used by Moncrieff, used as an electron collector is essentially an artificial delta function concerning electron capture if the beam width is less than the diameter of the hole. A beam width greater than the diameter of the Faraday cup will have extreme edge effects from the sides of the Faraday cup. Also, the smoothness of the hole is unknown with the smoothness of the base and sides of the Faraday cup depends on the drilling techniques used (Chen *et al.*, 2002).

Materials heated to a critical temperature and then allowed to cool back down (a process referred to as annealing) can provide a smoother surface (Raoufi *et al.*, 2007). High energy ion bombardment over time can lead to the formation of ripple-like features in the surface of a material thus leading to a classification of “rough” (Cuerno *et al.*, 1995). If the sample is annealed at sufficient temperature for sufficient time after ion bombardment these ripple features, can be attenuated if however, annealing does not occur after intense ion bombardment a surface will remain rough. The primary purpose of ion bombardment is to liberate contaminants from the sample. It is also possible, however, that for very high energy the bombarding ion may be embedded in the sample. Bonds for atoms on rough surface features can be broken by sputtering and these atoms can subsequently preferentially fall into the valleys, therefore smoothing the surface. Contamination of samples can occur in clumps, thin films, or even high aspect ratio structures (Ichinokawa *et al.*, 1985; Vladár *et al.*, 2008; Vladár *et al.*, 2001). It is very difficult to determine a definite morphology of a contaminated surface without examining it under a microscope to determine the bonding strength and directionality of deposited layers along with the mobility of the deposited atoms over the surface. For this reason, we assume that an *in situ* contaminated sample has a roughened surface due to the possible irregularity of the contaminant deposition.

The surface of a spacecraft will change, as the space environment acts upon it, and those changes should be taken into account when modeling (Chang *et al.*, 2000) (see Section 4.3.2). We have qualified the SEY data specifically so that the surface effects of data can be used to better mimic the environmental effects that a proposed spacecraft will experience. A technique to quantify these surface conditions is discussed later in Section 4.3.2.

### 3.3 Data Compilation

*Microsoft Excel* was used to compile the data with specific columns prepared to transition into the online database vehicle. *DataThief* and existing databases, as was previously mentioned, were the main tools used in acquiring data (see Section 3.1). The data were then imported into *Excel* where surface conditions were qualified and recorded. The resultant data file contains data divided into the sections “Material, Reference E (keV), SE yield, Surface Morphology, and Surface Contamination.” These categories are vital to either data reporting or data classification.

Initial data analysis identified outliers within the data as well as mistakes made in data reporting in the primary data acquisition process and allowed us to remove the most obvious problems. By using an Excel pivot table, immediate outliers within the dataset were identified and their sources were investigated further. We will now investigate two data variances that we identified with this pivot table (See Figs. 3.5, 3.6.).

A graph of different allotropes of carbon allowed for the immediate identification of an outlier. Mearini reports SEY values for a disordered carbon film that does not peak but instead continue to grow (see Fig. 3.5.). We reexamined the original paper and found that the data were in agreement. Upon further investigation, the source of the exponential growth of SEY values was found to be caused by the deposition of chemical vapor deposited (CVD) diamond onto a relatively high electropositive Mo substrate that was contaminated by CsI, which is a very good electron emitter. We removed this data from the final database because of its extreme nature and uncharacteristic contamination by CsI.

Bulk diamond, a pure carbon allotrope is a very large band gap semiconductor ( $E_{\text{gap}} = 5.46\text{eV}$ ), in contrast to graphitic C which has a very low band gap (Dennison *et al.*, 2007). This difference in the band gap for diamond-like and graphitic carbon allotropes has profound consequences. Bulk crystalline diamond is an optically transparent hard, insulator (or large band gap semiconductor), while graphite is an optically opaque, soft, conductor (semi-metal). Diamond has a SEY  $\delta_{\text{max}}$  of 2.8 (Kishimoto *et al.*, 1977), while graphite has a SEY  $\delta_{\text{max}}$  of 1.22 (Dennison *et al.*, 2016). Indeed, Corbridge (2014) found that SEY of graphitic amorphous carbon films decreased from 1.74 to 1.22 as thermal annealing of the g-C films reduced the band gap from 0.6 eV to 0 eV.

Other examples of potentially extraneous data values, however, were not removed. Several low  $\delta$  values were found for Cu (see Fig. 3.6.) (Cimino *et al.*, 2015; Gimpel and Richardson, 1943; Myers, 1952; Petry, 1926; Warnecke, 1936). Data were investigated to verify that accurate reporting was made, and they were included in the database.

The datasets were formatted and uploaded into an online repository for easy access by the *HTML* database vehicle (see Appendix A). *JavaScript Object Notation* (JSON) was selected to format our data file. The data were uploaded to *GitHub* (an online programmer's reference repository). *GitHub* allows access to the data at any time and precludes any possible attacks upon local servers.

Several *JavaScript* libraries were researched and utilized in the *HTML* coding process for this database. The USU Material Physics Group (MPG) has made successful use of *HTML* pages in the past. As discussed in Section 3.2.1 (Wilson *et al.*, 2018b) developed an online range-modeling tool (see Fig. 3.3.). There were, however, a few important differences in the coding and libraries utilized in the development of the USU SEY Database. Specifically, the range approximation tool utilized *d3* for the backbone of its user interface, whereas, the USU SEY Database has used *jQuery*. For this reason, the libraries utilized by the code and the roles that each library plays in making the database function will be analyzed in some detail below.

The libraries used in the development of this code were *PivotTable.js*, *jQuery*, *touch-punch*, *GitHub*, and *Gchart*. Each library serves a specific purpose and assists in creating a database that is easy to access, versatile, and user-friendly. See Appendix A for details of each aspect of the code.

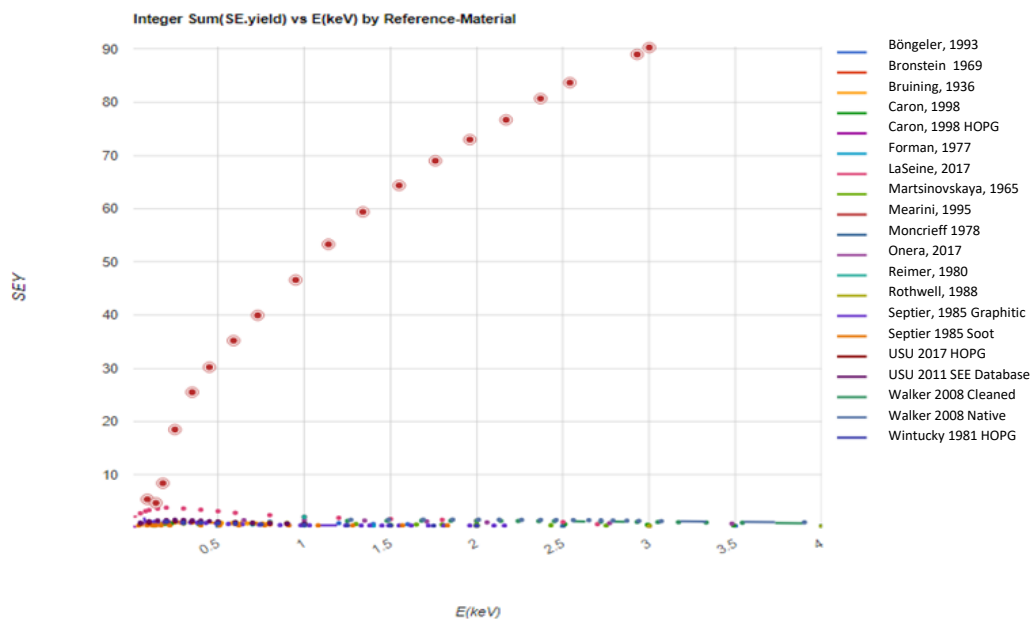


FIG. 3.5. Values for different allotropes of carbon. With the data for Mearini appearing as an obvious outlier and mistake.

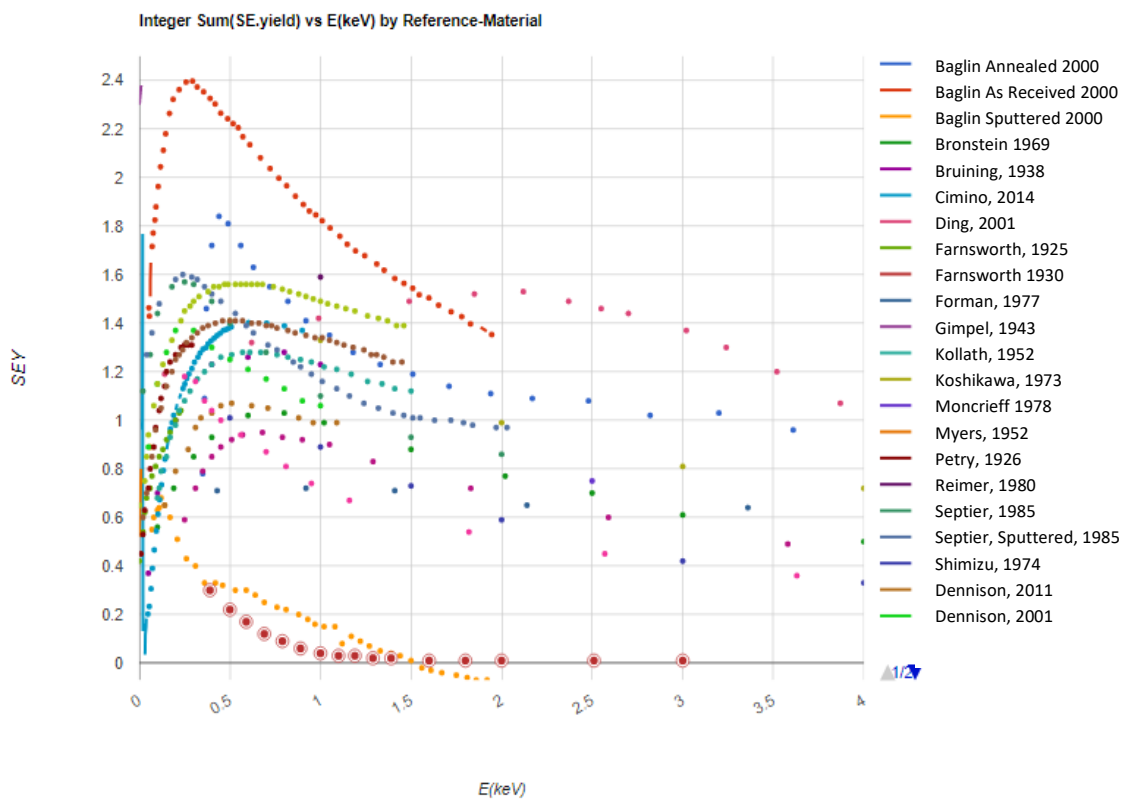


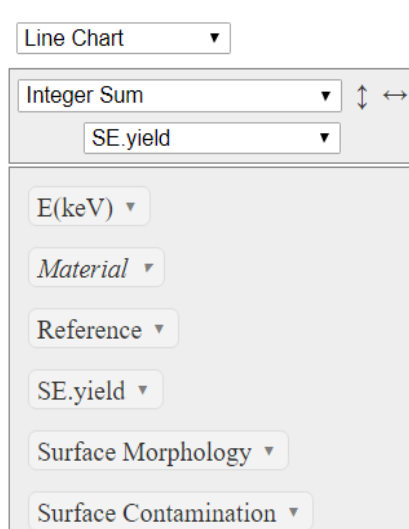
FIG. 3.6. SEY Values for Copper. Exhibiting specifically those low energy values which had veracity confirmed before inclusion in the database.

### 3.4 Database Options

Users can select a few different options when generating reports. The options are report type, material(s), and data filter (see Fig. 3.7.). Through this section, these different methods of differentiating data are highlighted. For a more thorough analysis and suggestion of various reports to generate see Appendix B.

#### 3.4.1 Report Types

The USU SEY Database allows for a variety of report types (see Table 3.1.). A line graph is the default type of report utilized by the database. The USU SEY Database pulls up as the default material: copper with no filters applied to surface or contamination designations. This type of report permits plotting of  $\delta$  versus E in a visible graph. These graphs are useful to get an initial idea for the spread of historical data reported for a given material and to see the number of datasets available within the database for a specific material (see Fig. 3.8.).



The image shows a screenshot of a web-based reporting interface. At the top, there is a dropdown menu set to "Line Chart". Below this is a section with a dropdown menu set to "Integer Sum" and a double-headed vertical arrow icon to its right. Underneath that is another dropdown menu set to "SE.yield". The bottom half of the interface consists of a vertical stack of seven dropdown menus: "E(keV)", "Material", "Reference", "SE.yield", "Surface Morphology", and "Surface Contamination".

FIG. 3.7. Snapshot of the different reporting options available in the USU SEY database.

Table 3.1. Chart types available in USU SEY database.

- Table
- Table Barchart
- Heatmap
- Row Heatmap
- Col Heatmap
- Line Chart
- Bar Chart
- Stacked Bar chart

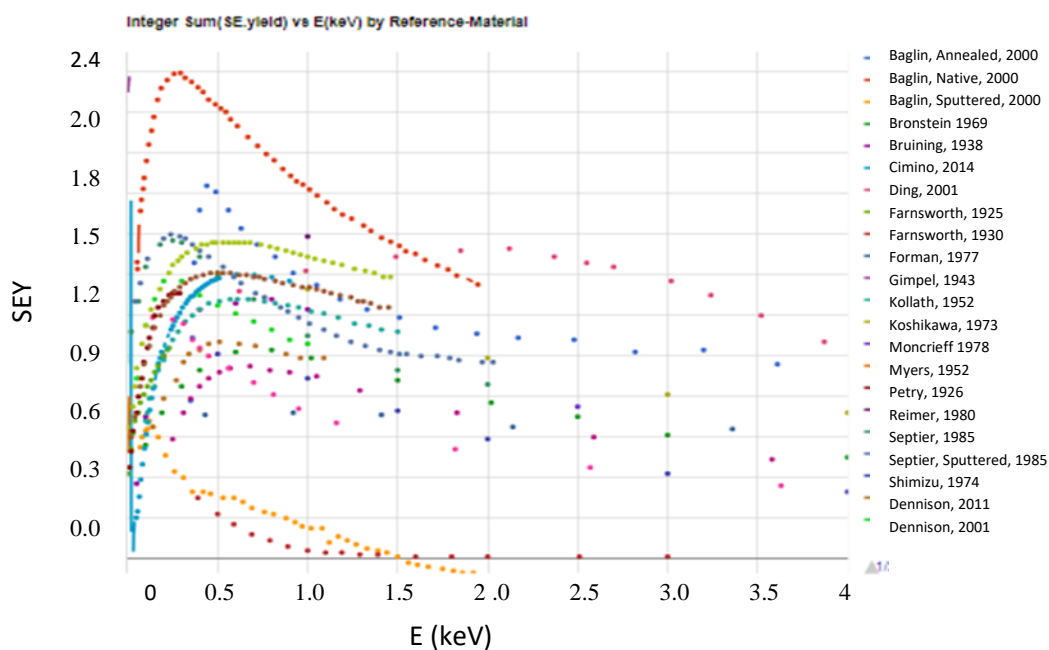


FIG. 3.8. The default USU SEY Pivot Tool settings. Displayed is a line chart displaying Cu data from multiple sources that are not filtered by either topography or contamination.

### 3.4.2 Data Filters

The USU SEY Database allows for filtering data based upon four criteria: Material, Reference, Surface Morphology, and Surface Contamination. To sort by one of these criteria, all a user need do is

select the button with the corresponding criteria title. For example, selecting “Material” will list all of the materials which are available (see Table 2.7.).

As of April 2020, the database contains 54 different materials. These materials are elemental samples useful to spacecraft or electron microscope applications. Stable metals or semi-metals make up the majority of available materials. Pure elements were emphasized in this preliminary database due to the prevalence of data and the simplicity of categorization. The majority of spacecraft modelers require information related to more complex spacecraft materials. To address this need, a preliminary framework has been developed for various multi-element compounds, this is not currently available, and will be relegated to future work.

Reference sorting is another option available. Users wishing to include/exclude a particular reference in the report can do so. Sorting data by a particular publication date range is also possible. For example, to include only data sets reported in the 2000s click on the reference pulldown, click “Select None”, enter the first three digits of the decade you wish to search, for example, “200”, into the Filter values field, click the “Select All” button and then click apply. This selection method by publication date is illustrated for Cu datasets published in the 2000s in Fig. 3.9..

Surface morphology or “roughness” can affect SEY values (Bergeret *et al.*, 1985). As was discussed in Section 3.2.2, each dataset has been categorized in one of 3 ways: smooth, rough, or unknown. This categorization can be used to sort data by making a selection in “Surface Morphology”.

Surface morphology can be altered from its initial conditions as the mission progresses by interaction with the space environment. It is advisable to model spacecraft with initial characteristics to mimic the situation immediately after launch and then model it again with modified morphologic characteristics based upon appropriate environmental effects (see Section 4.3.1).

Morphologic differences are readily discernable by comparing smooth versus rough results (see Fig. 3.10.). In an analysis for Cu samples, it can be seen that rough samples tend to have lower  $\delta_{max}$  values (average  $\delta_{max}=1.04$ ) while smooth samples tend to have higher  $\delta_{max}$  values (average  $\delta_{max}=1.34$ ). A more thorough analysis of morphological variability and its effects on  $\delta_{max}$  values is made in Section 4.1.2.

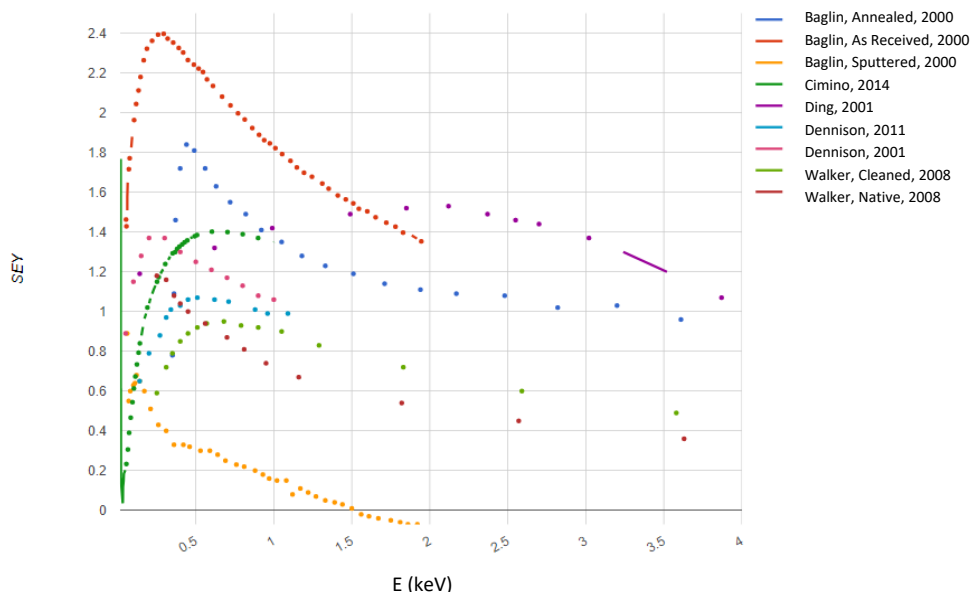


FIG. 3.9. Screen shot of the USU SEY Database. Displayed is a chart showing Cu datasets from multiple sources reported from 2000 to 2020.

Surface contamination can also be used to filter data by employing the same method used to filter data by morphology (see Fig. 3.11.). A comparison of the graphs associated with Al shows a trend with clean samples having lower  $\delta_{max}$  values (average  $\delta_{max} = 1.43$ ). Moreover, oxidized samples have higher  $\delta_{max}$  value (average  $\delta_{max} = 2.83$ ) and behave more like  $\text{Al}_2\text{O}_3$  ( $\delta_{max} = 5.0$ ) (see Fig. 3.11b.) (Christensen, 2017). An analysis of the physics behind the effects of surface contamination and  $\delta_{max}$  adjustment will be made in Section 4.1.1.

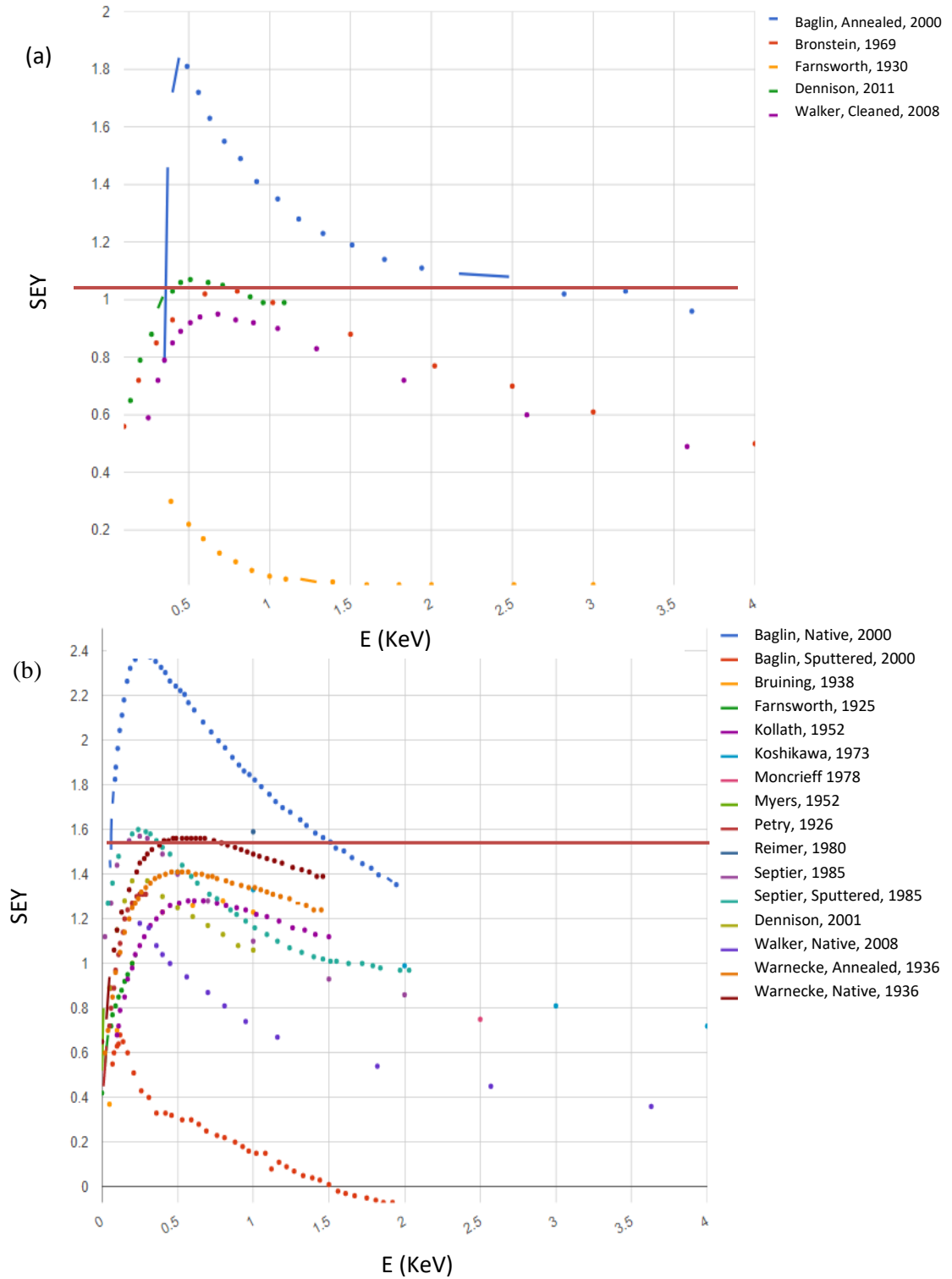


FIG. 3.10. Different copper SEY data sets sorted based upon surface morphology conditions. Figures show (a) smooth results and (b) rough results. Red lines are drawn in to indicate average  $\delta_{max}$  values.

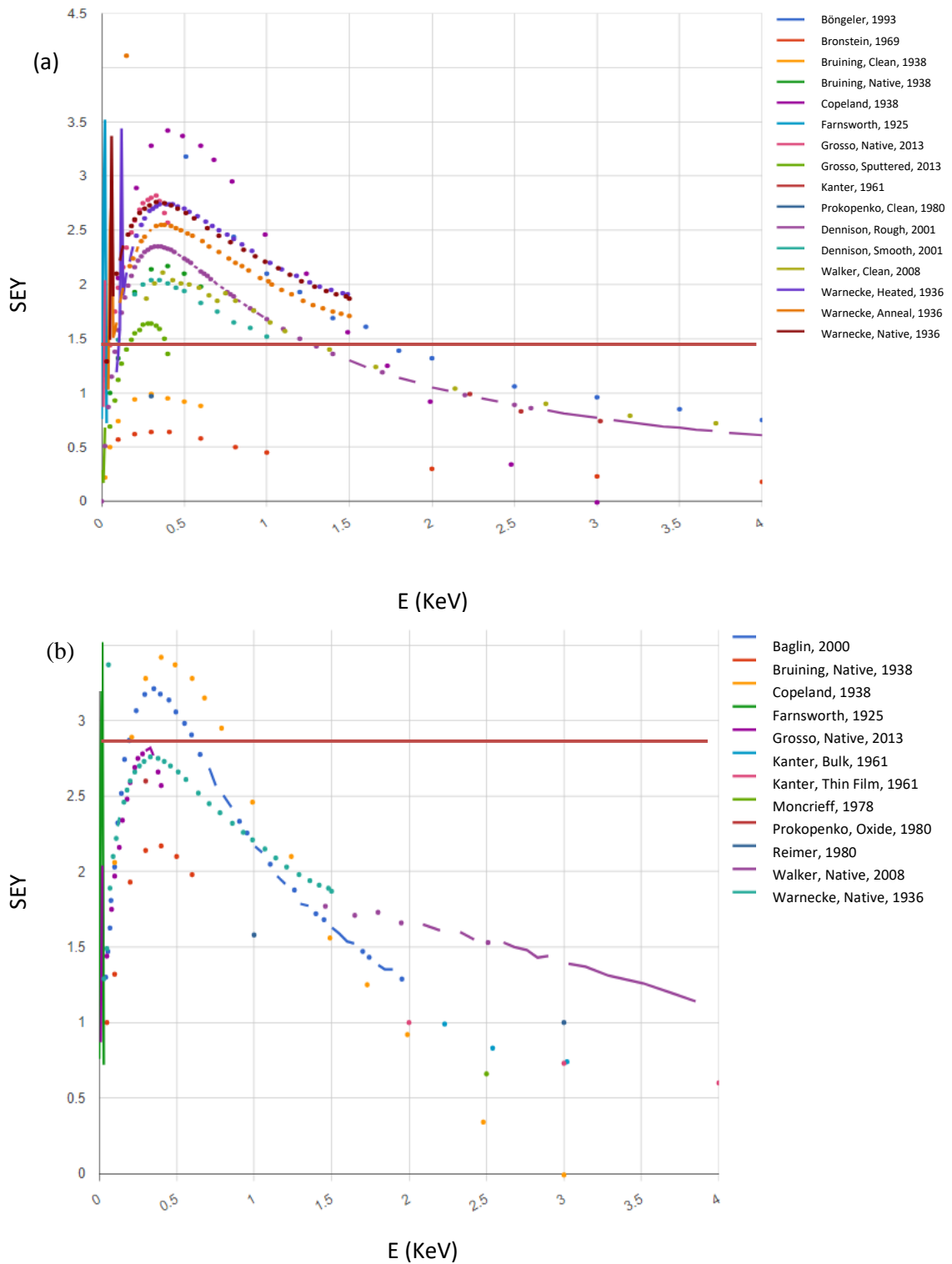


FIG. 3.11. Different aluminum SEY data sets sorted based upon surface contamination conditions. (a) clean, elemental and (b) contaminated and oxidized. Red lines are included to indicate average  $\delta_{max}$  values.



## CHAPTER 4

### RESULTS

Having established the need for the USU SEY Database and the physics foundations of SE emission in Chapter 1, a review of the availability and limitations of existing SEY databases in Chapter 2, and the structure and content of the new USU SEY Database in Chapter 3, it is natural to ask what the uses of the new database are. Application of the USU SEY Database has identified these specific applications: verification of previously reported historical SEY trends, identification and refinement of methods to better model spacecraft materials SEY properties (especially as the materials evolve due to environmental interactions), and identification of novel physics principles that can be garnered from analyzing big data sources. In this chapter, each of these tasks will be discussed. Much of this information has been presented previously.

Presentations at the American Physical Society Four Corners Meeting (Lundgreen and Dennison, 2018a) and the Applied Space Environments Conference (ASEC) (Lundgreen and Dennison, 2019) provided overviews of the database development and strategies. The conference proceeding of ASEC and a full-length peer-reviewed journal article focused on the results of compiled SEY studies of Al (Lundgreen and Dennison, 2020). This paper provides details of how trends observed in Al studies address the three applications of the new database enumerated above, including how coupling the database results with novel parameterized models of SEY can shed light on trends in SEY due to surface modification (see Fig. 4.1.). (Lundgreen and Dennison, 2019) presented a similar analysis of SEY studies of Cu. A presentation and conference proceedings paper for the 16th Spacecraft Charging and Technology (SCTC) 2021 will present similar analysis for the ubiquitous polymeric insulating spacecraft material polyimide or Kapton™; a peer-reviewed journal article for a special edition of IEEE Transactions of Plasma Science for the 16<sup>th</sup> SCTC 2021 is in preparation.

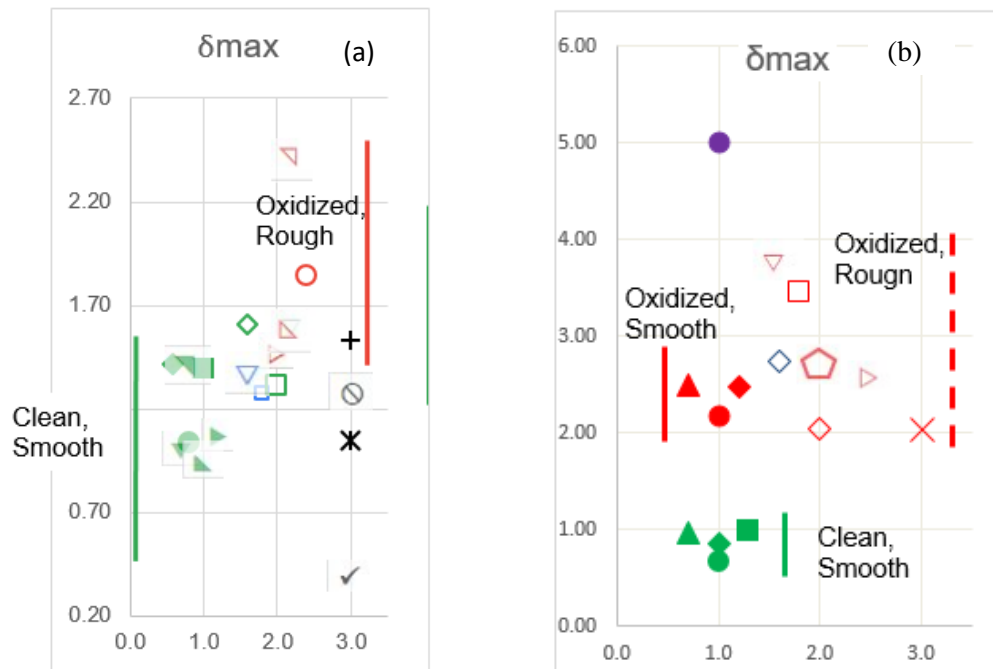


FIG. 4.1.  $\delta_{max}$  values for two conducting materials. (a) Copper and (b) aluminum, included with aluminum is a measurement of  $\text{Al}_2\text{O}_3$  (sapphire) to illustrate an extreme case of oxidation.

#### 4.1 Verification of Prior Established Physics Principles

This section describes efforts made towards verifying historically reported trends in SEY. To do this two conclusions were identified, analyzed, and corroborated through analysis of multiple datasets.

The first conclusion analyzed was that an oxide layer formed on metallic conductors would affect energy associated with yield differently depending on the conductivity of the oxide layer (Baglin *et al.*, 2000). Aluminum oxides ( $\text{Al}_2\text{O}_3$ ,  $\text{AlO}$ , and  $\text{Al}_2\text{O}$ ) and copper oxides ( $\text{CuO}$ ,  $\text{Cu}_2\text{O}$ ) were selected for these studies, because of their use in spacecraft construction. Studies of specific aluminum and copper samples treated to scan a range of oxidation layer thicknesses have established specific trends. Higher  $E_{max}$  values have been observed for oxidized insulating surfaces ( $\text{Al}_2\text{O}_3$ ) (Bruining and De Boer, 1938; Baglin *et al.*, 2000; Chang *et al.*, 2000; Christensen, 2017) and lower values have been observed for conducting surfaces ( $\text{CuO}$ ) (see Fig. 4.2.).

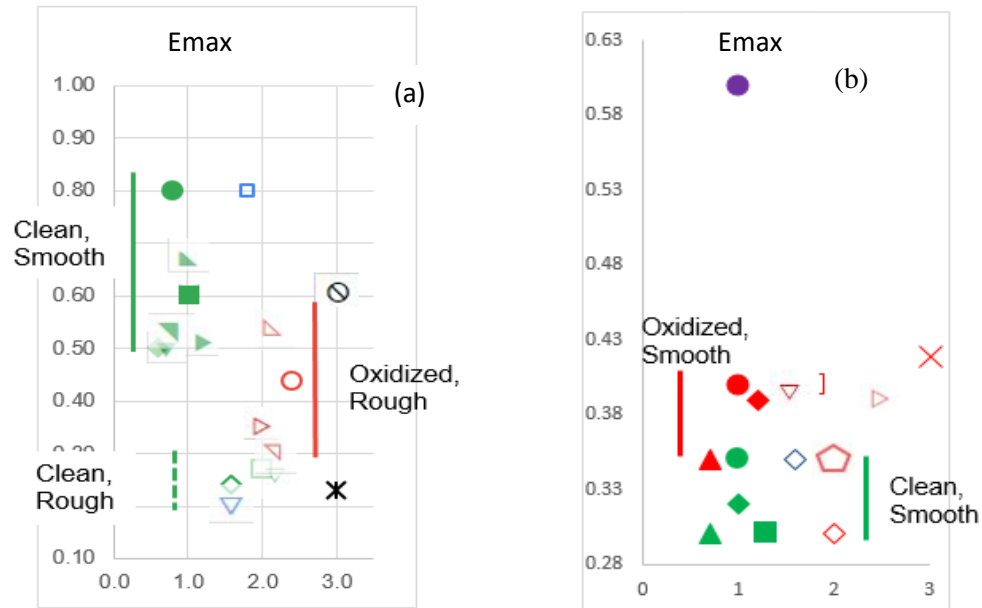


FIG. 4.2. Comparison of  $E_{max}$  values for various conducting samples. With (a) copper, and (b) aluminum. Included with aluminum is a measurement of  $Al_2O_3$  (Sapphire) to illustrate an extreme case of oxidation. Apparent from these graphs is the difference that an oxide layer has on  $E_{max}$  values. (Conductive oxides increase values, while insulating values decrease  $E_{max}$  values).

The second conclusion analyzed is that the modification of SEY for higher energy PE's is largely affected by the surface morphology of the sample.  $E_{max}$  values of clean-rough Cu have lower  $E_{max}$  values than oxidized rough samples. However, these trends are not as obvious when considering the full SEY curves, most likely because of other compounding differences between the various studies including roughness, C-layers, experimental methods, and calibration.

#### 4.1.1 Contamination Affects Yield

Surface coatings can change SEY (Baglin *et al.*, 2000), although their effects on SEY are more nuanced and varied than the effects due to roughness (Wilson *et al.*, 2018a). Coatings of low-Z conducting materials (*e.g.*, C) will typically lower SEY while high-Z conducting coatings (*e.g.*, Au) will typically increase SEY, though thin surface layers can produce complicated incident energy-dependent effects from the underlying substrate (Lundgreen and Dennison, 2019; Bruining and De Boer, 1938). As another

example, the presence of adsorbed water vapor can significantly increase SEY; for example, for Al or Cu surfaces, condensation of water can greatly enhance yields, while a vacuum bake-out, which can evolve surface water, reduces this increase in yield (Baglin *et al.*, 2000). Similar changes in yield can be affected by ion bombardment by sputtering or ion glow discharge using various gases (Baglin *et al.*, 2000). Ion sputtering can both remove contamination through sputtering and embed sputtered ions in the near surface layers of the substrate depending upon the energy of the sputtering particles (Davies and Dennison, 1999).

Two common coatings are considered, the formation of oxide layers and carbon-rich contamination layers. Formation of highly insulating oxides (*e.g.*, Al<sub>2</sub>O<sub>3</sub> or SiO<sub>2</sub>) can significantly increase the elemental material yields (Christensen, 2017). The formation of semiconducting oxides (*e.g.*, copper oxides) typically act to reduce yields (Baglin *et al.*, 2000). Copper does form multiple oxides, cupric oxide (CuO), and cuprous oxide (Cu<sub>2</sub>O). It is assumed that the primary species present is CuO as it has a lower enthalpy of formation (-156.06 kJ/mol) compared to Cu<sub>2</sub>O (-170 kJ/mol).

Aluminum oxide (Al<sub>2</sub>O<sub>3</sub>), known as alumina in its microcrystalline or ceramic form or as sapphire in its single crystalline form, behaves as an electrical and thermal insulator (Meyza *et al.*, 2003). By contrast, copper oxide has been shown to behave as a p-type semiconductor with a band gap of roughly 2.1-2.6 eV (Ogwu *et al.*, 2007). These energy levels are low enough that we can essentially consider copper oxide to be a conductor.

Carbon-rich contamination layers are often formed under electron bombardment; this is a phenomenon well known to electron microscopists (Baglin *et al.*, 2000; Reimer *et al.*, 1980). The formation of these contaminating layers is believed to result from the ionization of residual carbon species in the vacuum system (*e.g.*, CO, CO<sub>2</sub>, and hydrocarbons) or molecules desorbed from surfaces during electron irradiation. These ionized particles are then propelled toward the sample surface by the electron beam, or re-attracted as sample surface potential builds, and are subsequently cracked leaving disordered C-rich surface layers (Baglin *et al.*, 2000; Andritschky, 1989). C-rich surface layers are frequently encountered in studies in low vacuum (*e.g.*, scanning electron microscope systems) and systems employing diffusion pumps (*e.g.*, most—but not all—studies done before the mid-1960s) (Myers and Gwinn, 1952). C-rich surface layers are similarly present in space applications (Scialdone, 1972), due in many cases to

outgassing of volatile organic compounds and their subsequent reabsorption on spacecraft surfaces (Taylor *et al.*, 2020). Indeed, Caroline Purvis—one of the central developers of the original NASCAP code—once quipped, “All spacecraft surfaces eventually turn into carbon” via deposition of organic contamination and outgassing (Purvis, 1995).

*Microsoft Excel* was used to plot the data for the four SEY fitting parameters from the USU SEY

Table 4.1. SEY data for various Cu studies. Sources, plotting symbols and fitting parameters for Eq. 2.2 are listed.

Symbol	Source		Surface		Fitting Parameters			
	Author	Year	Contaminated	Morphology	$\delta_{\max}$	E(keV)	n	m
●	Bronstein IM and Fraiman	1969	X	S	1.03	0.80	0.64	1.59
▷	Hilleret (Sputtered)	2000	O	R	1.48	0.36	0.64	1.33
○	Hilleret (Annealed)	2000	O	R	1.84	0.44	-10.34	1.40
□	Bruining	1938	X	R	1.28	0.80	0.42	-
■	Cimino	2014	X	S	1.40	0.60	0.72	1.13
+	Ding	2001	?	?	1.53	2.12	0.87	1.49
X	Farnsworth & Goerke	1930	X	?	-	-	-	2.73
*	Farnsworth	1925	?	?	1.04	0.23	0.94	-
◇	Gimpel	1943	CO	R	-	-	-	0.90
◆	Koshikawa	1973	X	S	1.41	0.50	-	1.35
○	Moncrieff	1976	X	R	-	-	-	1.65
△	Myers	1952	CO	R	-	-	0.90	-
□	Petry	1926	X	R	1.31	0.27	0.54	-
—	Reimer	1982	?	?	-	-	-	1.84
▽	Septier (Cleaned)	1980	X	R	1.57	0.25	1.14	1.38
◇	Septier (Sputtered)	1985	X	R	1.60	0.24	0.85	1.38
▼	Shimizu	1974	X	S	1.01	0.50	-	-
▽	USU (Technical)	2001	CO	R	1.37	0.20	0.72	1.24
▶	See Database	2001	X	S	1.07	0.51	0.60	1.75
▶	Walker (Clean)	2008	X	S	0.95	0.68	0.60	0.60
△	Walker (Native)	2008	X	S	-	-	-	1.45
▷	Warnecke (Native)	1936	O	R	1.56	0.53	0.75	1.14
▼	Warnecke (Heated)	1936	X	S	1.41	0.53	-	1.03
✓	Wittry	1966	?	?	0.39	5.00	-	-
⊙	Kollath	1952	?	?	1.28	0.61	-	0.53
▽	Hilleret (Native)	2000	O	R	2.40	0.29	0.68	0.20

Contamination: X-Clean, O-Oxidized, C-Contaminated, ?-Unknown  
Morphology: S-Smooth, R-Rough, ?-Unknown

Database. For each of the materials, a table was generated with columns for symbol, source, surface, and fitting parameters (e.g., Table 4.1.). The surface column describes the contamination and roughness conditions of a sample for a specific study: X is clean, O is oxidized, C is contaminated, S is smooth, R is rough, and “?” is unknown.

The source column signifies the origin and date of the dataset, with a differentiation made for those sources that have reported multiple datasets. Surface is used to describe the contamination and roughness conditions of a material; X is clean, O is oxidized, C is contaminated, S signifies a smooth surface, R a rough surface and “?” unknown surface conditions.  $n$  and  $m$  are the fitting parameters required for modeling SEY with the reduced power-law (RPL) yield model, Eq (2), and will be discussed further in Section 4.3.2.

The “Symbol” column is a category selected specifically to portray the morphology and contamination level of a dataset. Each symbol shape has been chosen sequentially, with the color and fill properties of a symbol used to indicate surface characteristics of a sample (See Table 4.2.).

#### 4.1.2 Roughness Affects Yield

Surface morphology can affect SEY (Myers and Gwinn, 1952) and the difficulty in accurately describing the degree of surface modifications due to limited sample characterization in the original references. Figure 3.2(a) is repeated here as Fig. 4.3. to reemphasize this. Rougher surfaces, with features on the (typically sub- $\mu\text{m}$ ) scale of electron penetration depths and with higher depth-to-width aspect ratios, enhance the recapture of emitted electrons through surface collisions, thereby lowering SEY (Robertson and Dennison, 2020; Wood *et al.*, 2019; Bergeret *et al.*, 1985; Baglin *et al.*, 2000). The effects of surface

Table 4.2. The different symbols used in the comparison of different SEY fitting parameters.

Surface Morphology	Surface Layers			
	Clean	Oxidized	Contaminated	Unknown
Smooth	●■◆▲▼▶▷◂◃◄◅◆◇◈◉◊○◌◍◎●◐◑◒◓◔◕◖◗◘◙◚◛◜◝◞◟◠◡◢◣◤◥◦◧◨◩◪◫◬◭◮◯◰◱◲◳◴◵◶◷◸◹◺◻◼◽◾◿◸◹◺◻◼◽◾◿	●■◆▲▼▶▷◂◃◄◅◆◇◈◉◊○◌◍◎●◐◑◒◓◔◕◖◗◘◙◚◛◜◝◞◟◠◡◢◣◤◥◦◧◨◩◪◫◬◭◮◯◰◱◲◳◴◵◶◷◸◹◺◻◼◽◾◿	●■◆▲▼▶▷◂◃◄◅◆◇◈◉◊○◌◍◎●◐◑◒◓◔◕◖◗◘◙◚◛◜◝◞◟◠◡◢◣◤◥◦◧◨◩◪◫◬◭◮◯◰◱◲◳◴◵◶◷◸◹◺◻◼◽◾◿	●■◆▲▼▶▷◂◃◄◅◆◇◈◉◊○◌◍◎●◐◑◒◓◔◕◖◗◘◙◚◛◜◝◞◟◠◡◢◣◤◥◦◧◨◩◪◫◬◭◮◯◰◱◲◳◴◵◶◷◸◹◺◻◼◽◾◿
Rough	○□◇△▽▷◂◃◄◅◆◇◈◉◊○◌◍◎●◐◑◒◓◔◕◖◗◘◙◚◛◜◝◞◟◠◡◢◣◤◥◦◧◨◩◪◫◬◭◮◯◰◱◲◳◴◵◶◷◸◹◺◻◼◽◾◿	○□◇△▽▷◂◃◄◅◆◇◈◉◊○◌◍◎●◐◑◒◓◔◕◖◗◘◙◚◛◜◝◞◟◠◡◢◣◤◥◦◧◨◩◪◫◬◭◮◯◰◱◲◳◴◵◶◷◸◹◺◻◼◽◾◿	○□◇△▽▷◂◃◄◅◆◇◈◉◊○◌◍◎●◐◑◒◓◔◕◖◗◘◙◚◛◜◝◞◟◠◡◢◣◤◥◦◧◨◩◪◫◬◭◮◯◰◱◲◳◴◵◶◷◸◹◺◻◼◽◾◿	○□◇△▽▷◂◃◄◅◆◇◈◉◊○◌◍◎●◐◑◒◓◔◕◖◗◘◙◚◛◜◝◞◟◠◡◢◣◤◥◦◧◨◩◪◫◬◭◮◯◰◱◲◳◴◵◶◷◸◹◺◻◼◽◾◿
Unknown	X+*-✓	X+*-✓	X+*-✓	X+*-✓

roughness are less for higher energy BSE's, which have a narrower distribution of emission angles than lower energy SE (Wood *et al.*, 2019; Niemietz and Reimer, 1985; Nickles and Dennison, 2000). By contrast, smooth surfaces minimize recapture by maximizing the solid angle for the escape of emitted electrons without further collisions with the surface. The effects of surface roughness are more pronounced at lower incident energies, where more SE tend to be generated near the surface. Common methods affecting surface roughness include material preparation, deposition or formation of high aspect ratio textured or dendritic surfaces, chemical etching, mechanical abrasion, polishing, sputtering, and thermal annealing. Such methods are routinely used to intentionally reduce electron emission from surfaces (Baglin *et al.*, 2000; Bergeret *et al.*, 1985; Wood *et al.*, 2019; Robertson and Dennison, 2020). The examination of Fig. 4.1. again shows that roughened surfaces will have a lower yield value than a clean surface regardless of material. Of special interest is aluminum as it shows that rough oxidized datasets have higher yields than smooth oxidized datasets.

Figure 4.2 shows higher  $E_{max}$  values for oxidized insulating surfaces ( $Al_2O_3$ ) (Bruining and De Boer, 1938; Baglin *et al.*, 2000; Chang *et al.*, 2000) and lower values have been observed for conducting surfaces (CuO). The aluminum  $\delta_{max}$  values displayed in Fig. 4.1.(b) in general confirm that an insulating oxide layer will tend to increase on average  $\delta_{max}$  values, with the majority of oxidized surfaces (red symbols  $2.0 < \delta_{max} < 3.8$ ) lying between a lower bound for smooth clean Al (green symbols;  $\delta_{max} \sim 1.0$ ) and bulk  $Al_2O_3$  (purple symbols;  $\delta_{max} \sim 5.0$ ).

The opposite is true for  $E_{max}$  values plotted for copper in Fig. 4.2.(a), with clean-rough Cu (green,

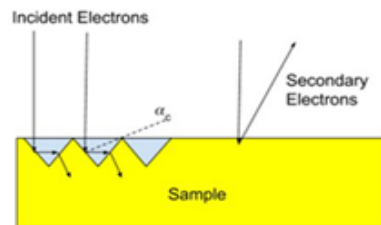


FIG. 4.3. Roughness facilitates the recapture of emitted electrons. This is accomplished by creating features on the surface, which can reabsorb emitted electrons and decrease net electron emission.

open symbols  $E_{max} < 0.3$ ) having lower  $E_{max}$  values than oxidized rough samples (Red open symbols;  $0.3 < E_{max} < 0.55$ ). These trends are similar to those found for Al with clean, smooth Al (green, solid symbols;  $\delta_{max} < 0.35$ ) occurring below oxidized smooth Al (red, solid symbols;  $0.35 < E_{max}$ ). However, these trends are not as obvious when considering the full SEY curves (see Fig. 3.10.), most likely because of other compounding differences between the various studies including roughness, C-layers, experimental methods, and calibration.

#### 4.2 Selecting Data for More Accurate Charge Modeling

This section presents strategies for determining the best available SEY data to use when modeling materials for use in specific spacecraft applications, and how to draw upon the requisite knowledge mentioned above to increase modeling accuracy. Two simple ubiquitous spacecraft material aluminum and copper are analyzed in detail. These results have been published separately in the past (Lundgreen and Dennison, 2018a; Lundgreen and Dennison, 2018b; Lundgreen and Dennison, 2019). Modeling space plasma environment-induced effects on spacecraft require knowledge of the following:

- Environment and impinging fluxes during spacecraft orbits, which are mission-specific and can be incorporated through environmental models and databases (Hastings and Garrett, 2004; Lai, 2013).
- Satellite geometry and orientation in the space environment accomplished through charging codes (see Fig. 2.5.). The three most prominent codes, NASCAP-2K (Mandell *et al.*, 2006; Katz *et al.*, 1977; Davis *et al.*, 1999; Mandell *et al.*, 1977), SPENVIS (SPENVIS, 2018), and MUSCAT (Muranaka *et al.*, 2008).
- Precise descriptions of the materials used in spacecraft construction, for the specific spacecraft design (Toyoda *et al.*, 2003; Dennison *et al.*, 2007).
- Relevant materials properties which characterize the interaction of these specific materials with the environment and how these properties may change with exposure to the space environment (Katz *et al.*, 1977; Dennison *et al.*, 2005; Dennison *et al.*, 2007; Parker and Minow, 2018).

This thesis focuses on the last requirement, the key material property of SEY, and how to address this topic for more extended and precise descriptions of specific materials and the evolution of their properties during mission lifetime. Listed here is a three-tiered strategy for determining appropriate electron yield material parameters for specific spacecraft charging modeling.

1. The easiest approach is to select parameterized yield properties from a limited database of materials tabulated for use with the standard charging codes mentioned above (Mandell *et al.*, 1977; Mandell *et al.*, 1993; Dennison *et al.*, 2005; Mandell *et al.*, 2006; Dennison *et al.*, 2007; Parker and Minow, 2018; Drolshagen, 1994)
2. A second method involves the review of available literature to identify data of more directly applicable materials not presently tabulated in these databases (Joy, 1995; Walker *et al.*, 2008).
3. The third, most sophisticated method requires selecting materials and specific data sets which are most mission specific to relevant charging concerns and possible changes in materials with prolonged exposure to the space environment. This is facilitated through the use of a much more extensive database, such as the USU SEY Database. This is discussed in Section 4.3.

Sections 4.2.1 and 4.2.2 address the first two methods, as they are the most common methods utilized in charge modeling. Section 4.3 focuses on a novel method that utilizes the newly created database to more accurately model materials with various surface conditions. Section 2.4 established that electron yield studies of nominally similar materials often show widely differing results. Indeed, even round-robin studies in different laboratories of carefully selected “standard” calibration materials such as Au and graphitic carbon show smaller but still significant, variation in yields (see Fig. 4.4.) (Dennison *et al.*, 2016). These can be attributed to subtle differences in instrument calibration, measurement methods, and sample preparation at the different facilities—details that are seldom provided in the standard literature. Indeed, even the definition of “secondary electron yield” can differ for different studies and lead to ambiguities (Lundgreen and Dennison, 2020).

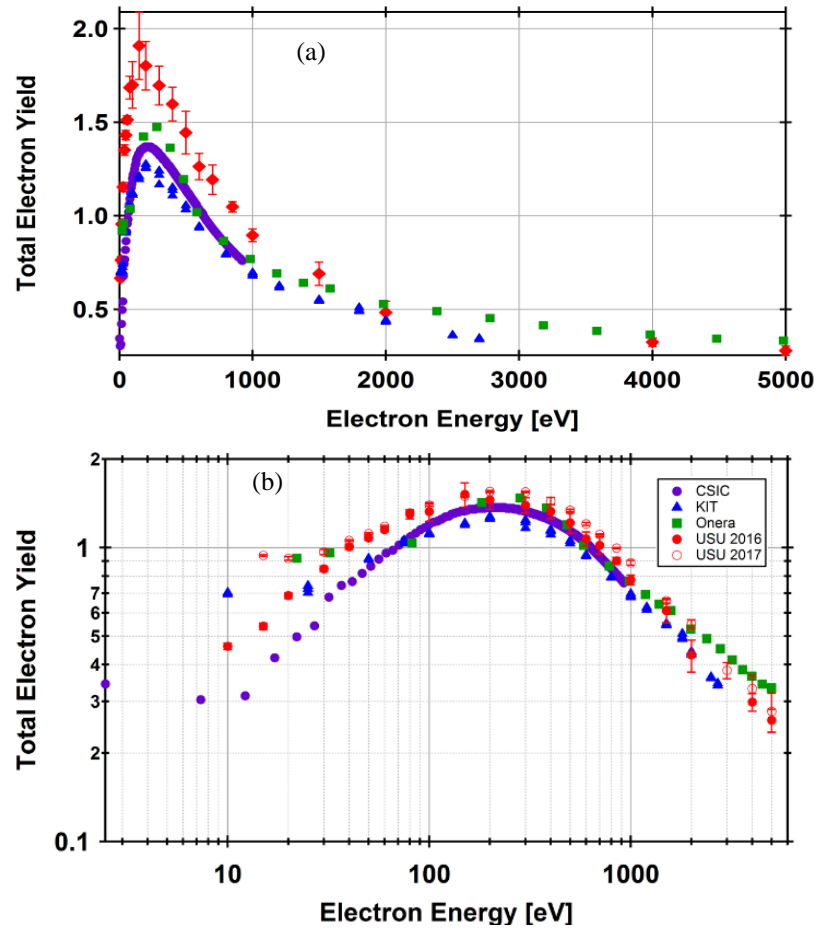


FIG. 4.4. Round robin comparison of various SEY curves. Displayed are (a) high purity polycrystalline Au and (b) atomically clean, flat highly oriented pyrolytic graphite (HOPG), from a round robin study performed by ONERA, LaSeine, CSIC, and USU (Dennison, 2017).

#### 4.2.1 Method 1: Select Parameterized Yield Properties

The easiest method for selecting electron yield material parameters entails selecting parameterized yield properties from a limited database of materials, as tabulated for use with standard charging codes. Table 4.3. lists the model parameters in the default materials database included with successive versions of NASCAP (Mandell et al., 1977; Mandell *et al.*, 1993; Davis *et al.*, 1999; Mandell *et al.*, 2006), these are used to characterize SEY with the Katz (1977) or far less accurate Feldman (1960) models mutually incorporated in the three charge modeling codes. The parameters are:

Table 4.3. SEY data for various Al studies. Sources, plotting symbols and fitting parameters for Eq. 2.2 are listed.

Symbols	Source		Surface		Reduced Power Law Fitting Parameters				NASCAP Fitting Parameters			
	Author	Year	Contam-inated	Morph-ology	$\delta_{max}$	$E_{max}$ (keV)	$n$	$m$	$RC1$ $\hat{n}_1$	$REXP$ $l$	$RC2$ $\hat{n}_2$	$REXP$ $2$
●	Prokopenko (Clean)	1980	X	S	0.97	0.30	-	-	-	-	-	-
●—	Bronstein	1969	X	S	0.66	0.35	0.79	1.58	0.00	0.80	1.0	1.5
■—	<b>Bruining (Cleaned)</b>	<b>1938</b>	<b>X</b>	<b>S</b>	<b>0.97</b>	<b>0.27</b>	<b>0.42</b>	<b>1.29</b>	<b>1</b>	<b>0.80</b>	<b>1.0</b>	<b>1.57</b>
◆—	Kanter (Bulk)	1961	X	S	-	-	-	-	0.27	0.40	1.0	1.9
▲—	Gibbons (Cleaned)	1964	X	S	0.97	0.30	-	-	-	-	-	-
●—	Bruining	1938	O	S	2.17	0.40	0.56	1.27	0.51	0.42	1.0	1.28
■—	Kanter (Thin Film)	1961	O	S	-	-	-	1.77	0.1	0.80	1.0	1.96
◆—	<b>Dennison (Oxidized)</b>	<b>2002</b>	<b>O</b>	<b>S</b>	<b>2.34</b>	<b>0.37</b>	<b>0.69</b>	<b>1.79</b>	<b>0.4</b>	<b>0.90</b>	<b>1.0</b>	<b>2.25</b>
▲—	Gibbons (Oxidized)	1964	O	S	2.50	0.35	-	-	-	-	-	-
●	Prokopenko (Technical)	1980	O	R	2.60	0.3	-	-	-	-	-	-
○--	Shimizu	1974	O-	R-	-	-	-	1.74	0.99	0.60	1.0	2.0
□--	<b>Baglin (Heavily oxidized)</b>	<b>2000</b>	<b>O</b>	<b>R</b>	<b>3.21</b>	<b>0.35</b>	<b>0.50</b>	<b>1.55</b>	<b>1</b>	<b>.35</b>	<b>1</b>	<b>1.84</b>
◇--	Dennison (Technical)	2005	O	R	2.04	0.30	0.55-	1.71	1.0	0.57	1.0	1.86
△--	Czaja	1966	O	R	-	-	-	1.43	-	-	-	-
▽--	Copeland	1938	O+	R	3.44	0.40	0.62	1.86	0	0.5	1.0	2.0
◁--	Farnsworth	1925	O+	R	-	-	0.51	-	-	-	-	-
◡--	Warnecke (heated)	1936	O+	R	2.70	0.35	0.60	1.37	1	.40	1.0	1.6
▷--	Warnecke (annealed)	1936	O	R-	2.55	0.39	0.62	1.42	1	0.42	1	1.64
x··	Walker, (Cleaned)	2008	O	?	2.04	0.42	-	1.66	0.32	0.67	1.0	1.65
○··	Reimer	1980	CO	R-	-	-	-	1.79	-	-	-	-
□··	Moncrieff	1978	CO	R+	-	-	-	1.64	0.3	0.6	1.0	1.7
◇··	Warnecke (Native)	1936	CO+	R	2.75	0.35	0.59	1.35	-	-	-	-
+··	Walker (Native)	2008	CO	?	-	-	-	1.79	0.3	0.8	1.0	1.7
●—	<b>Christensen (bulk Al<sub>2</sub>O<sub>3</sub>)</b>	<b>2017</b>	<b>O++</b>	<b>S</b>	<b>5.00</b>	<b>0.60</b>	<b>0.40</b>	<b>2.09</b>	<b>1.5</b>	<b>0.56</b>	<b>1.0</b>	<b>1.95</b>

**Contamination:** X- clean, O-oxidized, C-contaminated, ?-unknown **Morphology:** S-smooth, R-rough, ?- unknown  
**Bold Text:** Best fit for specific surface conditions

- The maximum SEY,  $\delta_{max}$ ;
- The energy  $E_{max}$ , associated with  $\delta_{max}$ ; and
- Two amplitudes,  $b_1$  and  $b_2$ , and two exponents,  $n_1$  and  $n_2$ , for an analytic bi-exponential

range expression.

(Note that there are only five independent parameters, including only  $(b_1/b_2)$  rather than  $b_1$  and  $b_2$  independently (Chang *et al.*, 2000; Purvis, 1995)).

Values selected from such parameterized yield properties tabulated in one of the standard charging codes, unfortunately, have multiple flaws associated with them, as detailed at length in Section 3.3.2.

#### 4.2.2 Method 2: Review of Available Literature

Modelers before the compilation work of Joy had to utilize individual published studies to identify datasets taken on materials that would mimic the environment to which their craft would be subject. This method involves a more extensive review of available literature to identify data of more directly applicable materials not presently tabulated in existing charge modeling databases. This requires investigations into source background information to select materials parameters based on specific knowledge of proposed mission-specific conditions and applications and on materials characteristics known for individual studies. It also requires expertise in both spacecraft charge modeling and materials science.

However, selecting appropriate values of  $\delta_{max}$  and  $E_{max}$  from such a thorough literature analysis is often confusing, as data can show a large variation. This is illustrated for representative data from 22 studies of the ubiquitous spacecraft materials Al in Fig. 4.5. and 17 studies of Cu in Fig. 4.6.. Table 4.1. lists the fitting parameters  $\delta_{max}$  and  $E_{max}$ , as well as limited details about Cu. Many studies have limited ranges of measured energies making it difficult, or impossible, to determine all the fitting parameters for SEY models. As noted above, often the literature does not provide sufficient details of sample characterization and preparation, experimental methods, or data analysis to choose from myriad and often conflicting results. Again, a word of caution is in order, to determine the appropriate use of SEY versus TEY (see Section 2.1.2 and (Lundgreen and Dennison, 2020)).

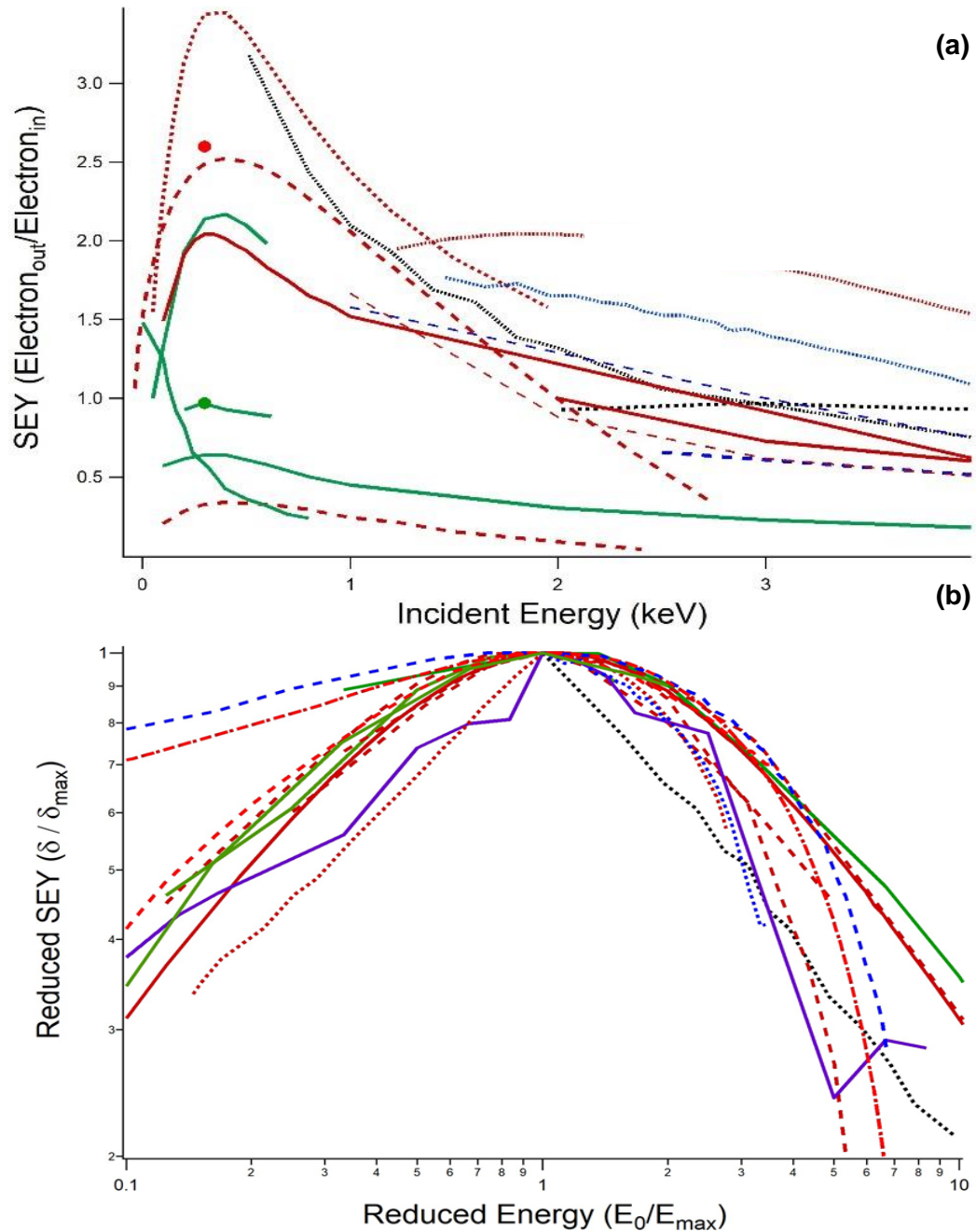


FIG. 4.5. SEY curves versus energy for Al studies. As listed in Table 4.3. (a) Linear plot of SEY versus energy. (b) Log-log plot of reduced SEY,  $\delta/\delta_{max}$ , versus reduced energy,  $E_0/E_{max}$ . A full listing of the various studies plotted and their associated symbols is given in Table 4.3. Solid, dashed, and dotted lines signify studies of smooth, rough and unknown surfaces, respectively. Green, red, and black lines signify studies of clean, contaminated, and unknown surface coverages, respectively. Bulk  $Al_2O_3$  (sapphire) SEY curve are indicated with purple lines (Christensen, 2017).

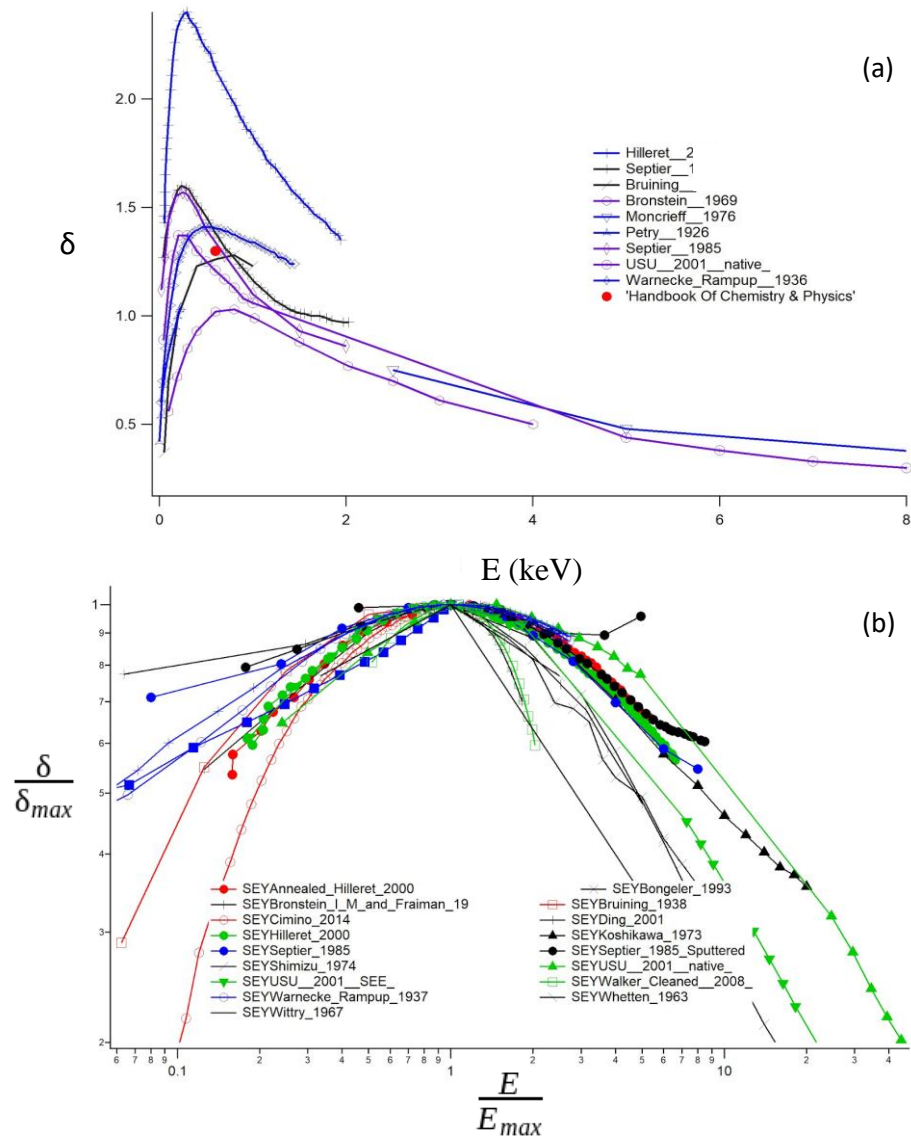


FIG. 4.6. Entirety of the Cu SEY data. Plot (a) is useful for showing  $\delta_{max}$  and  $E_{max}$  fitting parameters. Plot (b) is useful for determining  $n$  and  $m$  fitting parameters

An example of large variations in yield values can be manifest even in careful studies on ostensibly similar samples. As previously mentioned, calibration studies of TEY values for standard elemental materials, Au and graphitic carbon, (often used as calibration standards for electron yield instrumentation) (Kite, 2006) were performed by groups at USU, ONERA, LaSeine and CSIC (Dennison *et*

*al.*, 2016). In this round-robin study, where a good agreement for TEY values was expected, significant variations in maximum TEY were found, with values for Au varying from 1.3 to 1.8 and HOPG varying from 1.3 to 1.5 (see Fig. 4.4.).

Modelers should use data that more accurately mimics environmentally altered materials namely rougher, heavily oxidized surfaces typical of technical materials. Scialdone (1972) observes a trend that as altitude orbit increases the rate of contamination decreases (see Section 4.3.1). Thus, for spacecraft charging models, it is better to select studies of technical Al materials—which have SEY curves closer to those of bulk crystalline Al<sub>2</sub>O<sub>3</sub> (sapphire) (Christensen, 2017), and typically have  $\delta_{max}$  values 2 to 2½ times that of smooth, clean elemental Al—from the multitude of data shown in Fig. 4.3. and listed in Table 4.3..

### 4.3 Establishment of New Physics Principles

One cause of error in SEY reporting is the presence of contamination, specifically contamination of the surface layer of the sample. The most common surface contaminants are graphitic carbon (or related organic contaminants), water, and oxygen (Crutcher *et al.*, 1991). Each of these species can affect SEY in different ways. Because contamination and morphology have such a significant effect upon SEY values, the results found in the USU SEY Database pivot as well as the four-parameter SEY model developed by USU (see Eq. 2.2) were investigated.

#### 4.3.1 Determining Spacecraft Environment

In selecting which data to use to correctly model a spacecraft, the environment in which the craft will be operating first must be determined. A few key parameters of the environment are spacecraft outgassing rate, spacecraft dimensions, and orbit parameters. Scialdone (1972) proposes a method using these parameters to model the flux of molecules emitted by a spacecraft and reflected back to its surface that can then be used to calculate the rate of contamination for a specific craft orbiting at a specific altitude. To demonstrate the versatility of this proposed method, the amount of time required to form a monolayer of H<sub>2</sub>O on the Apollo spacecraft orbiting at 300 km is calculated. Apollo has been selected specifically because of the recently renewed interest in returning to the Moon.

To calculate the time required to form a monolayer of contaminant on a surface the density of that contaminant must be divided by the condensation rate of said contaminants. For this calculation, we will calculate the amount of time that it takes to form a monolayer of H<sub>2</sub>O (5.27 x 10<sup>14</sup> molecules-cm<sup>2</sup>).

$$\text{Monolayer formation} = \frac{\text{Density of H}_2\text{O}}{\text{Condensation rate}} \quad 4.1$$

The condensation rate for a monolayer of contaminant,  $\nu$ , can be calculated using Scialdone's (Scialdone, 1972) equation:

$$\nu = \frac{\alpha N_D (1 + \frac{\nu_0}{\nu_D})}{4\pi R_{sc} \lambda_0} \quad 4.2$$

Where  $N_D$  is the number of molecules being desorbed from the surface,  $\nu_0$  is the craft velocity,  $\nu_D$  is the velocity of a desorbed molecule,  $R_{sc}$  is the spacecraft radius,  $\lambda_0$  is the mean free path of desorbed molecules, and  $\alpha$  is the coefficient of condensation. A modified ideal gas law determines the number of molecules coming from a surface:

$$N_D = \frac{Q}{k_B T} = 1.01 \times 10^{21} \frac{\text{molecules}}{s} \quad 4.3$$

where  $k_B$  is Boltzmann's constant, and  $T$  is the temperature in Kelvins. For Scialdone's calculations, the standard temperature is assumed  $T=293 \text{ K}$ .  $Q$  is the outgassing coefficient (for water 0.133 N-m/s). The craft velocity ( $\nu_0$ ) is determined by:

$$\nu_0 = \sqrt{\frac{R_0}{R_{sc}}} \sqrt{g_0 R_0} = 7.9 \sqrt{\frac{R_0}{R_{sc}}} \quad 4.4$$

where  $g_0$  is the acceleration due to gravity,  $R_0$  is the radius of the earth, and  $R_{sc}$  is the altitude of the orbit of the craft from the center of the Earth. For this calculation  $R_{sc} = 300 \text{ km}$ . The velocity of desorbed molecules,  $\nu_D$  is determined as the mean velocity of a Boltzman distribution for an ideal gas as:

$$\nu_D = \sqrt{\frac{8k_B T}{\pi M_w}} \approx 4 \times 10^4 \frac{\text{cm}}{s} \quad 4.5$$

The mean free path,  $\lambda_0$ , of desorbed molecules is given by the 1962 version of the U.S. Standard Atmosphere as  $1 \times 10^5 \text{ cm}$  based on the atmospheric density at  $R_{sc}$  (*U.S. Standard Atmosphere, 1962*). The coefficient of condensation,  $\alpha$ , is generally taken as unity, implying that any molecules that are exposed to the surface adhere to the surface. The condensation rate is:

$$\nu = 9.6 \times 10^{13} \frac{\text{molecules}}{\text{cm}^2 \text{ s}} \quad 4.6$$

Then from Eq. 4.1.

$$t = 6 \text{ s} \quad 4.7$$

this is significant as it shows that a minimal amount of time is required for monolayer contamination to occur on a working craft at a working altitude. In general, an increase in altitude will decrease the rate of outgassed particle reabsorption exponentially as the mean free path and neutral particle density decrease with altitude (see Fig. 4.7.). Also increasing a craft's radius will increase the reabsorption rate. Studies of specific environments have been done which show that spacecraft charging, contamination, and the neutral atmosphere are of particular concern for all earth-orbiting environments (Silverman, 1995).

Assuming a monolayer thickness for H<sub>2</sub>O of ~0.3 nm, it would take 20 min to form a 100 μm thick layer of adsorbed H<sub>2</sub>O, assuming a constant condensation rate and no subsequent desorption. Incident electrons of <400 eV have a range of < 20 nm (Wilson *et al.*, 2018a). Hence the SEY of electrons <400 eV will be determined only by the H<sub>2</sub>O surface layer and not the bulk substrate, at least to first order (Wilson *et*

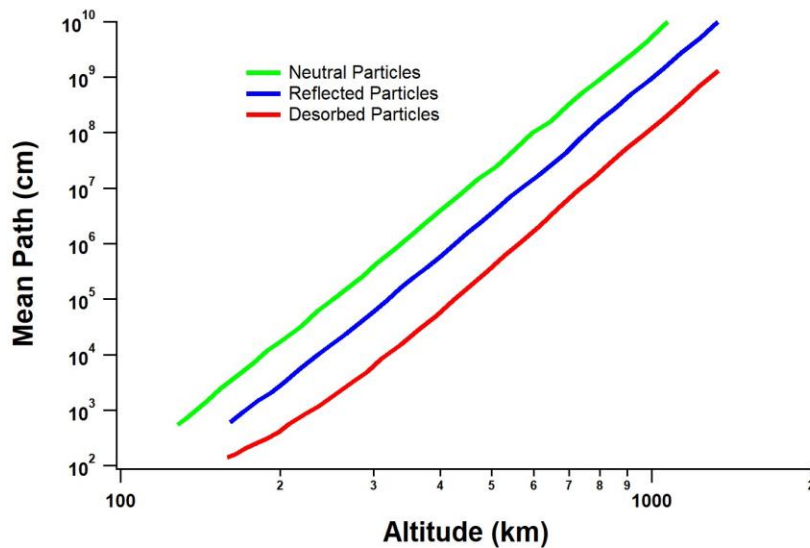


FIG. 4.7. Mean free paths versus altitude. The mean thermal velocity of the desorbed molecules is assumed to be  $v_D$  to be  $4 \times 10^4 \text{ cm s}^{-1}$ . The average velocity of the reflected particles is assumed to be one-third of the orbital velocity ( $v_R = v_0/3$ ) (Scialdone 1972).

*al.*, 2018a).

Scialdone offers many examples of LEO environment crafts. From this information, we can conclude that for a small craft in a low orbit it would be better to model the surface of the craft as being contaminated and, as contamination for many weakly bonded compounds is often not uniform, model it as rough.

For a higher LEO environment, the ISIS 1 craft provides an excellent model. Despite its radius being smaller (~55 cm), its extended altitude of 575 km has a pronounced effect on the time to form a monolayer ( $9.15 \times 10^3$  s) or roughly 2.5 hours. Although, 2.5 hrs. is significantly longer than 3 s, however, when you compare it with the lifetime of the mission (1969-90) it is still negligible. Modeling a craft at a high elevation LEO would be best accomplished by starting with smooth clean elemental samples that would last for a few hours, but then switching to a model of rough contaminated materials, as they would be more accurate to the sample in its environment.

For crafts that proceed to higher altitudes, like MEO, geosynchronous, or interstellar orbits the time to form a monolayer of contaminants will likely be more nuanced as other interstellar objects will have a greater effect upon the craft. For higher altitude missions it would be better to select either a lightly contaminated or a clean surface, and then proceed to a more contaminated surface. Determining a paper that reports data for a sample that is only lightly contaminated is tricky, however, as most researchers do not explicitly measure or quantify the contamination of their samples. A new method proposed here overcomes this difficulty by quantifying the effects of surface conditions on SEY through modeling.

#### 4.3.2 Method to Quantify Contamination and Morphology

A novel method for determining material characterization is outlined here, which involves the use of reduced format SEY curves. Figure 4.8(b) shows the same Al studies from Fig. 4.5.(a), plotted in a reduced format ( $\delta/\delta_{max}$  versus  $E_0/E_{max}$ ) on log-log axes. This method produces reduced yield curves with a consistent “inverted V” shape, which emphasizes the power-law behavior of the yield curves for the reduced data well above or below  $E_0=E_{max}$  (Bronstein *et al.* 1969). The reduced yield curve is modeled with a Reduced Power Law yield model (see Eq. 2.2). Where  $E_0$  is the incident energy and  $r_0$  is a constant fully

determined by  $n$ ,  $m$ , and  $E_{max}$  (Christensen, 2017)). This is similar to one of the SEY models employed in SPENVIS (Sims, 1992). The parameters  $m$  and  $n$  determine the slopes of the log-log plots of SEY well above and below  $E_0/E_{max}=1$ , respectively. Fig. 4.5.(a) emphasizes the parameters  $\delta_{max}$  and  $E_{max}$ , whereas the reduced yield curves in Fig. 4.8.(b) emphasize parameters  $n$  and  $m$ , as  $\delta_{max}$  and  $E_{max}$  have been factored out in the reduced format. Table 4.2. lists these four fitting parameters for the Al studies plotted in Fig. 4.5..

$n$  and  $m$  can be roughly calculated as the slope of the lines on the reduced log-log graph which lead up to and away from 1. Because the graph is a log-log plot, the slope is calculated by:

$$n \approx 1 - \frac{\log \frac{\delta_b}{\delta_a}}{\log \frac{E_b}{E_a}} \quad \text{for } E_a < E_b \ll E_{max} \quad 4.8$$

$$m \approx 1 - \frac{\log \frac{\delta_d}{\delta_c}}{\log \frac{E_d}{E_c}} \quad \text{for } E_{max} \ll E_c < E_d \quad 4.9$$

where  $E$  and  $\delta$  are points somewhat arbitrarily selected from the graph, which are separated enough that they can give a good approximation of the slope, and far enough from  $E_{max}$  that the log-log plot for the relevant energy region is a straight line. More accurate computer-generated fitting functions using Eq. 2.2 do exist and would be useful for further investigation into quantifying surface contamination through these fitting parameters, however that will have to be addressed in future work.

Table 4.1. also lists the studies plotted in Fig. 4.5.. Bulk smooth  $\text{Al}_2\text{O}_3$  (sapphire) SEY curves are also included in Fig. 4.8.(a) and associated fitting parameters are shown in Figs. 4.9. and 4.10. (Christensen, 2017). Sapphire represents a limiting case for fully oxidized Al, as the bulk limit of an infinitely thick fully oxidized aluminum sample.

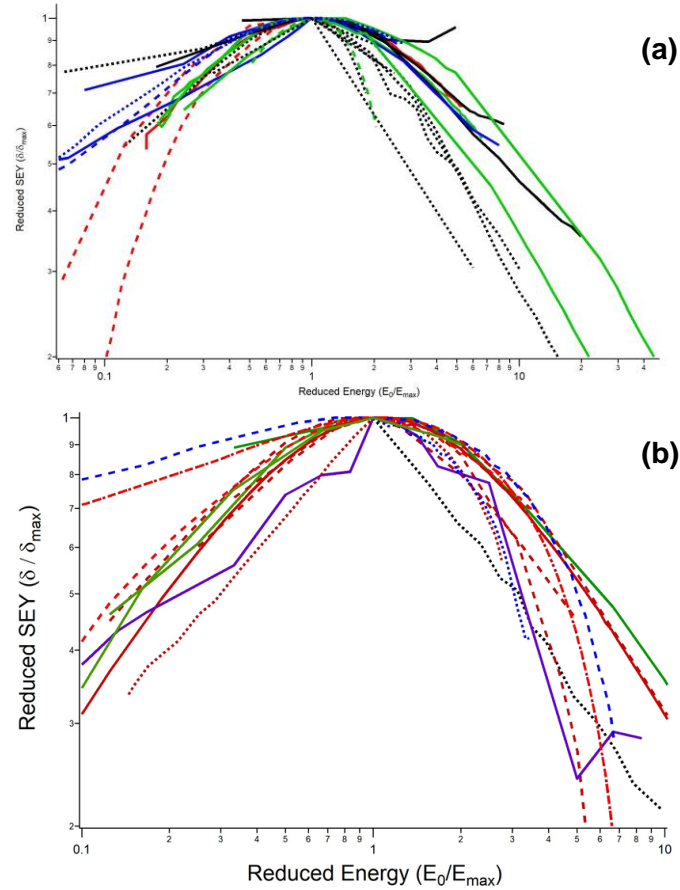


FIG. 4.8. Log-log plot of reduced SEY,  $\delta/\delta_{max}$ , versus reduced energy,  $E_0/E_{max}$ . For (a) Copper, (b) Aluminum. A full listing of the various studies plotted and their associated symbols is given in Tables 5.1.1 and 4.1. Solid, dashed, and dotted lines signify studies of smooth, rough and unknown surfaces, respectively. Green, red, and black lines signify studies of clean, contaminated, and unknown surface coverages, respectively. The bulk  $Al_2O_3$  (sapphire) SEY curves are indicated with purple lines (Christensen, 2017).

Each study has been characterized in terms of surface morphology as smooth or rough and in terms of surface layers as clean, oxidized, or C-rich contamination. The conventions established for the plotting symbols for each study used in Figs. 4.7 and 4.8 based on these designations are shown in Table 4.2., as are the line symbols used for Fig. 4.8.. Using the results displayed in Figs. 4.1., 4.2., 4.9., 4.10. and Table 4.1., attempts to establish correlations between the various yield curves and their surface properties

$E_{max}$  values are shown in Fig. 4.2.. In general, they show lower values for clean Al samples (green symbols) and higher values for rough or oxidized Al samples (open or red symbols). Interestingly the opposite trend is witnessed for CuO. AlO (an insulator  $E_g=8.5\text{eV}$ ) has higher  $E_{max}$  values than pure Al, while CuO (a semiconductor  $E_g=1.2\text{eV}$ ) has lower  $E_{max}$  values than pure Cu. Again, this trend is not as immediately apparent in the unreduced yield plots of Fig. 4.1. The curves displayed in Fig. 4.9. corroborate the trend that for low energies oxidized semiconductors (CuO) tend to have higher  $n$  values, while insulating semiconductors ( $\text{Al}_2\text{O}_3$ ) tend towards lower  $n$  values.

Correlations between the slopes  $m$  and  $n$  of the reduced yield curves in Fig. 4.8.—where the dependence on  $\delta_{max}$  and  $E_{max}$  have been removed through normalization—allow further discernment of

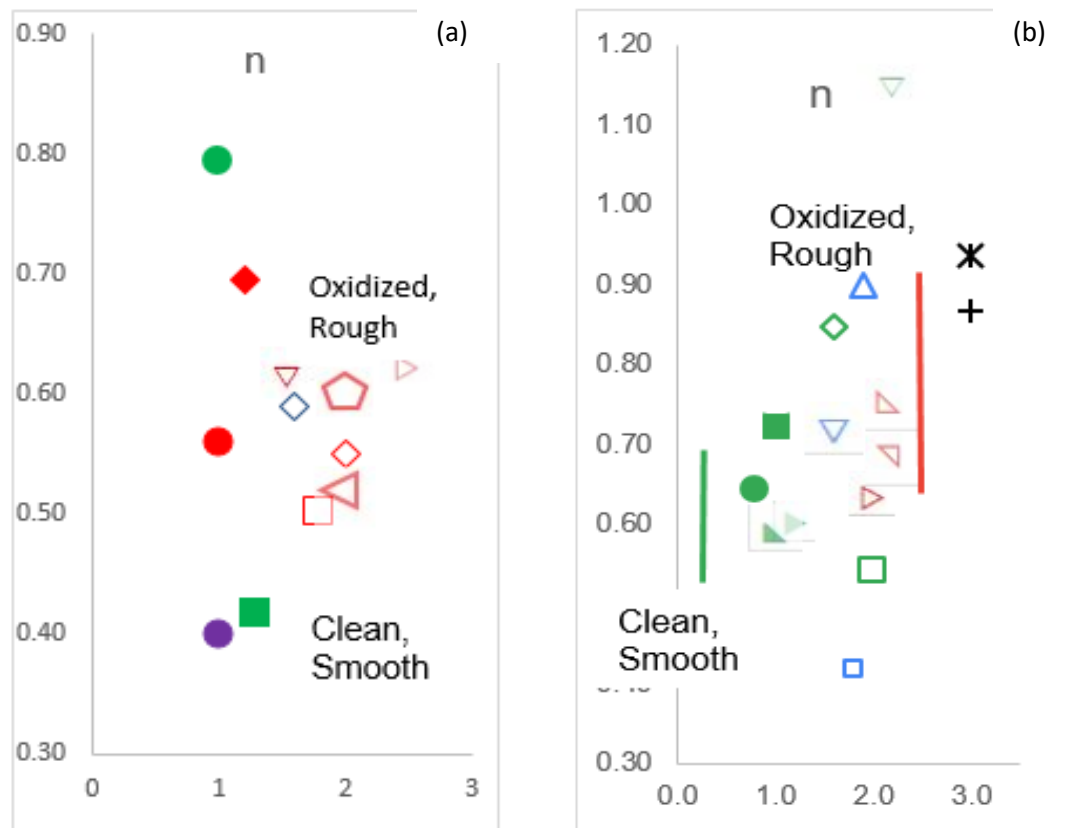


FIG. 4.9. Values of the high-energy SEY fitting parameter ( $n$ ) used in Eq. 2.2. Al studies (a) and Cu studies (b) listed in Tables 4.1, 4.3 are the source. The three columns of symbols in each plot displays values for smooth, rough, and unknown surface layers, respectively. Figure 4.2 identifies the plotting symbols used in these plots and listed for each specific study.

sample characteristics. Figure 4.9 shows that aluminum oxidized samples (red, solid symbols) and rough (red, open symbols) have consistently lower values for  $n$  ( $E_0/E_{max} < 1$ ) than smooth samples (green symbols).

Bruining's low energy  $n$  value (green solid square) is anomalously low (Bruining and De Boer, 1938). A possible reason why Bruining's  $n$  value correlates better with sapphire information than clean elemental aluminum; is the probable existence of a thin film of diffusion pump oil on the surface of the sample. As was previously mentioned often in historical measurements (before 1969) oil diffusion pumps cause contamination of samples. A thin film on the surface of an aluminum sample would affect low energy yield values, but as energy is increased, it would become insignificant. This would explain why Bruining's values behave like sapphire for low energy (Fig. 4.9.) and like clean elemental aluminum for high energy (Fig. 4.10.). Using Wilson's range model (Wilson *et al.*, 2018a), the maximum thickness of a thin film that would not be penetrated by electrons having energy less than 0.3 keV ( $E_{max}$ ) is about 1.5 nm or a few atomic layers. This is realistic when compared with experimental results (Campbell *et al.*, 1999).

In Fig. 4.10. it is apparent for both the materials that the high-energy SEY fitting parameter  $m$  values tend to range higher for smooth surfaces (solid symbols) than for rough samples (open symbols) for Al. Oxidized samples (red symbols) have  $m$  values between clean surfaces (green symbols) and heavily oxidized sapphire (purple symbol). Cu shows an interesting trend for smooth samples ranging farther while rough samples occupy only lower values. These trends are born out in the order of lines in Figs. 4.10.(a) and 4.10(b) for ( $E_0/E_{max} > 1$ ), with rough, oxidized Al (red, open symbols) falling below smooth oxidized aluminum (closed, red symbols) and heavily oxidized, smooth sapphire (purple) curves and clean, smooth copper (closed, green symbols) ranging above rough, clean copper (open, green symbols).

These apparent trends identified above are not entirely consistent, as exceptions and complications result from multiple surface modifications that have differing effects on the parameters but, for the most part, the conclusions are supported. In general, the observed trends are consistent with physics-based expectations discussed at the beginning of this section.

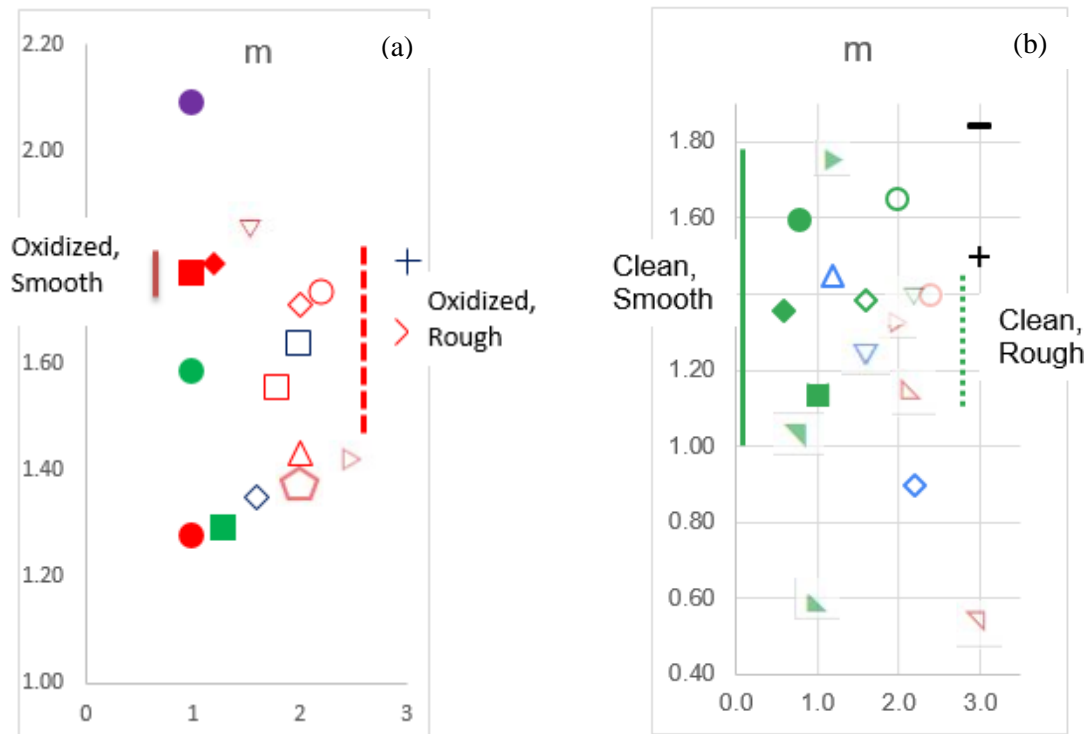


FIG. 4.10. Values of the low-energy SEY fitting parameter ( $m$ ) used in Eq. 2.2. (a) Al studies and (b) Cu studies listed in Tables 4.1, 4.3. The three columns of symbols in each plot displays values for smooth, rough, and unknown surface layers, respectively. Figure 4.2 identifies the plotting symbols used in these plots and listed for each specific study. Filled symbols indicate smooth samples, open symbols indicate rough samples, and lines symbols indicate unknown surface morphology. Green symbols indicate clean samples, red symbols indicate oxidized samples, blue symbols indicate samples with C-rich coatings, and black symbols indicate unknown surface layers. Bulk  $\text{Al}_2\text{O}_3$  (sapphire) fits are indicated with purple symbols (Christensen, 2017).



## CHAPTER 5

### CONCLUSION AND OUTLOOK

#### 5.1 Conclusion

Careful selection of appropriate materials SEY data can provide significantly improved modeling of spacecraft charging (Dennison *et al.*, 2007). The quantitative modeling of spacecraft charging using spacecraft charge-modeling software is only possible if there is sufficient experimental data on which to base the model and against which to test the predictions. The USU SEY Database, when coupled with an understanding of specific spacecraft design, flight attitude, and material selection has the potential to reduce spacecraft charging anomalies and assist in the preservation of spacecraft. This database is a continuation of the efforts of those researchers that have come before in preparing data repositories for spacecraft charging, particle accelerators, plasma physics devices, microelectronics, and electron microscopy.

To present data in the USU SEY Database data were acquired from existing databases, published journal articles, as well as the archival SEY data acquired by the USU Materials Physics Group. These data were then categorized based upon surface characteristics of the materials studied, as well as could be determined, through careful analysis of information in the journal articles and the types of materials studied. These data were then published as the USU SEY Database to facilitate researcher ease of access, as well as ease of data comparison and analysis.

Through the development of this database, a substantial increase has been made to the accessibility of qualified SEY data. Thorough examination and verification techniques were employed to report data in high fidelity. The quality of the data varies widely from source to source. Many of the samples are well qualified and well documented, but many are not. If readers require more information they are encouraged to read the original source as it has been reported in the references section.

Specific examples were given for Al and Cu as they are very common technical materials. Specifically, for these metals, the use of values for technical alloys with thicker oxide layers and rougher

surfaces is most often preferred over values for elemental clean, smooth surfaces for beginning-of-life space simulations, technical Al with thin C-rich contamination is often more appropriate for end-of-life modeling. Thus, utilizing only the default tabulated NASCAP SEY values for Al best suited for clean, smooth elemental Al can often introduce large uncertainties in spacecraft charging models. For this reason, care must be made in selecting specific data sets that apply to mission specifications and the charging concern associated with the environment and objectives proposed.

Trends observed in fitting parameters for numerous reported SEY studies under varying sample conditions presented in this database can be exploited to the spacecraft modeler's advantage through the use of specific data to identify which experimental studies best match conditions for a specific space mission. This requires knowledge of both the specific mission environments, objectives, and materials, as well as the potential causes of variations in materials surface conditions and SEY of the materials. This evaluation can identify which studies of similar materials are most applicable for specific mission parameters and can provide guidance on the extent of changes expected from environmentally induced materials surface interactions. For example, many samples will develop an oxide coating (typically 0.001  $\mu\text{m}$  to 0.1  $\mu\text{m}$  thick) before launch or as they are exposed to atomic oxygen in space. Outgassing of various spacecraft surfaces will cause many samples to develop C-rich contamination layers (typically 0.001  $\mu\text{m}$  to 1  $\mu\text{m}$ ), or they will develop some type of roughened surface (roughness on the order of 0.1  $\mu\text{m}$  to 10  $\mu\text{m}$ ) due to mechanical treatment of the material or to environmental effects such as ion-sputtering from the solar wind. To facilitate this approach the USU SEY Database can sort and identify individual data sources based upon materials characteristics of the various studies.

The majority of individuals requesting an updated SEY database require data for highly specialized insulating or semiconducting materials and typically do not utilize pure elements for their purposes. In the spacecraft design industry, elemental samples are used, however more frequently, highly disorganized insulating materials are used on the surface of a craft where environmentally-induced spacecraft charging is of most concern. Frequently questions concerning yield values for materials such as Kapton<sup>TM</sup> (polyimide), Teflon<sup>TM</sup> (polytetrafluoroethylene), or other manufactured compounds are asked. The aim of this initial database was establishing a framework on which to add more complex insulating

materials at a later date. Indeed, work has already begun on acquiring and qualifying Kapton™ data for inclusion in the database.

In the initial development stage of this database, many individuals questioned the capabilities of a materials database with regards to adding any new value to the existing physics knowledgebase. By bringing large numbers of data together into specific materials based graphs, this database has quickly verified trends previously reported by researchers regarding surface effects upon electron yield. Also by analyzing the data, a new semi-empirical model has been developed which begins to address some of the variety in industry-reported SEY values. By creating a model that addresses surface roughness and contamination, spacecraft charge modelers are more accurately able to predict SEY and charge rates of specific materials in specific environments. The model is still progressing and needs to be tested for applicability to other, highly insulating, spacecraft materials.

## 5.2 Further Developments

Further developments of this research are planned to include research into highly disorganized insulating materials, the inclusion of SEY fitting parameters, real-time curve fitting of individual datasets, and an update to the NASA SEE database. Work has already begun on some of these projects, and their initial stages are promising.

As previously mentioned, work has already begun on the iconic materials polyimide (Kapton™) and PTFE (Teflon™). In addition to these, some 81 other compounds from 61 different sources have been determined. Initial investigation has determined 17 of them to be organic, which some researchers have determined to be significant especially in regards to carbon contamination (Kishimoto *et al.*, 1977).

Research into polyimide and PTFE was begun with the intent of presenting the information at the 16<sup>th</sup> Spacecraft Charging Conference in March 2020, but due to travel restrictions caused by the Covid-19 pandemic, this conference has been rescheduled for 2021. The work on obtaining, categorizing, and presenting the data on the USU SEY database will continue forward however, with the intent of making available to the public the data by fall 2020.

An initial effort to include SEY model fitting parameters into the USU SEY Database has been as crude as including a linked spreadsheet. This spreadsheet lists each of the studies, the materials they studied, and the fitting parameters for both Eq. 2.2 and the NASCAP SEY fitting formula (see Table 5.1.). Future work will allow users to hover over a specific dataset on the USU SEY Database and have fitting parameters appear on the screen.

For this thesis, general calculations of  $n$  and  $m$  were made using log-log graph slope calculations. In the future, we plan to utilize computer-fitting programs to achieve more accurate values for  $n$  and  $m$  and incorporate these programs into our online database allowing users to fit specific datasets from the database with a specific SEY model.

Additionally in an effort to continue to increase materials knowledge an update to the NASA SEE database has been funded and is in progress. It will include historical reports analysis (much like those done

Table 5.1. Fitting parameters for aluminum. As will be included in USU SEY Database.

Material	Reference	E <sub>max</sub>	DeltaMax	RExp1	RC1	RExp2	RC2	Chi-Squared
Aluminum	Baglin, 2000*	0.334817693	3.210389179	0.540107708	1.316208174	2.0243797	1	0.02556679
	Baroody 1950	0.306582721	2.484137949	0.557215358	6.096183285	1.434729614	1	0.000575213
	Bongeler, 1993	0.304981383	3.585291523	1.372285939	5.534406973	2.309334142	1	0.01482083
	Bronstein I M and Fraiman 1969	0.252192693	0.64831856	1.858636745	0.830843334	0.615737012	1	0.001113495
	Bruining Clean Elemental 1938	0.288187366	0.985249217	1.762801414	0.880361604	0.700556877	1	0.000852481
	Bruining, As received 1938	0.357253543	2.148522612	2.010500883	0.620653968	0.45924394	1	0.012705969
	Copeland, 1938	0.455578873	3.430827814	3.193993553	0.235772276	0.800166954	1	0.126742276
	Czaja, 1966	0.254873164	4.072236567	0.149082719	0.4286875	1.724991323	1	0.014231618
	Farnsworth 1925	0.333	2.5	0.498993973	1.839041971	1.647049694	1	0.003701684
	Grosso as received 2013	0.325	2.8	0.478566838	0.8	1.6	1	0.863310429
	Grosso sputtered 2013	0.255230647	1.643792496	0.431906572	0.673129299	2.735609561	1	0.060469059
	Kanter Bulk, 1961	0.243326628	2.939236258	0.452368146	1.406188347	1.841579773	1	0.005465511
	Kanter Thin Film, 1961	0.243326628	2.939236258	0.527641771	1.404899195	1.847628733	1	0.001665645
	Moncrieff, 1978	0.291617114	1.747996542	0.84167189	0.834841134	1.76084123	1	0.000132273
	Reimer 1980	0.85	1.6	0.8	1	1.89	1	0.057435342
	Shimizu 1974	0.583444531	2.0255708	1.51454776	1.052042788	1.967300818	1	0.0024429
	USU Roughed 2001	0.331428214	2.350708346	0.834858191	1.791864931	2.019285389	1	0.022136529
	USU Smooth 2001	0.317838888	2.031454729	0.813855892	2.165842175	2.075314498	1	0.002648859
	Walker Cleaned 2008	0.429868361	2.047370503	0.813855892	2.165842175	1.980689636	1	0.02331166
	Walker Native 2008	1.86417244	1.710612845	0.788017726	0.651592158	2.088382187	1	0.066606368
	Warnecke Annealed 440C 1936	0.392710531	2.780739188	0.331710216	0.229323571	1.391685237	1	0.116667892
	Warnecke Annealed 570C 1936	0.338855773	2.522648488	0.442303575	1.131366612	1.666050214	1	0.067209175
	Warnecke Native 1936	0.297419716	2.746390565	0.442303575	0.932866527	1.588771188	1	0.049243616

in Chapter 4), specific materials properties native to a material, as well as measurements made on specific samples. This project intends to make available to a spacecraft modeler any information they may need with regards to the charging of a material.

Through these efforts to increase the availability of highly disorganized insulating material information, SEY fitting parameters for specific datasets, application of an SEY curve fitting algorithm to the database, and an update to the NASA SEE database we plan to continue to push forward the knowledge base and capabilities of the USU SEY Database.



## REFERENCES

- Andritschky, M., 1989, "Damage of Oxide Layers on an Al-Alloy by Electron Bombardment," *Vacuum* **39**, 649.
- Baglin, V., J. Bojko, C. Scheuerlein, O. Gröbner, M. Taborelli, B. Henrist, N., and Hilleret, 2000, "The secondary electron yield of technical materials and its variation with surface treatments." (No. LHC-Project-Report-433).
- Barut, A., 1954, "The Mechanism of Secondary Electron Emission," *Physical Review* **93**, 981.
- Baroody, E. M., 1950, "A theory of secondary electron emission from metals," *Physical Review* **78**, 780.
- Bedingfield, K. L., R. D. Leach, and M. B. Alexander, 1996, "Spacecraft System Failures and Anomalies Attributed to the Natural Space Environment," (National Aeronautics and Space Administration, MSFC).
- Bengtson, M., J. Hughes, and H. Schaub, 2019, "Prospects and Challenges for Touchless Sensing of Spacecraft Electrostatic Potential Using Electrons," *IEEE Transactions on Plasma Science*. **47**, 3673-3681.
- Bergeret, H., A. Septier, and M. Drechsler, 1985, "Nottingham Effect of a Superconducting Metal," *Physical Review B* **31**, 149.
- Bilgin, I., F. Liu, A. Vargas, A. Winchester, M. K. Man, M. Upmanyu, K. M. Dani, G. Gupta, S. Talapatra, and A. D. Mohite, 2015, "Chemical Vapor Deposition Synthesized Atomically Thin Molybdenum Disulfide with Optoelectronic-Grade Crystalline Quality," *ACS nano* **9**, 8822.
- Böngeler, R., U. Golla, M. Kässens, L. Reimer, B. Schindler, R. Senkel, and M. Spranck, 1993, "Electron-specimen interactions in low-voltage scanning electron microscopy," *Scanning*, **15**(1), pp. 1-18.
- Bronstein, I. M., J. Moiseevich, and B. S. Freiman, 1969, "Secondary electron emission" Moscow, Russia: Atomizdat, 408(rus)
- Bruining, H. and J. De Boer, 1938, "Secondary Electron Emission: Part I. Secondary Electron Emission of Metals," *Physica* **5**, 17.
- Burke, E., 1980, "Secondary Emission from Polymers," *IEEE Transactions on Nuclear Science* **27**, 1759.
- Campbell, T., R. K. Kalia, A. Nakano, P. Vashishta, S. Ogata, and S. Rodgers, 1999, "Dynamics of Oxidation of Aluminum Nanoclusters Using Variable Charge Molecular-Dynamics Simulations on Parallel Computers," *Physical review letters* **82**, 4866.
- Chang, W., J. R. Dennison, J. Kite, and R. Davies, 2000, "Effects of Evolving Surface Contamination on Spacecraft Charging," 38th Aerospace Sciences Meeting and Exhibit AIAA **868** 2000
- Chen, D.C., T. Gaynor, and B. Comeaux, 2002, "*Hole quality: why it matters*," *SPE International Petroleum Conference and Exhibition: Villahermosa, Mexico*.

- Cho, M., T. Sumida, H. Masui, K. Toyoda, J. H. Kim, S. Hatta, F. K. Wong, and B. Hoang, 2012, "Spacecraft Charging Analysis of Large Geo Satellites Using Muscat," *IEEE Transactions on Plasma Science* **40**, 1248.
- Christensen, J., 2017, "Electron Yield Measurements of High-Yield, Low-Conductivity Dielectric Materials." Senior Theses and Projects. Paper 44.
- Christensen, J., P. Lundgreen, and J. R. Dennison, 2018, "Parameterization of Secondary and Backscattered Electron Yields for Spacecraft Charging," SCTC. Posters. Paper 75.
- Cimino, R., L. A. Gonzalez, R. Larciprete, A. Di Gaspare, G. Iadarola, and G. Rumolo, 2015, "Detailed Investigation of the Low Energy Secondary Electron Yield of Technical Cu and Its Relevance for the LHC," *Physical Review Special Topics-Accelerators and Beams* **18**, 051002.
- Copeland, P. L., 1935, "Secondary Emission of Electrons from Complex Targets," *Physical Review* **48**, 96.
- Corbridge, J., J. R. Dennison, and A. M. Sim, 2014, "Density of State Models and Temperature Dependence of Radiation Induced Conductivity," Abstract 113, Proceedings of the 13th Spacecraft Charging Technology Conference, (Pasadena, CA, June 25-29, 2014), pp 8.
- Crutcher, E., L. Nishimura, K. Warner, and W. Wascher, 1991, "Quantification of Contaminants Associated with Ldef," in *LDEF, 69 months in space: first post-retrieval symposium*. **1** p 141-154 (SEE N92-23280 14-99)
- Cuerno, R., H. A. Makse, S. Tomassone, S. T. Harrington, and H. E. Stanley, 1995, "Stochastic Model for Surface Erosion Via Ion Sputtering: Dynamical Evolution from Ripple Morphology to Rough Morphology," *Physical Review Letters* **75**, 4464.
- Czaja, W., 1966, "Response of Si and Gap P-N Junctions to a 5-to 40-Kev Electron Beam," *Journal of Applied Physics* **37**, 4236.
- Darlington, E. and V. Cosslett, 1972, "Backscattering of 0- 5-10 Kev Electrons from Solid Targets," *Journal of Physics D: Applied Physics* **5**, 1969.
- Davies, R. E. and J. R. Dennison, 1997, "Evolution of Secondary Electron Emission Characteristics of Spacecraft Surfaces," *Journal of Spacecraft and Rockets* **34**, 571.
- Davies, R. E. and J. R. Dennison, 1999, "Measurement of Angle-Resolved Secondary Electron Spectra." PhDT 5574
- Davis, V., I. Katz, M. Mandell, and B. Gardner, 1999, *37th Aerospace Sciences Meeting and Exhibit: Spacecraft Charging Interactive Handbook*, p. 378
- Davis, V., L. Neergaard, M. Mandell, I. Katz, B. Gardner, J. Hilton, and J. Minor, 2002, *40th AIAA Aerospace Sciences Meeting & Exhibit: Spacecraft Charging Calculations-Nascap-2k and See Spacecraft Charging Handbook*, p. 626
- Davis, V. and M. Mandell, 2014. *Nascap-2k scientific documentation for version 4*, San Diego, CA: Leidos, p. 4.
- Dekker, A.J. and A. Van der Ziel, 1952, "Theory of the production of secondary electrons in solids," *Physical Review*, **86** (5), p.755.
- Dennison, J. R., J. Gillespie, S. Hart, J. Dekany, A. Sim, C. Sim, and D. Arnfield, 2009, "Engineering Tool for Temperature, Electric Field and Dose Rate Dependence of Low Conductivity Spacecraft Materials,"

*47th AIAA Aerospace Sciences Meeting Including the New Horizons Forum and Aerospace Exposition*, p. 562.

Dennison, J. R., A. R. Frederickson, and P. Swaminathan, 2003, "Charge Storage, Conductivity and Charge Profiles of Insulators As Related to Spacecraft Charging," *All Physics Faculty Publications*. Paper 1485. [https://digitalcommons.usu.edu/physics\\_facpub/1485](https://digitalcommons.usu.edu/physics_facpub/1485)

Dennison, J. R., A. R. Frederickson, N. W. Green, C. Benson, J. Brunson, and P. Swaminathan, 2005, "Materials Database of Resistivities of Spacecraft Materials," Final Report, NASA Space Environments and Effects Program, Contract No. NAS8-02031.

Dennison, J. R., R. Hoffmann, and J. Abbott, 2007, "Triggering Threshold Spacecraft Charging with Changes in Electron Emission from Materials," *Proceedings of the 45th American Institute of Aeronautics and Astronautics Meeting on Aerospace Sciences: Reno, NV*, p. 1098.

Dennison, J. R., A. Evans, D. Fullmer, and J. L. Hodges, 2011, "Charge-enhanced contamination and environmental degradation of MISSE-6 SUSpECS materials," *IEEE Transactions on Plasma Science*, **40** (2), pp.254-261.

Dennison, J. R.; J. Christensen, J. Dekany, C. Thomson, N. Nickles, R. E. Davies, M. Belhai, K. Toyoda, A. R. Khan, K. Kawasaki, S. Inoue, I. Montero, M. E. Davila, and L. Olano, 2016, "Absolute Electron Emission Calibration: Round Robin Tests of Au and Polyimide," 14th Spacecraft Charging Technology Conference. Presentations. Paper 121. [https://digitalcommons.usu.edu/mp\\_presentations/121](https://digitalcommons.usu.edu/mp_presentations/121)

Diaz-Aguado, M. F., J. W. Bonnell, S. D. Bale, J. Christensen, P. Lundgreen, J. Lee, J. R. Dennison, B. Wood, and M. Gruntman, 2020, "Experimental Investigation of the Secondary and Backscatter Electron Emission from Spacecraft Materials," *Journal of Spacecraft and Rockets*, 1.

Ding, Z., X. Tang, and R. Shimizu, 2001, "Monte Carlo Study of Secondary Electron Emission," *Journal of Applied Physics* **89**, 718.

Dionne, G. F., 1973, "Effects of Secondary Electron Scattering on Secondary Emission Yield Curves," *Journal of Applied Physics* **44**, 5361.

Drolshagen, B., 1994, "Studierende Mit Sehschädigungen an Bundesdeutschen Hochschulen," (Verlag nicht ermittelbar) (Doctoral dissertation, Verlag nicht ermittelbar).

Farnsworth, H., 1925, "Electronic Bombardment of Metal Surfaces," *Physical Review* **25**, 41.

Farnsworth, H. and V. Goerke, 1930, "Distinction between Contact-Potential Effects and True Reflection Coefficients for Low-Velocity Electrons," *Physical Review* **36**, 1190.

Feldman, C., 1960, "Range of 1-10 Kev Electrons in Solids," *Physical Review* **117**, 455.

Ferguson, D. C., 2012, "New Frontiers in Spacecraft Charging," *IEEE Transactions on Plasma Science* **40**, 139.

Flower, A., 2016, "Validity and reliability of GraphClick and DataThief III for data extraction," *Behavior Modification* **40**, 396-413

Forman, R., 1977, "Secondary-electron-emission properties of conducting surfaces with application to multistage depressed collectors for microwave amplifiers," NASA Technical Report: 1097, E-9233

Gimpel, I. and O.W. Richardson, 1943. "The secondary electron emission from metals in the low primary energy region," *Proceedings of the Royal Society of London, Mathematical and Physical Sciences*, **A182**(988), pp.17-47.

Goto, K. and K. Ishikawa, 1968, "Secondary Electron Emission from Diffusion Pump Oils II.  $\Delta$ -H Analysis for DC-705," *Japanese Journal of Applied Physics* **7**, 227.

Grimmer, D., K. Herr, and W. McCreary, 1978, "Possible Selective Solar Photothermal Absorber: Ni Dendrites Formed on Al Surfaces by the CVD of Ni (Co) 4," *Journal of Vacuum Science and Technology* **15**, 59.

Hastings, D. and H. Garrett, 2004, *Spacecraft-Environment Interactions*, (Cambridge University Press).

Hughes, J. and H. Schaub, 2018, "Space Weather Influence on Electromagnetic Geosynchronous Debris Perturbations Using Statistical Fluxes," *Space Weather* **16**, 391.

Ichinokawa, T., H. Ampo, S. Miura, and A. Tamura, 1985, "Formation of Surface Superstructures by Heat Treatments on Ni-Contaminated Surface of Si (110)," *Physical Review B* **31**, 5183.

Joy, D. C., 1995, "A Database on Electron-Solid Interactions," *Scanning* **17**, 270.

Jun, I., H. B. Garrett, W. Kim, and J. I. Minow, 2008, "Review of an Internal Charging Code, Numit," *IEEE Transactions on Plasma Science* **36**, 2467.

Kanaya, K. and H. Kawakatsu, 1972, "Secondary electron emission due to primary and backscattered electrons," *Journal of Physics D: Applied Physics*, **5** (9), pp. 1727.

Kanter, H., 1961, "Contribution of Backscattered Electrons to Secondary Electron Formation," *Physical Review* **121**, 681.

Katz, I., M. Mandell, G. Jongeward, and M. Gussenhoven, 1986, "The Importance of Accurate Secondary Electron Yields in Modeling Spacecraft Charging," *Journal of Geophysical Research: Space Physics* **91**, 13739.

Katz, I., D. Parks, M. Mandell, J. Harvey, D. Brownell, S. Wang, and M. Rotenberg, 1977, "A Three Dimensional Dynamic Study of Electrostatic Charging in Materials." *IEEE Transactions on Nuclear Science* **24**, no. 6 (1977): 2276-2280.

Kishimoto, Y., T. Hayashi, M. Hashimoto, and T. Ohshima, 1977, "Secondary Electron Emission from Polymers and Its Application to the Flexible Channel Electron Multiplier," *Journal of Applied Polymer Science* **21**, 2721.

Kite, J. T., 2006, "Secondary Electron Production and Transport Mechanisms by Measurement of Angle-Energy Resolved Cross Sections of Secondary and Backscattered Electron Emission from Gold." All Graduate Theses and Dissertations. 2089. <https://digitalcommons.usu.edu/etd/2089>

Kollath, R., 1956, "Sekundärelektronen-emission fester Körper bei Bestrahlung mit Elektronen," *Electron-Emission Gas Discharges I/Elektronen-Emission Gasentladungen I*: Springer, pp. 232-303.

Koons, H. C., J. E. Mazur, R. S. Selesnick, J. B. Blake, and J. F. Fennell, 1999, "The impact of the space environment on space systems." No. TR-99 (1670)-1. AEROSPACE CORP EL SEGUNDO CA EL SEGUNDO TECHNICAL OPERATIONS.

Koshikawa, T. and R. Shimizu, 1973, "Secondary Electron and Backscattering Measurements for Polycrystalline Copper with a Spherical Retarding-Field Analyser," *Journal of Physics D: Applied Physics* **6**, 1369.

Lai, S.T., 2013, "Spacecraft charging: incoming and outgoing electrons," arXiv preprint arXiv:1309.4660.

Lane, R. and D. Zaffarano, 1954, "Transmission of 0-40 Kev Electrons by Thin Films with Application to Beta-Ray Spectroscopy," *Physical Review* **94**, 960.

Lee, S., N. Mettlach, N. Nguyen, Y. Sun, and J. White, 2003, "Copper Oxide Reduction through Vacuum Annealing," *Applied Surface Science* **206**, 102.

Lin, Y. and D. C. Joy, 2005, "A New Examination of Secondary Electron Yield Data," *Surface and Interface Analysis* **37**, 895.

Lundgreen, P., and J. R. Dennison, 2018a "An Analysis of Variations in Published Secondary Electron Yield Measurements of Copper" (2018). Fall 2018 Four Corner Section Meeting of the American Physical Society. Posters. Paper 76

Lundgreen, P., and J. R. Dennison, 2018b, "Rectifying Garbage-in Equals Garbage-out Using a Secondary Electron Yield Materials Database," USU Colloquium Oct. 2018

Lundgreen, P., and J. R. Dennison, 2019, "Strategies for Determining Electron Yield Material Parameters for Spacecraft Charge Modeling," in *Applied Space Environments Conference*, Los Angeles, California.

Lundgreen, P., and J. R. Dennison, 2020 "Strategies for Determining Electron Yield Material Parameters for Spacecraft Charge Modeling." *Space Weather* **18**, no. 4 (2020): e2019SW002346.

Mandell, M. J., J. Harvey, and I. Katz, 1977, "Nascap User's Manual [Contractor Report, Jul. 1976- Jul. 1977]."

Mandell, M. J., P. Stannard, and I. Katz, 1993, "Nascap Programmer's Reference Manual."

Mandell, M. J., V. A. Davis, D. L. Cooke, A. T. Wheelock and C. J. Roth, 2006, "Nascap-2k Spacecraft Charging Code Overview," *IEEE Transactions on Plasma Science* **34**, 2084.

Marchand, R. and P. A. R. Lira, 2017, "Kinetic Simulation of Spacecraft-Environment Interaction," *IEEE Transactions on Plasma Science* **45**, 535.

Matéo-Vélez, J.-C., J.-F. Roussel, V. Inguibert, M. Cho, K. Saito, and D. Payan, 2012, "SPIS and MUSCAT Software Comparison on Leo-Like Environment," *IEEE Transactions on Plasma Science* **40**, 177.

Meyza, X., D. Goeriot, C. Guerret-Piécourt, D. Tréheux, and H.-J. Fitting, 2003, "Secondary Electron Emission and Self-Consistent Charge Transport and Storage in Bulk Insulators: Application to Alumina," *Journal of applied physics* **94**, 5384.

Miller, E.R., 1984, "Induced Environment Contamination Monitor-Preliminary Results from the Spacelab 1 Flight" (No. NASA-TM-86461). National Aeronautics and Space Administration Huntsville Al George C Marshall Space Flight Center.

Moncrieff, D.A., and Barker, P.R., 1978, "Secondary electron emission in the scanning electron microscope," *Scanning*, **1**(3), pp.195-197.

- Muranaka, T., S. Hosoda, J.-H. Kim, S. Hatta, K. Ikeda, T. Hamanaga, M. Cho, H. Usui, H. O. Ueda, and K. Koga, 2008, "Development of Multi-Utility Spacecraft Charging Analysis Tool (Muscat)," *IEEE Transactions on Plasma Science* **36**, 2336.
- Myers, H., 1952, "The Secondary Emission from Copper and Silver Films Obtained with Primary Electron Energies Below 10 Ev," *Proc. R. Soc. Lond. A* **215**, 329.
- Myers, R. J., and W. D. Gwinn, 1952, "The Microwave Spectra, Structure, Dipole Moment, and Chlorine Nuclear Quadrupole Coupling Constants of Methylene Chloride," *The Journal of Chemical Physics* **20**, 1420.
- Nakamura, M., S. Nakamura, R. Kawachi, and K. Toyoda, 2018, "Assessment of Worst Geo Plasma Environmental Models for Spacecraft Surface Charging by Spis," *Transactions of the Japan Society for Aeronautical and Space Sciences, Aerospace Technology Japan* **16**, 556.
- Nickles, N., and J. R. Dennison, 2000, "Instrumentation and Measurement of Secondary Electron Emission for Spacecraft Charging," *All Physics Faculty Publications*. Paper 1488.
- Niemietz, A., and L. Reimer, 1985, "Digital Image Processing of Multiple Detector Signals in Scanning Electron Microscopy," *Ultramicroscopy* **16**, 161.
- Ogwu, A., T. Darma, and E. Bouquerel, 2007, "Electrical Resistivity of Copper Oxide Thin Films Prepared by Reactive Magnetron Sputtering," *Journal of achievements in materials and manufacturing engineering* **24**, 172.
- Olano, L., M. E. Davila, A. Jacas, M A Rodriguez, and J. R. Dennison, 2017, "Dynamic Secondary Electron Emission in Dielectric/Conductor Mixed Coatings" *Mulcopim. Conference Proceedings*. Paper 42.
- Pandya, A., P. Mehta, and N. Kothari, 2019, "Impact of Secondary and Backscattered Electron Currents on Absolute Charging of Structures Used in Spacecraft," *International Journal of Numerical Modelling: Electronic Networks, Devices and Fields*, e2631.
- Parker, L., and J. Minow, 2018, "Spacecraft Charging Material Database (Scmd) in the Free Space Environment," *42nd COSPAR Scientific Assembly*.
- Pearson, S., K. Clifton, and W. Vaughan, 1998, "NASA's Space Environments and Effects Program and Related Space-Borne Experiments," *36th AIAA Aerospace Sciences Meeting and Exhibit*.
- Petry, R. L., 1926, "Secondary Electron Emission from Tungsten, Copper and Gold," *Physical Review* **28**, 362.
- Prokopenko, S. M. L. and J. G. Laframboise, 1980, "High voltage differential charging of geostationary spacecraft," *Journal of Geophysical Research: Space Physics*, **85**(A8), pp. 4125-4131.
- Purvis, C., 1995, personal correspondence.
- Raoufi, D., A. Kiasatpour, H. R. Fallah, and A. S. H. Rozatian, 2007, "Surface Characterization and Microstructure of Ito Thin Films at Different Annealing Temperatures," *Applied Surface Science* **253**, 9085.
- Reimer, J. A., R. W. Vaughan, and J. Knights, 1980, "Proton Magnetic Resonance Spectra of Plasma-Deposited Amorphous Si: H Films," *Physical Review Letters* **44**, 193.
- Reimer, L., and C. Tollkamp, 1980, "Measuring the Backscattering Coefficient and Secondary Electron Yield inside a Scanning Electron Microscope," *Scanning* **3**, 35.

Robertson, M. and J. R. Dennison, 2020, "Electron Yield of a Carbon Fiber Composite," Utah NASA Space Grant Consortium End of Year Fellowship Report, Utah State University

Sakai, Y., T. Suzuki, and T. Ichinokawa, 1999, "Contrast of Scanning Ion Microscope Images Compared with Scanning Electron Microscope Images for Metals," *Journal of Analytical Atomic Spectrometry* **14**, 419.

Schmidl, W. D., W. A. Hartman, and R. Mikatarian, 2018, "Characterization of Rapid Charging Events Due to Sheath Capacitance and Impact on the International Space Station Plasma Hazard Process," *Atmospheric and Space Environments Conference*, p. 3652.

Scialdone, J. J., 1972, "Self-Contamination and Environment of an Orbiting Spacecraft."

Seiler, H., 1983, "Secondary electron emission in the scanning electron microscope." *Journal of Applied Physics* **54**, no. 11 R1-R18.

Septier, A. and M. Belgaroui, 1985, "Secondary electron emission yields of carbon coated copper and niobium real surfaces," *IEEE Transactions on Electrical Insulation*, **4**, pp. 725-728.

Shimizu, R., 1974, "Secondary electron yield with primary electron beam of kilo-electron-volts," *Journal of Applied Physics* **45**, no. 5: 2107-2111.

Shapiro, H., and J. Hanyok, 1968, "Monomolecular Contamination of Optical Surfaces," *Vacuum* **18**, 587.

Shen, Y., Y. Mai, Q. Zhang, D. McKenzie, W. McFall, and W. McBride, 2000, "Residual Stress, Microstructure, and Structure of Tungsten Thin Films Deposited by Magnetron Sputtering," *Journal of Applied Physics* **87**, 177.

Silverman, E. M., 1995, "Space environmental effects on spacecraft: LEO materials selection guide," NASA Contractor report 4661, part 1. tech. rep.

Sims, A. J., 1992, "Electrostatic charging of spacecraft in geosynchronous orbit." No. DRA-TM-SPACE-389. Defence Research Agency Farnborough (United Kingdom)

SPENVIS, 2018. Space Environment Information System (SPENVIS) Help page European Space Agencies (ESA), <https://www.spervis.oma.be/help/system/toc.html>.

Standards, E. E. C. F. S., 2008, (Standard ECSS-E-ST-10-04C, ESTEC, Noordwijk, NI, 2009 ESA Requirements and Standards Division.

Starke, H., 1898, "Ueber Die Reflexion Der Kathodenstrahlen," *Annalen der Physik* **302**, 49.

Sternglass, E. J., 1954, "Backscattering of Kilovolt Electrons from Solids," *Physical Review* **95**, 345.

Swinton, AA., 1899, "On the reflection of cathode rays," *Proceedings of the Royal Society of London*: 1899 Dec 31; **64** (402-411) p. 377-95.

Taylor, T., P. Lundgreen, and J. R. Dennison, 2020, "Secondary Electron Yield Analysis of Space-Induced Contamination on Long Duration Exposure Facility Panels," in *Student Research Symposium*, Utah State University.

Terrill, H. M., 1923, "Loss of Velocity of Cathode Rays in Matter," *Physical Review* **22**, 101.

Thomson, J. J., 1897, "Cathode Rays," *Phillip. Mag. Ser.* **5** 44, 293.

Toyoda, K., T. Matsumoto, Y. Shikata, M. Cho, T. Sato, and Y. Nozaki, 2003, "Development of Solar Array for a Wideband Internet Working Satellite: Esd Test" *8<sup>th</sup> Spacecraft Charging Technology Conference*.

Tummers, B., 2006, "DataThief III," <https://datathief.org/>

U.S. Standard Atmosphere, 1962, U.S. Government Printing Office, Washington, D.C. 1962.

Viatskin, A. I., 1958, "The Theory of Inelastic Scattering of Electrons in Metals. 2," *Soviet Physics-Technical Physics* **3**, 2252.

Vladár, A. E., M. T. Postek, and R. Vane, 2001, "Active Monitoring and Control of Electron-Beam-Induced Contamination," *Metrology, Inspection, and Process Control for Microlithography XV*, Vol. **4344**. International Society for Optics and Photonics.

Vladár, A. E., K. Purushotham, and M. T. Postek, 2008, "Contamination Specification for Dimensional Metrology Sems," in *Metrology, Inspection, and Process Control for Microlithography XXII*. Vol. **6922**. International Society for Optics and Photonics, 2008.

Voigt, M., S. Dorsfeld, A. Volz, and M. Sokolowski, 2003, "Nucleation and Growth of Molecular Organic Crystals in a Liquid Film under Vapor Deposition," *Physical Review Letters* **91**, 026103.

Walker, C., M. El-Gomati, A. Assa'd, and M. Zdražil, 2008, "The Secondary Electron Emission Yield for 24 Solid Elements Excited by Primary Electrons in the Range 250–5000 eV: A Theory/Experiment Comparison," *Scanning* **30**, 365.

Wang, S., X.-J. Tang, Z. Yi, Y.-W. Sun and Z.-C. Wu, 2017, "Transient Analysis of Spacecraft Exposed Dielectric Charging Using SICCE," *IEEE Transactions on Plasma Science* **45**, 275.

Warnecke, R., 1936, "Émission Secondaire De Métaux Purs," *J. Phys. Radium* **7**, 270.

Whiddington, R., 1912a, "The Transmission of Cathode Rays through Matter," *Proceedings of the Royal Society of London, Series A*, **86**, 360.

Whiddington, R., 1912b, "The Velocity of the Secondary Cathode Particles Ejected by the Characteristic Röntgen Rays," *Proceedings of the Royal Society of London. Series A*, **86**, 370.

Whipple JR, E., 1982, "Impact Ionization Study." NASA Technical Report: NASA-CR-169545

Wilson, G., J. R. Dennison, and A. C. Starley, 2018a, "Electron Range Computational Tool for Arbitrary Materials over a Wide Energy Range." Conference Proceedings, Paper 47.

Wilson, G., M. Robertson, J. Lee, and J. R. Dennison, 2018b, "Electron Yield Measurements of Multilayer Conductive Materials," Fall 2018 Four Corner Section Meeting of the American Physical Society. Presentations. Paper 178.

Wintucky, E. G., A. N. Curren, and J. S. Sovey, 1981, "Electron Reflection and Secondary Emission Characteristics of Sputter-Textured Pyrolytic Graphite Surfaces," *Thin Solid Films* **84**, 161.

Wittry, D. B., 1966, "Cathodoluminescence and Impurity Variations in Te-Doped GaAs," *Applied Physics Letters* **8**, 142.

Wolfley, O. H., 2018, "Simulation of Charge Collection to Spacecraft Surfaces: Freja Satellite." NASA MSFC

Wood, B., J. Garrett, G. Meadows, V. Raghavan, E. Lay, W. Bertrand, K. Albyn, and A. Montoya, 2007, "Updated Version of the Nasa See Program Spacecraft Contamination and Materials Outgassing Effect Knowledgebase," in *45th AIAA Aerospace Sciences Meeting and Exhibit*. p. 907.

Wood, B., J. Lee, G. Wilson, T.-C. Shen, and J. R. Dennison, 2019, "Secondary Electron Yield Measurements of Carbon Nanotube Forests: Dependence on Morphology and Substrate," *IEEE Transactions on Plasma Science* **47**, 3801.

Young, J., 1957, "Some Observations on Transmission Secondary Emission," *Journal of Applied Physics* **28**, 512.



APPENDICES

## APPENDIX A. LIBRARIES USED IN CODING

This appendix includes the specific HTML code utilized to present the USU SEY database information. The various libraries and repositories called by the code are addressed in the main thesis body. The libraries used in the development of this code were *PivotTable.js*, *jQuery*, *touch-punch*, *GitHub*, and *Gchart*. Each library serves a specific purpose and assists in creating a database that is easy to access, versatile, and user-friendly.

Specific HTML database-specific *JavaScript* (JS) libraries such as *pivottable.js*, *jQuery*, and *Gchart* are used to program the web page. These libraries allow for the presentation of data in a dynamic manner which allows users flexibility of access, and data reporting style.

*Pivottable.js*© was developed by a Canadian programmer Nicolas Kruchten. This bit of code allows users to generate any chart that they wish and still be able to download a CSV of the data and plot the data using whatever program they desire (for examples of these charts and graphs see Appendix B). The USU SEY Database uses ver. 2.23.0. It is a *Javascript* Pivot Table library with drag'n'drop functionality built on top of *jQuery/jQueryUI* and originally written in *CoffeeScript*. The code is freeware and is available from Nicolas Kruchten's personal *Github* website: <https://github.com/nicolaskruchten/pivottable>. If a user does not wish to use *pivottable.js* a link is included in the USU SEY Database to the JSON file which contains the raw data. This may be used to plot the data in Excel, Igor Pro, or any other graphing program.

Java chart-making tools (jQuery) were utilized to pull external libraries from CDNJS a Cloudflare hosted public content delivery network (CDN), which hosts multiple JavaScript libraries. JQuery is the library that contains all the code for the user interface (UI). JQuery v 1.11.2 (<https://cdnjs.cloudflare.com/ajax/libs/jquery/1.11.2/jquery.min.js>) and jqueryui v 1.11.4 (<https://cdnjs.cloudflare.com/ajax/libs/jqueryui/1.11.4/jquery-ui.min.js>) were used to facilitate javascript interaction. While it is true that these versions are slightly older (circa 2014), they were the versions utilized by Kruchten in his example of *pivottable.js*, so they were included to prevent any potential issues that may occur with communication between new versions. An analysis of the UI code is not necessary for

an understanding of the workings of this database, so it is sufficient to say that using jQuery allows access to the UI library.

The database is required to support mobile compatibility. The specific reasons for this database to have mobile compatibility are real-time data validation, accurate instantaneous access, and because it is possible. This database allows users access to historical data and creates a tool that offers a capability for instant comparison of lab values to historical values. As an example, consider a recent conversation at a conference on spacecraft charging. SEY results were presented that seemed dubious, but corroborating or disproving them without online access and researching original journal articles was not possible. This situation created a desire for a mobile-capable spacecraft-charging database so that values presented could be verified on the spot. Another motivation is simply because it is possible. Our modern world has allowed vast improvements in data access, presentation, and reporting; choosing not to use them when they can be included with minimal additional work seems unwise.

*GitHub* is an online programmer's reference repository selected specifically for its hosting capabilities and its functionality concerning HTML coding. Online cloud hosting of data was chosen to limit bandwidth requirements on local USU MPG servers, and also to limit exposure of USU MPG servers to outside requests to preserve data security.

Google chart-making tools (*Gchart*) is a library provided by Google. These tools are loaded from a local repository (the "src" file in our local directory). It assists in drawing data charts using Google Chart application programming interfaces (API). This portion of code allows users to select dynamically a chart type, data source, and filter data as defined in Section 3.5 and Appendix B. This *Gchart* code also allows the pilotable framework to be more flexible in its data reporting. The adjustment of dataset colors, fonts, and error-bars are accomplished through *Gchart*. The source code is listed below.

```

1
2 <!DOCTYPE html>
3 <html>
4   <head>
5     <title>USU SEY Pivot</title>
6     <script type="text/javascript" src="https://www.google.com/jsapi"></script>
7
8     <!-- external libs from cdnjs -->
9     <script type="text/javascript" src="https://cdnjs.cloudflare.com/ajax/libs/jquery/1.11.2/jquery.min.js"></script>
10    <script type="text/javascript" src="https://cdnjs.cloudflare.com/ajax/libs/jqueryui/1.11.4/jquery-ui.min.js"></script>
11
12    <!-- external libs from highchart DELETE ME IF NEEDED
13    <script type="text/javascript" src="https://code.highcharts.com/highcharts.js"></script>-->
14
15    <!-- PivotTable.js libs from ../dist -->
16    <link rel="stylesheet" type="text/css" href="../dist/pivot.css">
17    <script type="text/javascript" src="../dist/pivot.js"></script>
18    <script type="text/javascript" src="../dist/gchart_renderers.js"></script>
19    <style>
20      html { height:100%; }
21      body {
22        font-family: Times_New_Roman;
23        min-height: 200%;
24      }
25    </style>
26    <!-- optional: mobile support with jqueryui-touch-punch -->
27    <script type="text/javascript" src="https://cdnjs.cloudflare.com/ajax/libs/jqueryui-touch-punch/0.2.3/jquery.ui.touch-punch.min.js">
28    </script>
29  </head>
30  <body>
31    <script type="text/javascript">
32    // This example adds Google Chart renderers.
33    google.load("visualization", "1", {packages:["corechart", "charteditor"]});
34    $(function(){
35      var derivers = $.pivotUtilities.derivers;
36      var renderers = $.extend($.pivotUtilities.plotly_renderers,
37        $.pivotUtilities.gchart_renderers);
38      //$.getJSON('https://raw.githubusercontent.com/elbeef/github-SEY/master/Data/Experimentalv6.json', function(SEY) {
39      //references the entire DB file
40      $.getJSON('https://raw.githubusercontent.com/elbeef/github-SEY/master/Data/Experimentalv7.json', function(SEY) {
41      //references the Aluminum and Copper DB file
42      //$.getJSON('Experimentalv5.json', function(SEY) { //This is the code to use if local data is requested
43      //$("#output").pivotUI(SEY, {
44      //This loads the renderers, sets chart size and allows for zooming on chart
45      //Google renderer options: https://developers.google.com/chart/interactive/docs/gallery/barchart#configuration-options
46      renderers: renderers,
47      cols: ["E(keV)", "rows: ["Reference", "Material"],
48      sorters: { Material: $.pivotUtilities.sortAs(["Hydrogen", "Lithium", "Beryllium", "Carbon", "Carbon (Graphite)",
49      "Carbon (MOFG)", "Magnesium", "Aluminum", "Silicon", "Silicon (Amorphous)",
50      "Titanium", "Vanadium", "Chromium", "Iron", "Nickel", "Copper", "Zinc", "Germanium", "Zirconium", "Niobium",
51      "Molybdenum", "Silver", "Cadmium", "Tin", "Caesium", "Barium", "Gadolinium",
52      "Tantalum", "Tungsten", "Platinum", "Gold", "Lead", ])}, //method to rearrange materials as reporting order
53      "inclusions": {"Material": ["Copper"], //selects which materials will appear "on load"
54      // "Surface Topography (SRU)": ["R"] //selects materials conditions which appear on load
55      },
56      rendererName: "Line Chart",
57      aggregatorName: "Integer Sum",
58      vals: ["SE.yield"],
59      rendererOptions: { gchart: {width: 1200, height: 1000,explorer:{ KeepInBounds: true}, //Sets Graph bounds
60      hAxis:{title: 'Energy(keV)', titleTextStyle: {color: '#000000', fontSize: 18}}, //Labels Vertical Axis
61      vAxis:{title: 'SEY', titleTextStyle: {color: '#000000', fontSize: 18}}, //Labels Horizontal Axis
62      hAxis: {allowContainerBoundaryTextCutoff: true},
63      //vAxis: {scaleType: 'log'}, //Creates a log vertical axis
64      //hAxis: {scaleType: 'log'}, //Creates a log vertical axis
65      lineWidth: 3, //adjusts line width
66      hAxis: {viewWindow: {max: 4}}}, //This specifies the maximum horizontal axis value
67      }
68    });
69  });
70  </script>
71  <p><a href="https://rfs.usu.edu/materialsphysicsgroup/">&laquo; back to USU MPG examples</a></p>
72  <p><a href="http://mpg.physics.usu.edu/SEY_DB/SEY%2008/Fitting_Parametersv2.0.html">&laquo; Fitting parameters (Beta)</a></p>
73  <p><a href="http://mpg.physics.usu.edu/SEY_DB/SEY%2008/">&laquo; Log-Log version</a></p> <!-- This needs to be fixed!-->
74  <!--<p><a href="https://raw.githubusercontent.com/elbeef/github-SEY/master/Data/Experimentalv5.csv">&laquo; Download Raw Data</a></p>!-->
75  <p><a> This is Version 10 </a></p>
76  <p><a> The purpose of this page is to make available a plot of secondary electron yield values(SEY).
77  On the y axis the SEY is plotted, while on the x axis the Energy(keV) is plotted. By clicking on the </a></p>
78  <p><a>material or Reference tab the user can select which data to display.
79  The options in the leftmost column are the qualifications of the data and allow for users filter displayed
80  data by Topography or Contamination. </a></p>
81  <p><a>For Surface Contamination the options are Clean (C), Oxidized (O), Contamination (C) or Unknown (U). </a></p>
82  <p><a>For Surface Morphology the options are Smooth, Rough, or Unknown. </a></p>
83  <div id="output" style="margin: 10px;"></div>
84  </body>
85 </html>

```

## APPENDIX B. EXAMPLES OF VARIOUS REPORTS AND HOW TO USE THEM

The purpose of this appendix is to give an example of a few of the possible reports which can be generated using the USU SEY Database. Included with each report example are some of the advantages and disadvantages to a particular format. We will only look into a handful of examples in this thesis giving specific directions on useful data and analysis that can be done with specific chart types.

### 7.1 Removing Gaps Between Datapoints

This can be adjusted if a user double-clicks on a data point within the graph (Fig. B.1.) to bring up the “chart editor” under the tab customize in the features section selecting “plot null values” (Fig. B.2.) will allow the graph to ignore gaps in the  $\delta$  data values and will create an actual line chart.

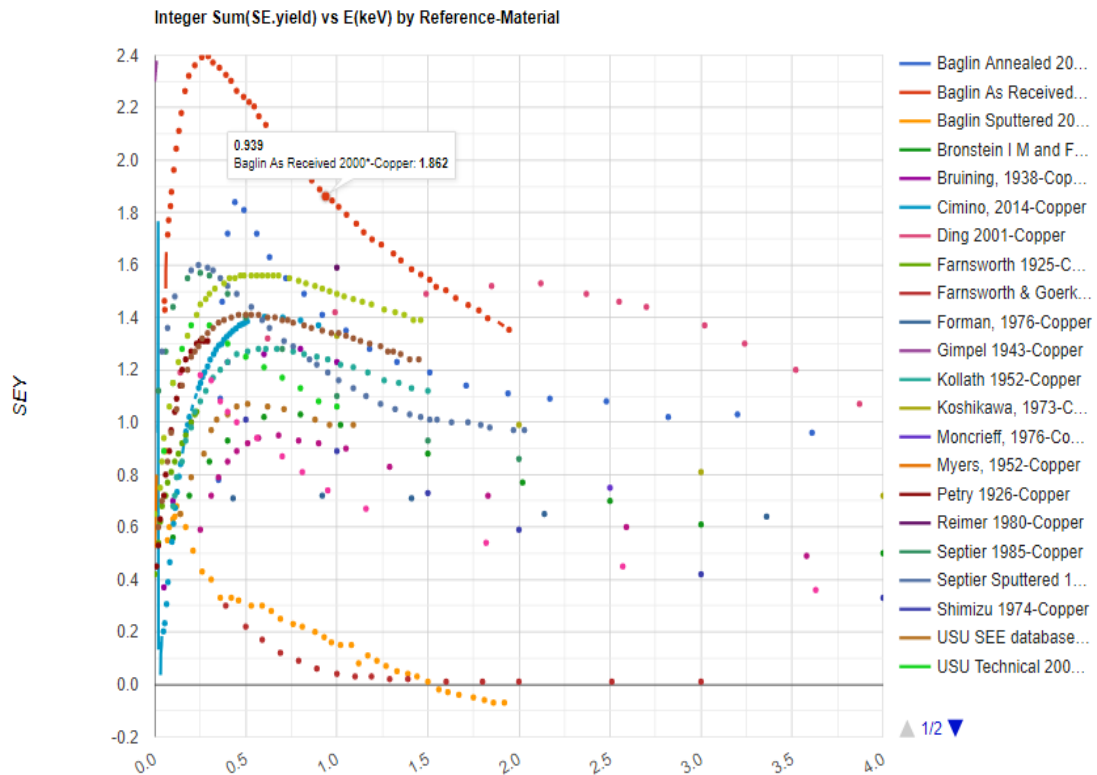


FIG. B.1. First step to remove gaps between data points. Double click on arbitrary data point.

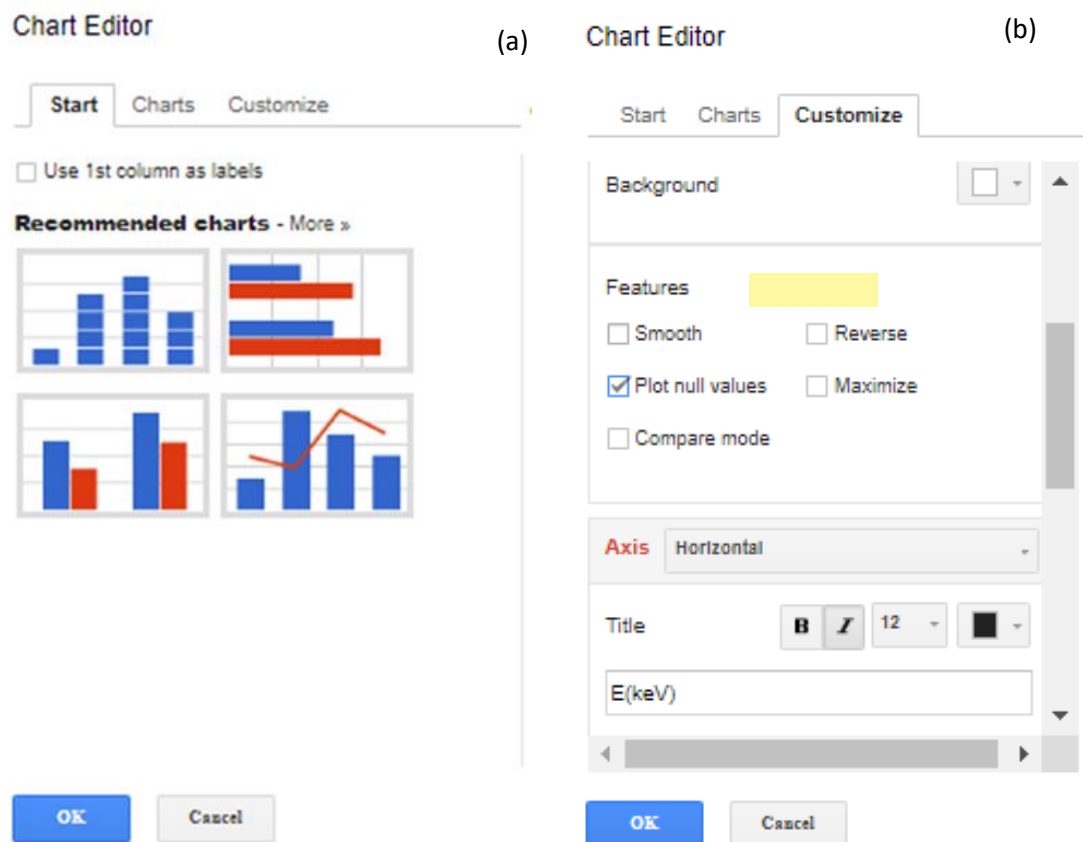


FIG. B.2. Second and third steps to remove gaps between data points. Step 2: (a) In the chart editor select customize. Step 3: (b) In the customize tab select “Plot null values”

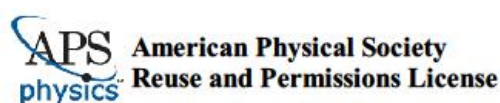
## 7.2 A Table Report

A table report is the simplest and most useful type of chart available (Fig. B.3.(a)). Table Report-1 is an example of the use and versatility of this report. It illustrates a list of multiple materials with multiple data sources and the  $\delta_{max}$  values associated with each measurement. A heat map report is a modified table report (Fig. B.3.(b)). Table Report-1 has been created to indicate extreme  $\delta_{max}$  values and could be useful when identifying the most extreme yield values which have been measured by researchers.



## APPENDIX C. BRUINING ARTICLE PERMISSIONS.

Permission granting use of Figures from “A Theory of Secondary Electron Emission from Metals” by E.M. Baroody.



28-Apr-2020

This license agreement between the American Physical Society ("APS") and Phillip Lundgreen ("You") consists of your license details and the terms and conditions provided by the American Physical Society and SciPris.

**Licensed Content Information**

<b>License Number:</b>	RNP/20/APR/025268
<b>License date:</b>	28-Apr-2020
<b>DOI:</b>	10.1103/PhysRev.78.780
<b>Title:</b>	A Theory of Secondary Electron Emission from Metals
<b>Author:</b>	E. M. Baroody
<b>Publication:</b>	Physical Review
<b>Publisher:</b>	American Physical Society
<b>Cost:</b>	USD \$ 0.00

**Request Details**

<b>Does your reuse require significant modifications:</b>	No
<b>Specify intended distribution locations:</b>	United States
<b>Reuse Category:</b>	Reuse in a thesis/dissertation
<b>Requestor Type:</b>	Student
<b>Items for Reuse:</b>	Figures/Tables
<b>Number of Figure/Tables:</b>	2
<b>Figure/Tables Details:</b>	Fig. 11. Variation of secondary emission with primary energy. Fig. 2 Correlation between the maximum secondary emission, and work function,
<b>Format for Reuse:</b>	Print and Electronic
<b>Total number of print copies:</b>	Up to 1000

**Information about New Publication:**

<b>University/Publisher:</b>	Utah State University
<b>Title of dissertation/thesis:</b>	THE GENERATION AND OPERATION OF SECONDARY ELECTRON YIELD DATABASE FOR SPACECRAFT CHARGE MODELING
<b>Author(s):</b>	Phillip Lundgreen
<b>Expected completion date:</b>	Jun. 2020

**License Requestor Information**

<b>Name:</b>	Phillip Lundgreen
<b>Affiliation:</b>	Individual
<b>Email Id:</b>	phillip.lundgreen@aggiemail.usu.edu
<b>Country:</b>	United States

## CURRICULUM VITAE

Phillip Lundgreen  
(August 2020)

## EDUCATION:

M.S. in Physics, Utah State University, Logan, Utah. (5/2020). GPA: 3.55. Thesis: The Development and Use of a Secondary Electron Yield Database for Spacecraft Charge Modeling

BS in Physics, Utah State University, Logan, Utah. (4/2014) GPA: 3.25, Minor in Chemistry

## STUDENT FUNDING:

USU Physics Department Undergraduate Student Summer Research Internship, “Developing a Database of Spacecraft Charging Materials Properties for Spacecraft Materials” (May 2019 to April 2020)

USU Physics Department Undergraduate Student Summer Research Internship, “Developing a Database of Spacecraft Charging Materials Properties for Spacecraft Materials” (May 2018 to August 2018)

USU Physics Department Ferrel and Ann Edwards Endowment “Methods to decrease error in Conductivity Measurements of Highly Disordered Materials” ( May 2013 to August 2013)

## PUBLICATIONS:

*In Preparation*

Phillip Lundgreen, Justin Christensen, and JR Dennison, “Comparison of Models for Materials Parameters Used in Spacecraft Charging Codes,” to be submitted to IEEE Trans. on Plasma Sci..

Phillip Lundgreen, “The Generation and Operation of a Secondary Electron Yield Database for Spacecraft Charging Modeling,” MS Thesis, May 2020.

*Published*

Millan F. Diaz-Aguado, John W. Bonnell, Stuart D. Bale, Justin Christensen, Phillip Lundgreen, Jordan Lee, JR Dennison, Brian Wood and Mike Gruntman, "Experimental Investigation of the Secondary and Backscatter Electron Emission from New Spacecraft Surface Materials," *Journal of Spacecraft and Rockets*, 2020.

Lundgreen, Phillip, and JR Dennison. "Strategies for Determining Electron Yield Material Parameters for Spacecraft Charge Modeling." *Space Weather* 18.4 (2020): e2019SW002346.

Phillip Lundgreen and JR Dennison, "Strategies for Determining Electron Yield Material Parameters for Spacecraft Charge Modeling," *Proceedings of the Applied Space Environments Conference 2019*, (Los Angeles, CA, May 12-17, 2019).

Christensen, Justin, Lundgreen, Phillip, and Dennison, JR, "Parameterization of Secondary and Backscattered Electron Yields for Spacecraft Charging" (2018). SCTC. Posters. Paper 75. [https://digitalcommons.usu.edu/mp\\_post/75](https://digitalcommons.usu.edu/mp_post/75)

Phillip Lundgreen (with JR Dennison and Justin Dekany), "Methods to Decrease Error in Conductivity Measurements of Highly Disordered Materials," *Senior Thesis*, Utah State University, Logan, UT, April 2014.

**PRESENTATIONS AND ABSTRACTS:***Accepted*

Trace Taylor, Phillip Lundgreen, and JR Dennison, "Optical Analysis of Contamination found on Long Duration Exposure Facility Panels," *USU Student Research Symposium*, Logan, UT, April 9, 2020.

Phil Lundgreen, Trace Taylor and JR Dennison, "Comparison of Secondary Electron Yield Studies of Polyimide through Parametrized Models," *16th Spacecraft Charging Technology Conference*, (Cocoa Beach FL, USA, March 30-April 3, 2020).

*Presented*

Phil Lundgreen and Milo Maughan, "Physics: Planting the SEEd of Science," Utah Science Teachers Association North Conference, (Weber State University, February 29, 2020).

Phil Lundgreen and JR Dennison, "Quantifying Materials Surface Conditions Through Electron Yield Analysis," (Physics Colloquium, Utah State University, October 15, 2019).

Phil Lundgreen and JR Dennison, "Quantifying Materials Surface Conditions Through Secondary Electron Yield Measurements," American Physical Society Four Corners Meeting, (Embry-Riddle Aeronautical University, Prescott, AZ, October 11-12, 2019).

Phil Lundgreen and JR Dennison, "Strategies for Determining Electron Yield Material Parameters for Spacecraft Charge Modeling," Applied Space Environments Conference 2019, (Los Angeles, CA, May 12-17, 2019).

Phil Lundgreen, Brenne Wilcox, Tonya Triplett and JR Dennison, "Getting administrator buy-in for Amusement Park Learning," Utah Science Teachers Association Conference, (Provo, UT, February 8, 2019).

Phil Lundgreen, Brenne Wilcox, Tonya Triplett and JR Dennison, "Getting administrator buy-in for Amusement Park Learning," Utah-Idaho American Association of Physics Teachers Meeting, (Logan, UT, February 20, 2019).

Phil Lundgreen, JR Dennison, "An Analysis of Variations in Published Secondary Electron Yield Measurements of Copper," American Physical Society Four Corners Meeting, (University of Utah, Salt Lake City, UT, October 12-13, 2018).

Justin Christensen, Phil Lundgreen, and JR Dennison, "Comparison of Models for Materials Parameters Used in Spacecraft Charging Codes," 15th Spacecraft Charging Technology Conference, (Kobe University, Kobe, Japan, June 25-29, 2018).

Phil Lundgreen and JR Dennison, "Development of Updated Spacecraft Materials Database for

Mitigation of Charging Risk,” American Physical Society Four Corner Section Meeting, (Colorado State University, Fort Collins, CO, October 20-12, 2017).

JR Dennison, Justin Dekany, Jodie Corbridge Gillespie, Phil Lundgreen, Allen Andersen, Amberly Evans Jensen, Gregory Wilson, Alec M. Sim, and Ryan Hoffmann, “Synergistic Models of Electron Emission and Transport Measurements of Disordered SiO<sub>2</sub>,” Invited Seminar, 13th Spacecraft Charging Technology Conference, (Pasadena, CA, June 25-29, 2014).

Phil Lundgreen, Justin Dekany and, JR Dennison, “Improved Conductivity Measurements of Highly Disordered Insulating Materials,” Utah State University Student Showcase, (Logan, UT, April 11, 2014).

Phil Lundgreen, Justin Dekany and, JR Dennison, “Methods to Decrease Error in Conductivity Measurements of Highly Disordered Materials,” Utah Conference on Undergraduate Research (UCUR) Meeting, Brigham Young University, (Provo, UT, February 28, 2014).

Phil Lundgreen, Justin Dekany and, JR Dennison, “Time Dependent Conductivity of Low Density Polyethylene,” American Physical Society Four Corner Section Meeting, (University of Denver, Denver, CO, October 18-19, 2013).